

Kristina Berg
Andrea Austjord Vik

Demonstration of PV Power to High-temperature Heat Storage for Solar Cookers

Master's thesis in Energy and Environmental Engineering
Supervisor: Ole Jørgen Nydal
June 2022

NTNU
Norwegian University of Science and Technology
Faculty of Information Technology and Electrical Engineering
Department of Energy and Process Engineering



Kristina Berg
Andrea Austjord Vik

Demonstration of PV Power to High-temperature Heat Storage for Solar Cookers

Master's thesis in Energy and Environmental Engineering
Supervisor: Ole Jørgen Nydal
June 2022

Norwegian University of Science and Technology
Faculty of Information Technology and Electrical Engineering
Department of Energy and Process Engineering

Preface

This master project is a part of a collaboration between the Norwegian University of Science and Technology, NTNU, and the University of Dar es Salaam, UDSM, and has been ongoing for several years. The thesis is written as a collaboration between two students at the master program Energy and Environmental Engineering at NTNU.

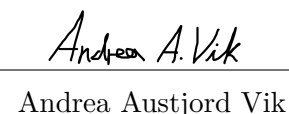
First, we would like to thank our supervisor Ole Jørgen Nydal for his support and help throughout the semester. His engagement and commitment to the project have been helpful and provided great insight. In addition, we would like to thank Paul Svendsen, Pernille Kristoffersen, Lars Konrad Sørensen and Stein Kristian Skånøy for guidance and help with work at the Thermal laboratory at NTNU. Without them, this project work would not have been possible. A special thanks to Alexander Peter Olsen for a great collaboration during the semester. He has been helpful regarding the project work and has become a good friend throughout the semester.

Due to Covid-19, we could not visit Tanzania as planned to execute experimental work in the canteen at the University of Dar es Salaam. Mapping the energy use and valuable information about the canteen would not have been provided without the help of the fieldwork conducted by Casiana Blasius Lwiwa in Tanzania.

Finally, we would like to thank the exchange students Mkufu Shabani Tindi and Leon Tshimuanga Kabongo from UDSM. They have provided valuable insight into Tanzanian culture and habits. The provided information has given a greater insight into why a transit to other cooking methods in Tanzania is still an issue.

Trondheim, June 8, 2022


Kristina Berg


Andrea Austjord Vik

Abstract

Although 72 % of the population in urban areas of Tanzania has access to electricity, charcoal and wood stoves are the conventional methods for cooking. This is due to cultural preferences, relatively low price and high availability of materials. These energy sources create thick smoke that releases heavy pollutants, causing serious health risks. A more clean and sustainable solution is, hence, required. As Tanzania is located near the equator, the location provides great potential to utilize solar power for cooking. This has established the ground for the development of different small-scale renewable cooking systems at NTNU in collaboration with several African universities.

This master thesis aims to demonstrate the concept of photovoltaic, PV, to high-temperature heat storage for cooking. The experimental work is carried out on a solar cooker developed at NTNU, referred to as the three-tank system. This thesis investigates the heating of the storage tank of the system and the ability to store high-temperature oil.

Furthermore, the thesis addresses how the concept can be demonstrated in three different system solutions. All system solutions are tested as off-grid systems with PV power; however, the setup and solar configurations differ. The three solutions consist of a battery system where excess power from a charge controller is directed to a heat battery, a direct system using PV power for direct heating of a storage, and a hybrid system that can accept power from PV and wind.

The weather conditions in Trondheim have limited the experimental work. As a consequence of poor solar conditions, the operating temperature was not reached for any tested system solutions. As the heating elements already were installed inside the heat storage tank, the controller and the solar array had to be dimensioned accordingly. This resulted in elements with too low resistance to match the solar conditions in Trondheim. These elements could not be changed due to comprehensive installation. A self-regulating heating element designed for water heating has been tested separately. However, the element was proven to be insufficient for operation at high temperatures due to the rapidly increasing internal resistance.

Implementation of a wind turbine provided a minimal capacity increase due to poor wind conditions. As a result, the system was not tested as a hybrid solution with wind energy as a secondary power source. However, the low power production from the turbine indicated that such a solution would not be beneficial.

When the system was tested with a battery, a large amount of the produced power was used to maintain the battery voltage. This is presumably a consequence of the batteries being old and worn out. A PWM controller is required by including a battery in the system, which has a lower efficiency than MPPT controllers. An overall higher temperature was achieved when testing the system with an MPPT controller.

If a system with an MPPT controller had been implemented in Tanzania, the operating temperature would most likely have been reached due to better solar conditions. In conclusion, a suitable *Geyserwise* MPPT controller has been installed and tested, creating a valuable basis for implementation and development of the system in the future.

Sammendrag

I Tanzania har 72% av den urbane befolkningen tilgang til elektrisitet, men matlaging gjennom kull- og vedfyrte ovner er fortsatt den mest brukte metoden. Det er grunnet kulturelle preferanser, høy tilgjengelighet og lav kostnad. Bruk av disse energikildene fører til et dårlig inneklima, som igjen kan forårsake en rekke helseproblemer. Dermed er det et stort behov for en bedre løsning. Med utgangspunkt i dette, er et samarbeid inngått mellom NTNU og afrikanske universiteter der hensikten er å utarbeide et bedre alternativ enn løsningen som benyttes i dag. Etersom Tanzania er lokalisert nærme ekvator gir dette godt utgangspunkt for utnyttelse av solenergi, noe som har resultert i et småskala oljebasert system drevet av fotovoltaisk, FV, paneler.

På bakgrunn av dette og tidligere arbeid, er formålet med masteroppgaven og demonstrere at FV paneler kan varme opp et varmelager til høye temperaturer. Eksperimentelt arbeid er utført på et kokesystem drevet av FV paneler på NTNU, kalt tretanks systemet. Oppgaven setter søkelys på oppvarming og energilagringsevne ved høye temperaturer.

Videre er tre variasjoner undersøkt for å demonstrere konseptet. Alle løsningene er testet som off-grid systemer driftet av FV paneler, men oppsettet og antall paneler varierer. Et oppsett er en batteriløsning der overskuddsenergi blir lagret i et varmebatteri via en ladekontroller. Deretter er et system der FV benyttes direkte til oppvarming av et varmebatteri testet. Til slutt er et hybrid system som kan driftes av både FV og en vindgenerator undersøkt.

Det eksperimentelle arbeidet har blitt begrenset av værforholdene i Trondheim. Som en konsekvens av dårlige solforhold, har ikke operasjonstemperaturen blitt nådd for noen av løsningene. Da varmeelementene i varmelageret allerede var installert, måtte solcellepanelene og kontroller dimensjoneres deretter. Dette resulterte i varmeelement med for lav resistans for solforholdene i Trondheim. Da utskifting av elementene var omfattende, ble de ikke byttet underveis i arbeidet. Derimot ble et selvregulerende element testet separat, men viste seg å fungere dårlig for operasjon ved høye temperaturer, grunnet en raskt økende indre resistans.

Implementering av en vindturbin i systemet førte til svært lav økning i produksjonskapasitet. Antagelig er det en konsekvens av lokasjonens dårlige vindforhold. Derfor har ikke systemet blitt testet som et hybridsystem drevet av både vind- og solenergi. Til tross for dette, er det antatt at implementering av vindturbin ikke vil være lønnsom grunnet den lave energiproduksjonen.

Testing av systemet med batterilagring avslørte at en stor andel av den produserte effekten gikk til å opprettholde batterispenningen. Dette er trolig en konsekvens av slitte og gamle batterier. Når systemet benyttes med batterier kreves det bruk av en PWM-kontroller. En slik kontroller har lavere effektivitet enn de testede MPPT-kontrollerene. Dette gjenspeiles i resultatene, der MPPT-kontrollere regulerte mer effektivt enn forsøkene med PWM-kontroller.

Til tross for at driftstemperaturen aldri ble nådd, kan det tenkes at dette er mulig ved bruk av MPPT-kontroller i Tanzania der solforholdene er bedre. Dermed kan det konkluderes med at den testede *Gesyserwise* MPPT-kontrollen er passende for systemløsningen uten batterier. Dette gir et verdifullt grunnlag for implementering og videreutvikling av systemet i fremtiden.

Table of contents

| | |
|--|------------|
| Preface | ii |
| Abstract | iii |
| Sammendrag | iv |
| List of terms | vii |
| List of abbreviations | ix |
| List of symbols | x |
| 1 Introduction | 1 |
| 1.1 Background | 2 |
| 1.2 Objective | 4 |
| 1.3 Project description | 4 |
| 1.4 System description | 5 |
| 1.5 Structure of thesis | 6 |
| 2 Literature review | 7 |
| 2.1 PV power to heat | 7 |
| 2.2 Hybrid wind and solar off-grid systems | 8 |
| 2.3 Cooking methods in Tanzanian university canteens | 9 |
| 2.4 Self-regulating heating elements | 10 |
| 3 Theory | 12 |
| 3.1 Off-grid systems | 12 |
| 3.2 Renewable energy sources | 13 |
| 3.2.1 Wind power | 13 |
| 3.2.2 Solar power | 15 |
| 3.3 Solar charge controllers | 16 |
| 3.4 Excess power to an external load | 18 |
| 3.5 Dimensioning an external load for a controller | 18 |
| 3.6 Electrochemical energy storage | 20 |
| 3.7 Thermal energy storage | 22 |
| 3.8 Volume in tank | 22 |
| 4 Experimental work | 26 |
| 4.1 Data collection | 29 |
| 4.2 Case 1: PV panels, batteries, and Tristar PWM controller | 32 |
| 4.2.1 Methodology | 32 |
| 4.2.2 Results 1.1 | 36 |
| 4.2.3 Results 1.2 | 39 |

| | | |
|----------|--|------------|
| 4.2.4 | Results 1.3 | 43 |
| 4.2.5 | Discussion | 47 |
| 4.3 | Case 2: Wind turbine and batteries | 49 |
| 4.3.1 | Methodology | 49 |
| 4.3.2 | Results | 51 |
| 4.3.3 | Discussion | 54 |
| 4.4 | Case 3: PV panels, wind turbine, batteries, and Tristar PWM controller | 55 |
| 4.4.1 | Methodology | 55 |
| 4.4.2 | Results and discussion | 56 |
| 4.5 | Case 4: PV panels and Geyserswise MPPT controller | 57 |
| 4.5.1 | Methodology | 57 |
| 4.5.2 | Results 4.1 | 59 |
| 4.5.3 | Results 4.2 | 62 |
| 4.5.4 | Discussion | 64 |
| 4.6 | Case 5: PV panels and homemade MPPT controller | 66 |
| 4.6.1 | Methodology | 66 |
| 4.6.2 | Results | 67 |
| 4.6.3 | Discussion | 71 |
| 4.7 | Case 6: PTC heating element and Geyserswise MPPT controller | 71 |
| 4.7.1 | Methodology | 71 |
| 4.7.2 | Results | 75 |
| 4.7.3 | Discussion | 78 |
| 4.8 | Cooldown | 80 |
| 4.8.1 | Methodology | 80 |
| 4.8.2 | Results | 80 |
| 4.8.3 | Discussion | 82 |
| 5 | Summary | 84 |
| 6 | Discussion | 86 |
| 7 | Conclusion | 90 |
| 8 | Further Work | 91 |
| | References | 92 |
| | Appendix A Manuals and Data Sheets | A-1 |
| | Appendix B PV panel configurations with heating elements | B-1 |
| | Appendix C Wind turbines | C-1 |
| | Appendix D Design of test rig | D-1 |

| | |
|--|-----|
| Appendix E Python script for calculation of u-value | E-1 |
| Appendix F Risk assessment: Oil based heat storage rig | F-1 |

List of terms

| Term | Description |
|---------------------------|--|
| Absorption charge voltage | The level of charge that can be applied without overheating the battery. |
| Angle of gradient | The tangent of the angle of a surface to the horizontal |
| Conduction | Diffusion of thermal energy within a material, or between materials in contact. |
| Convection | Heat transfer by the motion of fluid and, hence the motion of energy. |
| Cut-in speed | The wind velocity where a wind turbine start to produce power. |
| Cut-off speed | The wind velocity where a wind turbine is turned off to prevent damage. |
| Duty cycle | The duty cycle of a signal is defined as a ratio of the. time the signal is on to the total period of the cycle. |
| Flash point | The lowest temperature of an oil where the produced vapor ignite if given an ignition source. |
| Semiconducting material | A material that has a conductivity between conductors and nonconductors or insulators. |
| Smoke point | The critical temperature where an oil starts to produce smoke. |
| Solar array | PV panels wired together. |
| Sweep area | The area of the circle created by the blades of a wind turbine. |
| Thermal conductivity | Thermal conductivity is a measure of the ability to transfer heat by conduction, through a material. |
| Thermocouple | Sensor for measuring temperatures, consisting of metal wires in contact at the end. |
| Variable transformer | Variable AC power that supply adjustable AC voltage. |

List of abbreviations

| | |
|-------------------|-----------------------------------|
| AC | Alternating current |
| DC | Direct current |
| DIP | Dual in-line package |
| DOD | Depth of discharge |
| HAWT | Horizontal axis wind turbine |
| HE | Heating element |
| HTF | Heat transferring fluid |
| ISEC | Insulated electric cooker |
| MPPT | Maximum Power Point Tracking |
| PTC | Positive Temperature Co-efficient |
| PV | Photovoltaic |
| PWM | Pulse-width modulation |
| SOC | State of charge |

List of symbols

| | | |
|-------------|-------|---|
| A | | Cross sectional area [m^2] |
| A_s | | Surface area [m^2] |
| A_{Oil} | | Cross sectional area of oil inside tank [m^2] |
| A_{Slice} | | Cross sectional area of a slice in the tank [m^2] |
| C_p | | Specific heat capacity [$J/(Kg \cdot K)$] |
| h | | Height of the oil inside the tank [m] |
| I | | Current [A] |
| L | | Length of tank [m] |
| l | | Width of oil inside tank [m] |
| m | | Mass [kg] |
| P | | Power [W] |
| P_{oil} | | Perimeter of oil inside a tank [m] |
| t_f | | Final temperature [K] |
| t_i | | Initial temperature [K] |
| Q | | Heat transferred to or from a system [J] |
| Q_s | | Heat possible to store with sensible heat storage [J] |
| q | | Rate of heat transfer [W] |
| R | | Resistance [Ω] |
| R_{tot} | | Total resistance [Ω] |
| r | | Radius inside tank [m] |
| U | | Voltage [V] |
| u | | Overall heat transfer coefficient [$W/(m^2 \cdot K)$] |
| V | | Volume [m^3] |
| v | | Air velocity [m/s] |
| W | | Work [J] |
| ΔT | | Temperature difference [K] |
| η | | Efficiency [%] |
| ρ | | Density [kg/m^3] |

Φ_{in} Average light intensity of solar irradiation [W/m^2]
 ϕ Angle for calculating tank volume [$^\circ$]

1 Introduction

According to the World Trade Bank, the population in Tanzania with access to electricity increased with 13.7 % from 2015 to 2020. However, in 2020 only 22 % of the population in rural areas had access to electricity, while 72.9 % of the urban population had access. As the world is leaning against a more sustainable energy supply, electricity prices will become highly vulnerable to fluctuations. Consequently, energy independence solutions have become more important. Tanzania is still under rapid development and aims to expand the electricity grid further, as well as increase power generation while reducing greenhouse gas emissions. [1, 2]

Although the electricity grid in urban areas in Tanzania is relatively good, wood and charcoal fueled stoves are still the conventional methods for cooking. Instead of transitioning to electricity, there has been a transition from firewood to charcoal or charcoal with other additional fuel types. The extended use of charcoal is due to the relatively low price and high availability, and cultural preferences. In rural areas, charcoal and firewood, or other types of biomass, are the most commonly used power supply for cooking. This is a consequence of high electricity prices, inadequate grid connections, and limited infrastructure. [3]

When such fuels are used for indoor cooking, thick smoke releases heavy pollutants. Prolonged use of these traditional cooking methods can harm human health and the environment. According to the World Health Organization, WHO, 3.6 million premature deaths were caused by indoor air pollution in 2016. In addition, fuel gathering is a time-consuming and dangerous activity that can cause damage to the muscles and skeleton, which women and children usually perform. This extensive use of biomass causes deforestation in Tanzania, contributing to a huge amount of the CO_2 emissions when removed and used. Additionally, deforestation increases the risk of wildlife and biodiversity extinction. [4–8]

Since only 5 % of the population has access to clean fuels and technologies for cooking, there is a large potential for a stand-alone, renewable cooking system. Tanzania is also located near the equator, which provides great opportunities for utilizing solar energy. Consequently, giving potential for off-grid installations and establishing the background for this project work. [9, 10]

On this basis, a more sustainable and healthy cooking solution could be interesting to implement in bigger cities and rural areas. However, such a system can be expensive. An interesting opportunity could, thus, be to install a rig at a university or restaurant in the urban areas to test the system on a larger scale. Large scale testing could help improve the system and increase its efficiency faster before implementing it in rural areas. This can contribute to a less expensive and more efficient small-scale cooking solution for households in rural areas, as a stand-alone, renewable system is less expensive than developing a grid connection. [10, 11]

1.1 Background

The work towards developing a sustainable cooking solution to substitute the current solutions in Tanzania has been an ongoing project for several years. This project is a collaboration between NTNU and a group of African universities, where the work in this thesis is a continuation of previous testing and development. One of the systems that have been built and developed is a three-tank system consisting of separate tanks for heat storage. There are two versions of this system, one experimental rig at NTNU and one in Arusha. Previous projects have aimed to improve the existing system at NTNU and modify the system in Arusha to suit the local conditions in the best possible way.

An experimental rig of the three-tank system was built at NTNU in 2019 and has been modified multiple times since then. This system is a cooking apparatus designed to heat a frying pan and a cooker. The design can be divided into efficiency and user-friendliness of the cooker and heat storage ability at high temperatures. This thesis focuses on heating the storage tank and energy storage capability. As the work in this thesis is a continuation of prior work, conclusions and proposals from previous projects are briefly described in the following paragraphs.

The prior master thesis *Photovoltaic Solar Cooker with Heat Storage*[12] aimed at testing the three-tank system in Arusha with PV panels. This was to understand the surrounding conditions of the possible locations for implementation. Due to the limited availability of materials and costs, the rig in Arusha has some differences from the experimental rig at NTNU. The main differences are the use of a different oil as the heat transferring fluid and higher ratings of the PV panels and heating elements than the setup at NTNU.

Experimental work revealed that the heat storage could be heated up to 230 °C. However, the temperature did not reach 230 °C until around 11.00 or 12.00, dependent on the starting temperature. Even though the operating temperature was reached, a test with the intended PV panels, oil, and heating elements needs to be conducted to demonstrate the original design at NTNU fully.

When this experiment was conducted, the rig in Arusha had not been used for a year. Before starting the experimental work, maintenance was already needed. The demand for maintenance exposed a potential for improvements in components and material choices. Although this must be considered regarding price, as components can be at risk for theft. Furthermore, several modifications are also needed at the rig at NTNU. Among these is an improvement of the insulation of the heat storage, as heat loss prolongs the time to heat oil to the operating temperature. However, budget is a limiting factor. Improvement of the insulation should, hence, be a priority as long as it is economically viable.

Due to the rainy seasons in Tanzania and poor solar conditions in Norway, PV panels would not be sufficient to power the system at all times. Therefore, it is interesting to investigate the implementation of a backup energy source to ensure the demand for cooking is met. This issue has been further investigated in the thesis *Excess solar, wind, and hydro power to charge heat storage for cooking*[13]. The test rig at NTNU has been tested with solar power and batteries.

However, this test was performed with artificial sunlight from a lamp with batteries as a backup power source. As it did not produce enough power to heat the heat storage tank, the rig should be tested with actual sunlight. This will reveal how the heating elements respond to an alternating power supply.

Because of time restrictions and practical limitations, the thesis did not include a test with an additional power supply. A test with an additional power source would expand the use area and provide great insight to test the system as a hybrid solution with multiple power sources. A test with another power source, or an additional power source, would be interesting and should be performed.

Previous project work has disclosed that the system at NTNU still needs final testing of the working principle without power supply from the grid. Furthermore, there is a distinct need for further testing and improvements regarding the controller, power source, and heating elements, as the three-tank system has not changed since it was built in 2019. Since several projects at NTNU, with different design solutions, have aimed at substituting conventional cooking methods in Tanzania, it could be feasible to transfer the findings to other designs.

This master work is a continuation of the preliminary work *Small Scale PV Solar Cooker*[14] performed during fall 2021. The preliminary work suggested improvements to the design to increase the system efficiency. However, due to time limitations, it was decided to perform the experimental work on the already existing system at the Thermal Laboratory instead of building the new version. Such a system would require more knowledge from the user and would be more difficult to implement in Tanzania. Therefore, it was considered more beneficial to test single components of the existing system to transfer the findings to other setups for solar cooking technologies.

1.2 Objective

The main objective of this master's work is to demonstrate the concept of the off-grid cooking solutions developed at NTNU, with a primary focus on the three-tank system. This is to replace wood or charcoal fueled stoves as the conventional cooking method, as these methods create thick smoke leading to a poor indoor climate.

Developing an off-grid cooking solution powered by renewable energy has been an ongoing project for multiple years. Through these projects, a three-tank system has been developed and built. However, the concept has only been demonstrated with AC power from the grid. Therefore, the system needs to be demonstrated only powered by solar power before it can be implemented. Furthermore, an investigation of variations of renewable solutions for powering the system and examination of single components and their performance are needed. The results can be transferred to other small-scale heat storage methods.

The aim of this master thesis is, thus, to demonstrate that excess power from photovoltaic, PV, panels or wind can be directed to high-temperature heat storage, consisting of an insulated tank filled with thermal oil. Furthermore, to investigate and test if the system can take advantage of combining PV panels and wind power. Also, examine the possible advantages of connecting the power source directly to the heat storage.

1.3 Project description

Based on the objectives and previous work, the following project description has been developed: Several small-scale heat storage methods for cooking have been explored in the past as part of a long-term collaboration with a group of African universities. Systems based on electrical heating powered by PV panels, wind power, hydropower, or a combination, can be designed with and without batteries. This master thesis work will aim at demonstrating:

1. Battery system: Excess power from a charge controller is directed to a heat battery
2. Direct system: PV power is used for direct heating of a heat storage
3. Hybrid system: A heat storage that can accept power from PV and wind generator

The objective of the experimental work is to demonstrate these system solutions with new controllers with the available heating elements. All system solutions will be tested as off-grid systems by using solar power to demonstrate the working principle of the systems without supplementing power from the grid. In addition, look at wind as a supplementing power source in a hybrid system. Based on the findings and research, an evaluation will be performed regarding which system combination is recommended for implementation.

A potential challenge of the experimental work is the local weather conditions in Trondheim. The experimental work is highly dependent on the weather conditions, as good solar conditions are a prerequisite for the experiments. Trondheim is characterized by unpredictable weather, with frequently fluctuating solar conditions. Unpredictable weather is, hence, perceived as a challenge since the experimental work aims to test the system with solar and wind power.

The work will be made as a collaboration between four students, two from NTNU and two exchange students from UDSM under the NORPART project *UDSM-NTNU Mobility Program in Energy Technology*. This collaboration aims to include and support the exchange students with the experimental work concerning their thesis. The workload is distributed such that the NTNU students will work as a connection for the exchange students regarding communication with the people at the lab and handling the logistics, in addition, to coordinate and being present during their experiments. It is considered a part of the master thesis to get experience with multicultural collaborations during the experimental work.

1.4 System description

The following section is copied from the preliminary project work *Small Scale PV Solar Cooker*.^[14] The existing system consists of three tanks connected to a boiler and a frying pan. This system is powered by PV panels, which power the heating elements placed in the heat storage tank. The power from the solar array is regulated by a controller that connects the three-tank system to the PV panels placed on the roof of the Thermal Laboratory at NTNU. External batteries can also be connected to heat the system on days with no sun, or to power small household supplies.

A heat transferring fluid, HTF, is used to transfer heat from the heating elements to the cooker by circulation. The thermal oil Duratherm 630 is selected as the HTF, as this has provided great results in previous project work. However, multiple vegetable oils have been previously tested with satisfactory results. The HTF is stored in the upper tank, referred to as tank 1, before it is heated in the heat storage tank, referred to as tank 2. The heat storage tank is insulated with two layers of the high-quality insulation material Fyrewrap, serving as a hot oil reservoir. Furthermore, a thermostat placed next to a heating element regulates flow from the upper tank to the heat storage tank. The thermostat is a bimetallic spring that should open when the surrounding fluid reaches a temperature of $220\text{ °C} \pm 11\text{ °C}$.

After the oil has reached the operating temperature of 230 °C , the flow is directed to either the frying pan, the cooker, or both, dependent on valve openings. The three-tank system consists of several valves that need to be regulated during use, making the system more complex and less user-friendly. After rejecting heat to the frying pan or cooker, the oil is directed to a third tank, referred to as tank 3. This tank is not insulated and serves as a cold oil reservoir. When the oil level in the upper tank is low, the oil has to be manually pumped by a hand pump connected to the lower tank. To prevent high pressures, the tanks are vented to the ambient. Additionally, an electric thermostat is connected to the heat storage tank to prevent the system from overheating. A flow scheme of the system is shown in Figure 1.1.

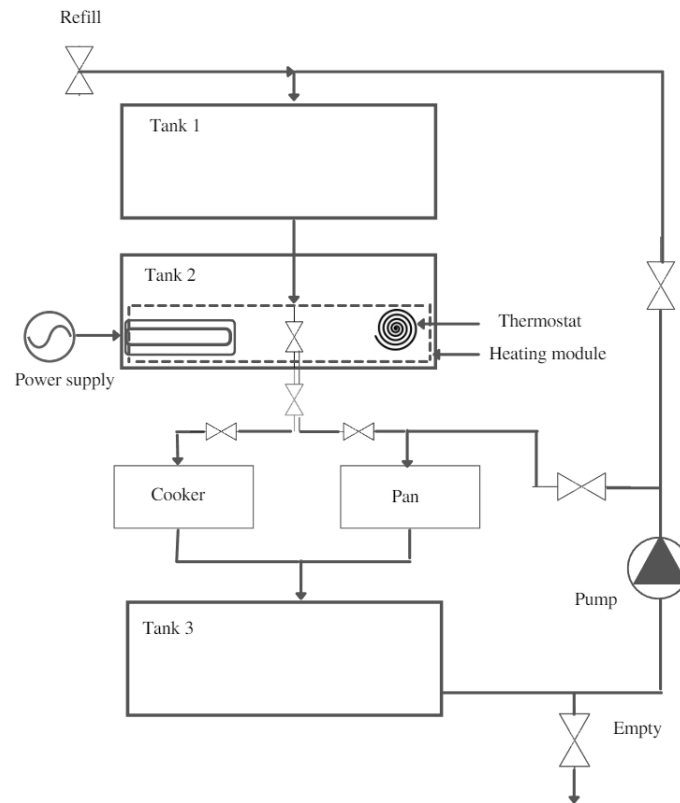


Figure 1.1: Schematic illustration of the system setup and components of the three-tank system. [14]

1.5 Structure of thesis

First, the background and origin of this work are described, followed by a brief description of the relevant work performed by previous students in addition to a literature review. Further on, the relevant theory is presented.

Chapter four consists of the experimental work performed concerning this master thesis. The work has been divided into six cases, all consisting of a solar array, a controller, and a load. The setup and methodology for each case are described, followed by a presentation of the findings and an experimental discussion of each case. Additionally, a section regarding data collection has been included.

The following chapter consists of a summary of the main results of each case, followed by a discussion of the findings and challenges. Lastly, a conclusion is presented together with the recommended further work.

2 Literature review

The utilization of solar power for cooking purposes is a well-known concept that has been applied for years. However, the field is constantly developing due to new and improved technologies. Though the specific concept of PV power to high-temperature storage is limited in literature, similar systems have been tested and developed. In this literature review, the benchmark technologies for solar cooking will be elaborated, followed by a description of the current area of use. Lastly, research on self-regulating heating elements in related systems will be described.

2.1 PV power to heat

Off-grid systems can be divided into direct-coupled and non-direct coupled systems. The load is connected directly to the solar array or a controller in-between in directly coupled systems. Non-direct systems are systems where the solar array is not directly coupled to the load, often including an energy storage unit such as a battery. In systems with batteries, a controller must be included to control the charging voltage to avoid overcharging and damage to the battery.[15, 16] Direct systems can also include a maximum power point tracking, MPPT, and a controller to optimize the power utilization of the solar array. According to the findings in the research article by T. Matuska and B. Sourek[17] direct systems with an MPPT controller can achieve a 20 % to 35 % higher annual yield than a system with the solar array coupled directly to the load.

Both direct and non-direct systems have been tested for cooking purposes with good results; however, the results differ. A standard design of direct PV systems for cooking is an insulated electric cooker connected to a solar array. This method is often referred to as ISEC cooking. ISEC cooking is proven to provide good results for cooking; however, with a limited area of use. Such systems are restricted by the heating element size and have no opportunity to store excess power. In a study by T. Watkins et al. [18], it was disclosed that the power limitation caused an increase in cooking time, which could be problematic. In this system, the cooking is highly weather dependent and has very low user flexibility. A benefit of this system is the cost and operation, as it consists of a few components. ISEC cooking is not suitable for large-scale cooking as the main advantage is simplicity and low costs.

A survey on the use of solar cookers for food vendors in Tanzania conducted by Modern Energy Cooking Services[19], MECS, revealed that durability and power were the most critical factors for the user to implement a new cooking solution. Better durability and power can be achieved for solar cookers by implementing an energy storage unit to reduce weather dependence. A study by S. Batchelor et al. [20] investigated the possibility of implementing a PV solar cooker with a battery as a cooking solution. The study revealed that the cost of energy was tripled by including a battery. However, the advantages of including a battery were so great that it might be a better solution, despite the increased cost.

A cooking system where a battery was included to store energy and a pot of water was serving as an excess load has been reviewed in experimental work performed by J.Barton[21]. The system provided good results with the opportunity to utilize excess energy. A drawback of this system is that the excess energy must be used immediately, as it is stored as hot water in a pot. This issue could be solved by storing the hot water in an insulated tank. A well-known solution is storing excess energy from PV systems in hot water tanks. However, there has not been conducted much research on combining this type of storage with cooking solutions. By combining these solutions, the excess energy could be stored without increasing the battery storage capacity. Such a solution would provide great user flexibility and reliability. This idea has created the basis for the design and development of the three-tank system.

2.2 Hybrid wind and solar off-grid systems

An additional power source can be added to increase the capacity and ensure a consistent power supply of an off-grid solar system. Implementing a wind turbine is considered beneficial for small-scale production and households due to its low impact on the environment and relatively easy installation. Systems with multiple power sources are referred to as hybrid systems. Such systems are commonly used with a battery for energy storage. Further, it consists of the power sources, a converter, and a controller connected to a load and the battery. [22]

The research on the implementation of small-scale hybrid systems in Norway is limited. However, such systems are commonly used in cabins to provide a consistent power supply where wind turbines are implemented to top off the batteries. According to the online forum *Byggehytte.no*, [23] the turbines can be mounted on the roof of the cabin, while the most common method is to mount them on the ground. However, mounting on the roof can create some vibration and noise issues.

The conventional setup is to connect the wind turbine and solar array to the controller and batteries. When the batteries are fully charged, the wind turbine breaks and the solar panels stop producing power. These systems can be purchased off-the-shelf where some turbines have a DC converter mounted in the turbine tower, whereas others come with a separate controller. In the master thesis *Mulighetsstudie: bruk av distribuert fornybar energiproduksjon på turisthytter*[24] H. R. Olsen investigated the opportunity to implement a similar system at a Norwegian tourist cabin. The results disclosed that it is possible to implement a renewable system solution; however, the solution was not economically competitive compared to the power supply from a diesel generator. Most systems with wind turbines cannot utilize the excess energy after fully charging the batteries due to the braking mechanism of the wind turbine in the controller.

However, some controllers have an operational mode where an extra load can be connected to utilize excess energy after fully charging the batteries. Examples of such loads are electric heaters or fans. In order to direct power from the turbine to the controller, it must be converted to DC first. The conversion to DC can be done in a converter or a separate control unit connected to the wind turbine. Suppose that the turbine is mounted with a separate control unit and a hybrid controller, the braking voltage of the turbine must be higher than the reference voltage of the controller. If this is not fulfilled, the turbine will break when the batteries are fully charged, and no excess power will be diverted to the excess load.

If the turbine is mounted with only a converter connected to the hybrid controller, without a separate control unit, the turbine has no braking mechanism. In this case, the turbine will produce energy as long as the wind conditions are higher than the cut-in speed. The external load will receive all excess power when batteries are fully charged. If the external load is an electric heater, an issue occurs when the room is considered sufficiently hot as the turbine cannot stop production. It is, hence, necessary to have a reliable additional load to burn off the excess energy. According to the online forum *Byggehytte.no*, [25], when the cabin is in use, a connection of an external load can be performed. In this case, the external load can be changed when the energy demand is covered. The external load can, for example, be a coil that heats outside air to burn off excess energy.

The challenge is implementing a solution where the excess energy can be stored when the batteries are fully charged and the system is unattended. To achieve this, a system that can switch between loads must be developed to ensure that safety is maintained continuously and to prevent overheating. An opportunity to store excess energy is thermal storage in an insulated tank filled with a heat transferring fluid. Although such a solution is limited in literature and research, it is considered to have great potential.

2.3 Cooking methods in Tanzanian university canteens

An unpublished study performed at the canteens located at the College of Engineering and Technology, University of Dar es Salaam, Tanzania, revealed that the primary energy source for cooking is briquette charcoal and liquefied petroleum gas, LPG. Briquette charcoal is preferred because it has low costs, is readily available and requires little maintenance, despite the long cooking time. LPG is preferably used for food with a shorter cooking time. With the recent increase in the costs of LPG, there is an opportunity to replace this fuel with other renewable solutions.

The frequent use of briquette charcoal creates a large amount of dust, making indoor air pollution a crucial issue. During the study, vast amounts of smoke and dirt from charcoal were observed in the cooking facilities. The daily average energy demand was estimated to 64.7 kWh/day, which corresponds to 21 440 W solar panels based on local solar conditions. Additionally, it was disclosed that the kitchen had space to install a solar cooker, and the roof was large enough to install the required amount of PV panels. The study concluded that implementing a solar cooker in the canteen could be feasible without compromising the operational and social demands. [26]

2.4 Self-regulating heating elements

Self-regulating heating elements are often called positive temperature coefficient elements, PTC elements. A PTC element is a ceramic-based electrical component where internal resistance is dependent on temperature. There is an intrinsic increase in internal resistance with an increase in temperature. With an increase in resistance and temperature, there is a decrease in current conductivity and power output until the design temperature of the element is reached. When the internal resistance reaches the value corresponding to the design temperature of the element, the current can barely flow anymore and keeping the temperature constant. Therefore, such elements will warm up quickly to the respective design temperature. The self-regulating characteristics prevent these elements from overheating, making this technology safe and reliable. [27]

Wire heating elements are more suitable for very high temperatures from 240 °C up to 950 °C, using temperature-resistant alloy compared to PTC elements. Wire heating elements are durable by being corrosion-resistant, insensitive to moisture and mechanically resilient. However, such elements can quickly overheat when not operated properly. Therefore, they must be installed with an appropriate protection control to switch off the heating elements if overheating occurs. [28, 29]

Heating water with PTC elements and PV panels is a well-known technology that has been used for years. Other areas of use are hair curlers or coffee machines. The design temperature of the PTC elements depends on the application. When used for water heating, the design temperature is commonly around 60 °C or higher. However, the design temperatures of PTC elements can range from from 40 °C to 220 °C.[27, 30]

According to the South-African company *Gesyserwise*, PV panels combined with an MPPT controller to power the PTC heating unit for water heating have been proven successful. The system can set time intervals for heating the elements during the day and set the maximum temperature within the storage tank. This setup has resulted in reduced energy demands in many heating applications. In addition, to save power, this system can prolong a lifetime of up to 30 years with only minimal requirements for maintenance, according to the manufacturer. Many households utilize this kind of setup for water heating today, as a higher temperature is achieved per kWh to heat the element than a standard spiral element. Furthermore, this saves money after the investment of the PTC element is repaid, which is approximately 5 to 6 years. [31, 32]

Shared experience retrieved from the online forum *4x4community.co.za*[33] and *powerforum.co.za* [34], expressed that PTC elements have been tested using PV and MPPT controllers to heat water with batteries to store excess power. However, if the temperatures in the water storage tank drop to a low temperature after usage, the batteries would heat the water. This works poorly if the heating element is rated at a high wattage. Powering a high wattage heating element would drain the batteries and damage them. Therefore, the setup works better with an element with lower wattage for a setup including batteries. However, heating the water to 50 to 60 °C takes a longer time to heat with a lower wattage. Although batteries are not shown to be efficient for powering heating elements during down periods independent of a lower wattage rating on the element.

There is limited information and research on the experience with the use of PTC elements for heating high-temperature oil. However, PTC elements with design temperatures of 180 °C, which can be heated up to 230 °C, exist. In addition, the principle is a well-known technology for heating water, which can be transferred to heating other fluids. [30]

3 Theory

An overall understanding of the main principles behind off-grid systems, power sources, and components related to the design and operation of a stand-alone system will be evaluated in this chapter. This is to furthermore develop a fundamental understanding of this project and the experimental work.

3.1 Off-grid systems

An off-grid system is a system that generates and distributes energy independently of a distribution grid. Such systems are typically installed to provide power to rural areas, reduce energy costs, or be independent of external power sources. The energy source can be renewable, fossil, or both. PV panels are often used as an energy source because they have great potential for energy production and are easy to install. This energy source can also be easily combined with wind or hydropower to increase electricity production. [35]

A battery is often used as an energy storage device, where the size of the battery should match the total power generation capacity of the system. In addition to an energy source, a controller, measuring devices, and safety equipment are essential for a functioning system. When using renewable energy sources, energy storage is also required to provide reliability and flexibility for the user.

The current output in an off-grid system can be either alternating current, AC, or direct current, DC, depending on the desired application. An inverter can be used in this scenario to change the output current from DC to AC. A control unit is also required to regulate the current and voltage from the source before it is sent to the storage unit or a load. Figure 3.1 illustrates a general setup of an off-grid system. [16]

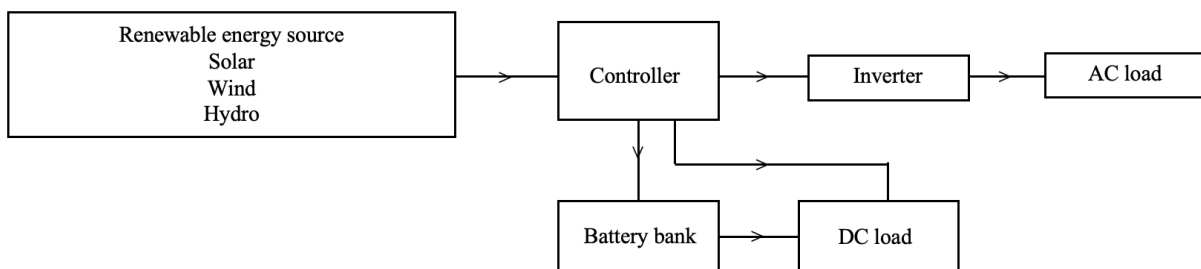


Figure 3.1: Flow scheme of a general setup of an off-grid system with necessary components. [16]

3.2 Renewable energy sources

Renewable energy sources are energy sources that are naturally replenished and produce sustainable energy with little or no carbon emissions. The main types are solar energy, wind energy, geothermal energy, hydropower, and biomass, with hydropower accounting for the highest share of renewable energy in electricity generation. [36, 37]

However, some of these energy sources are weather-dependent, where production is sensitive to weather fluctuations. Therefore, energy storage is needed to provide user flexibility in off-grid systems or ensure stability in systems connected to the electric grid. [38]

3.2.1 Wind power

Wind power can be harnessed by converting the kinetic energy of the wind into electrical energy using a wind turbine. Wind turbines are classified according to the axis of rotation, with the most common type being the horizontal axis wind turbine, referred to as HAWT. A less common type is the vertical axis wind turbine. The HAWT can be divided into five subsystems, given in the following list. [39]

1. Rotor
2. Nacelle
3. Tower and foundation
4. Machine control
5. Electrical system

The most important part of a wind turbine is the rotor, which consists of the blades and the hub. Most turbines have three blades, varying in length from 1 m on a small scale to 107 m for offshore turbines. As air flows over the blades, the pressure difference creates a lift force that causes the rotor to rotate. Blade length determines maximum power generation, as the available wind power is given by Equation 3.1, where P is the power given in W , ρ is the air density given in kg/m^3 , v is air velocity given in m/s , and A is the sweep area of the rotor given in m^2 . [40]

$$P = \frac{1}{2} \cdot \rho \cdot A \cdot v^3 \quad (3.1)$$

The mechanical energy of the turbine blades is converted into electrical energy in the nacelle, which is also called the turbine housing. The nacelle consists of a shaft, and a generator mounted on top of the turbine tower. Regarding the turbine tower, the height is critical to achieving sufficient wind velocity. The average height of the tower is 1 to 1.5 times the rotor diameter. The most common type is a free-standing tower mounted on a foundation of steel and concrete. For an illustration of a HAWT and the major components, see Figure 3.2. [41, p.3-7]

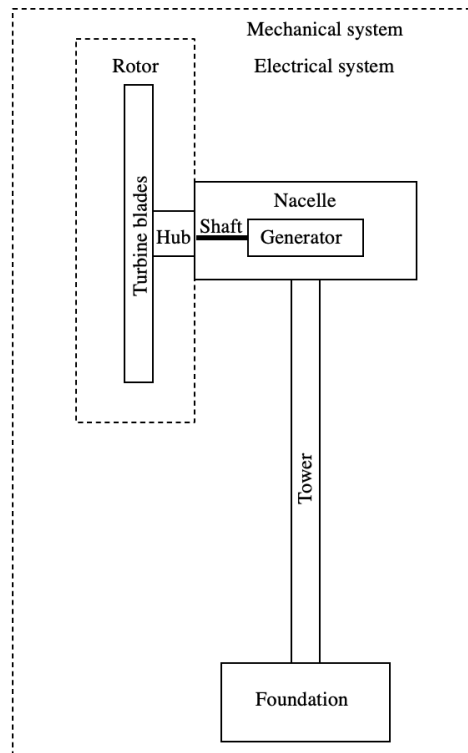


Figure 3.2: Main components of a horizontal axis wind turbine. [41, p.4]

To ensure that the wind turbine does not rotate uncontrollably at high velocities and regulates the speed of the rotor blades, a machine control system is needed. The electrical system includes all electrical components such as cables, converters, and transformers. Also, it includes the control system. The control system is often located in the nacelle and regulates the voltage out of the generator, which is transmitted to the grid or battery bank. The velocity where the blades start to rotate is referred to as the cut-in speed. The cut-out speed is the velocity where the control unit prevents the blades from rotating. In some turbines, the control system is separate from the wind turbine. [41, p.3-7]

3.2.2 Solar power

Solar power has great potential as the sun is a readily available renewable energy source. Sunlight can be harnessed by converting it into electricity using PV panels. This is done through a semiconducting material, with crystalline silicon being the most commonly used. [42, 43]

In Norway, an average PV panel can produce about 100 to 170 kwh/m^2 . How much electricity can be generated depends on the location, tilt angle, system solution, and efficiency of the solar cells. A limitation of PV panels is the unreliable power supply due to periods without sun, during the night or due to clouds. Therefore, the energy must be used immediately, stored or sold to the electricity grid to provide a flexible energy supply. [44–46]

The average solar irradiation in Norway on a horizontal surface ranges from 700 kWh/m^2 to 1 000 kWh/m^2 per year. The average solar irradiation in Norway for a winter and summer day is illustrated in Figure 3.3. In comparison, the average annual horizontal solar irradiation in Tanzania ranges from 1 753 to 2 337 kWh/m^2 , which is high. However, PV panels have higher efficiency in colder climates, which can be an advantage for installation in Norway. [9, 44]

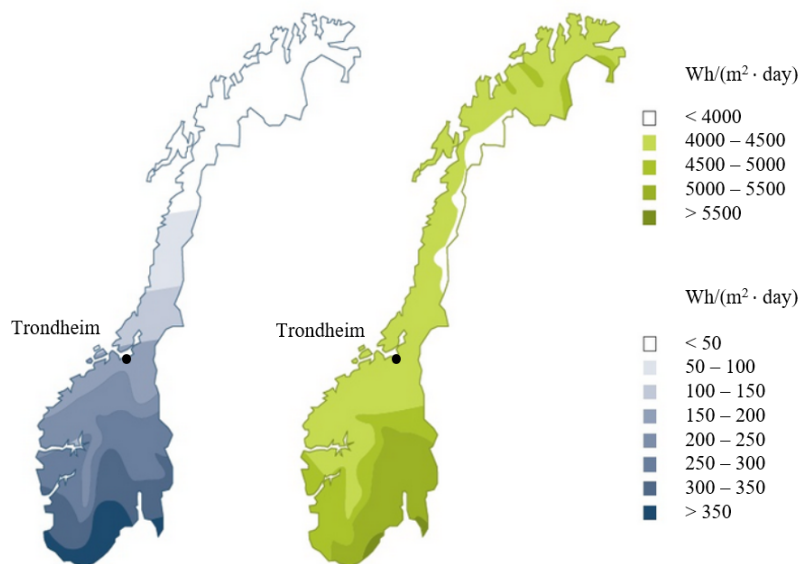


Figure 3.3: The average horizontal solar irradiation distribution in Norway for a winter day to the left and for a summer day to the right. [47]

Tanzania is located near the equator, giving it a great potential to exploit the high solar irradiation. The average horizontal solar irradiation distribution for a day in Tanzania is given in Figure 3.4, including the yearly average solar irradiation for a region. The highest solar irradiation is in the central region, with the least connections to the national grid and other mini-grids, creating great potential for a small-scale PV Solar Cooker with Heat Storage. [9]

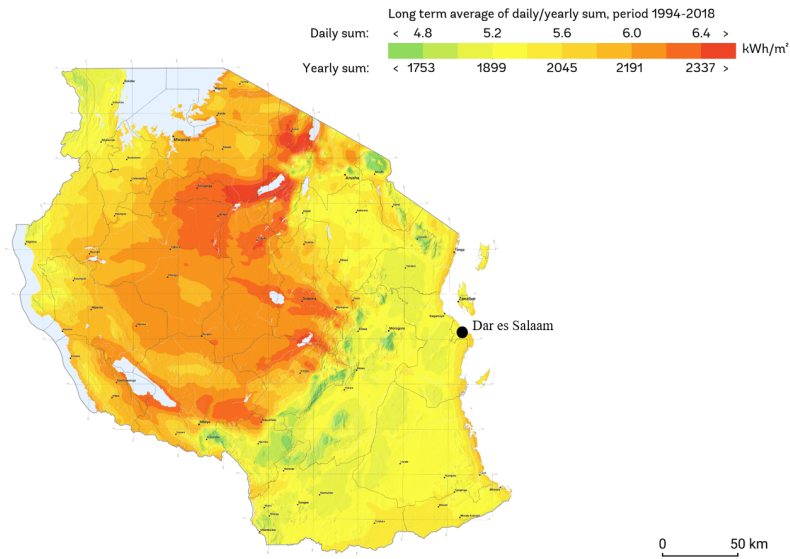


Figure 3.4: The average horizontal solar irradiation distribution for a day in Tanzania, in addition to the yearly average. [9]

Calculation of the maximum power output, P , of a selected solar cell, can be derived from Equation 3.2. The average light intensity of solar irradiation is represented as Φ_{in} , measured in W/m^2 , A is the effective surface area of the solar cells, measured in m^2 , and η is the efficiency. [48]

$$P = \eta \cdot \Phi_{in} \cdot A \quad (3.2)$$

3.3 Solar charge controllers

Solar charge controllers regulate voltage and current and are often used in off-grid or hybrid off-grid systems to regulate power from renewable energy sources. A controller ensures optimal power output for operating electrical loads and charging batteries. These regulators can keep batteries at their highest state of charge, SOC, without overcharging them. This is achieved by reducing the power flow to the batteries when a certain voltage is reached. If the voltage decreases due to less power produced from the power source or power consumption increases, the controller allows maximum charge. These adjustments are called voltage regulation, which prevents damage to the batteries and increases their life expectancy. [49, 50]

The voltage and current in an off-grid system can change quickly. How quickly and well a controller responds to these changes determines the life expectancy of the batteries. Therefore, a good investment in a controller can reduce the cost of an off-grid system as controllers typically account for 10 % of the investment in an off-grid system, while batteries account for approximately 40 %. [49]

A solar charge controller is selected based on the system in which it will be used, as controllers are designed according to the maximum input voltage and charge current. These parameters determine how many PV panels can be connected to the controller. [51]

There are two main types of solar charge controllers: pulse width modulation, PWM, and maximum power point tracking, MPPT. PWM controllers are connected directly from the PV panels to the batteries and use a transistor to modulate or control the battery charge. The transistor allows the current to flow until the battery reaches the absorption charge voltage. When this voltage is reached, the transistor begins to open and close at a high frequency to regulate the current flowing through and maintain a constant battery voltage. A disadvantage of the PWM controller is that the source voltage is reduced to match the battery voltage, which reduces the output power and operating efficiency of the PV panel. [51, 52]

The MPPT controllers can operate at voltages higher than the battery voltage, unlike the PWM controller. Furthermore, this offers greater design flexibility and is the preferred option for larger systems. However, these controllers are more expensive than PWM controllers due to the more complex control. The MPPT controller can control both input voltage and current and is capable of finding the optimal operating point of the power source, as illustrated in Figure 3.5. Since this controller is constantly iterating for the most optimal combination of voltage and current, it can operate more efficiently than the PWM controller. [53, 54]

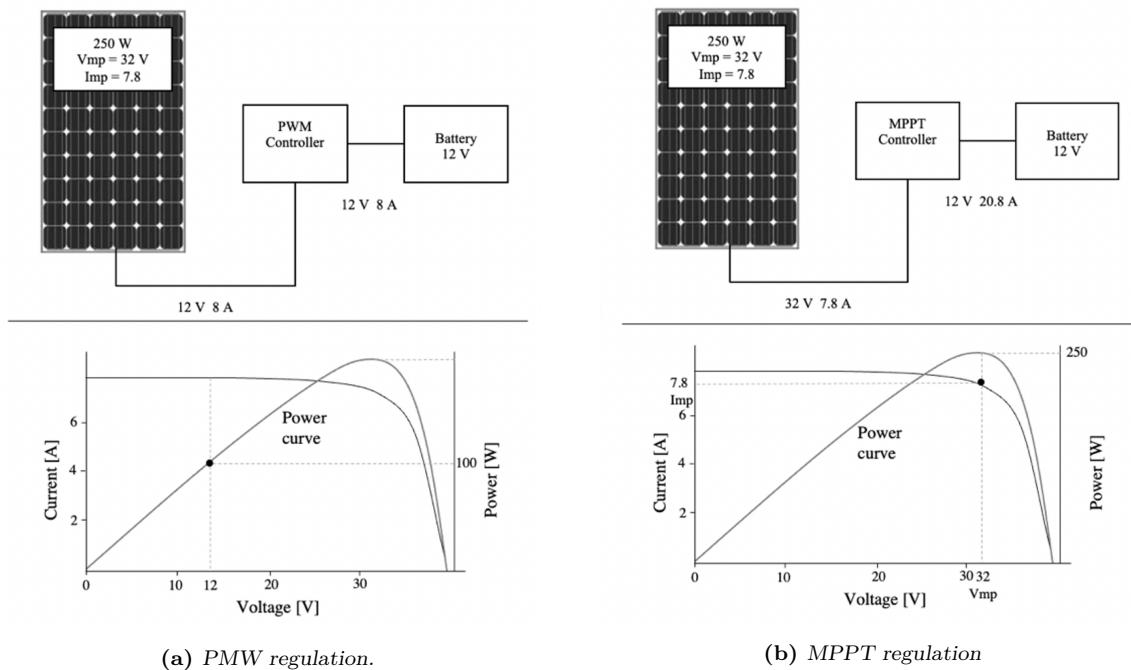


Figure 3.5: The regulation principle of PWM and MPPT controllers. [51]

An MPPT controller can regulate the voltage in different ways. It can regulate the input voltage either up, down, or both. The voltage regulation is dependent on the converter included in the controller. A converter that regulates the voltage up is called a boost converter, while a converter that regulates the input voltage down is called a buck converter. A converter that can both increase and decrease the output voltage compared to the input voltage is called a buck-boost converter. All three converters consist of an inductor, a diode, a capacitor, and a circuit breaker but are arranged differently. Regarding the experiments in this master thesis, three different controllers have been tested: a Tristar PWM controller, a Geysewise MPPT controller, and a homemade MPPT controller. Both the Geysewise controller and the homemade controller are buck controllers. [55]

3.4 Excess power to an external load

Excess energy cannot be fed back to the grid in off-grid systems and is often stored in battery storage. Energy is dumped when storage is full, often by converting energy to heat through a heating element. In off-grid systems with wind generators, an external load is required to reduce the number of times the turbine starts and, stops and in some cases to prevent the turbines from spinning uncontrollably at high wind velocities. When designing the external load, it is critical that it is capable of handling the entire power output of the connected source. This prevents damage when production is high and the batteries are fully charged.

Most controllers have an operational mode that allows power to be diverted to an external load. This is to avoid overcharging the batteries, which can cause damage and lower operating expectancy. When the controllers operate in this mode, the excess energy is dissipated to the connected load when the batteries reach a specific voltage. By placing the heating elements that serve as the external load in an insulated tank, the excess energy can be stored for an extended period. [56]

3.5 Dimensioning an external load for a controller

When operating a PWM controller in diversion mode, it is essential to correctly size the external load for the controller. The external load can, for instance, be a heating element. A load that is too small will not be able to divert power from the source and could result in overcharging of the batteries. On the other hand, an external load that is too large will draw more current than the rating of the controller. This activates the overload protection in the controller and disconnects the external load. As a result, all of the current from the source will flow to the batteries, resulting in overcharging or damage.

The external load should never exceed the current rating of the controller, making the choice of controller a limiting factor. Since the power source does not limit the load, it will draw its rated current from the batteries.

Some controllers require over-sizing. Consequently, the current from the power source must be lower than the current rating of the controller, depending on the safety margin specified in the manual. The power source must be sized appropriately not to exceed the voltage and current limits of the controller. It is also essential that the heating elements are large enough to dissipate the power produced by the source. This value is referred to as the minimum external load and is equal to the maximum battery voltage times the maximum current of the source, as shown in Equation 3.3. However, the external load should be sized for 150 % of the source current up to the current rating of the controller.

$$\textit{Minimum diversion load} = \textit{max battery voltage} \cdot \textit{max source current} \quad (3.3)$$

To prevent damage, the electrical ratings of the elements must be matched to the system. The required resistance can be calculated using Equation 3.4, where R is the resistance given in Ω , U is the system voltage given in V, and P is the system peak power given in W.

$$R = \frac{U^2}{P} \quad (3.4)$$

As long as the total resistance meets the requirements, the elements can be connected in series or parallel. The total resistance in series and parallel connections is given by Equation 3.5 and Equation 3.6, respectively.

$$R_{tot} = \sum_{i=1}^N R_i \quad (3.5)$$

$$R_{tot} = \left(\sum_{i=1}^N \frac{1}{R_i} \right)^{-1} \quad (3.6)$$

According to Ohm's law, the current is equal to the current drawn by each element in a series circuit. The solution of Ohm's law in terms of current is given by Equation 3.7, where I is the circuit current, U is the system voltage given in U, and R is the resistance of the heating elements given in Ω .

$$I = \frac{U}{R} \quad (3.7)$$

By using Equation 3.7 the current drawn by the heating elements can be calculated. This value is used to control that the current drawn from the elements are within the current rating of the controller.

3.6 Electrochemical energy storage

Solar and wind energy are intermittent energy sources and thus are not continuously available for electricity conversion. This is due to limiting factors that cannot be controlled, such as weather. The energy production cannot be turned on and off in response to the energy demand in the system. Energy storage devices such as lead-acid or lithium-ion batteries can solve this problem by storing the energy for later use. Energy storage in batteries is referred to as electrochemical energy storage. [57]

Lithium-ion batteries have a higher energy density than lead-acid batteries. In addition, they can be cycled more profound, giving them a longer life expectancy and lower maintenance. However, they currently have a much higher investment cost compared to lead-acid. [58]

Although lead-acid are considered to have a lower investment cost than lithium-ion batteries, the battery cost will still constitute a large amount of the total investment for an off-grid solar system. The batteries in a larger off-grid solar system can consist of approximately 45 % of the total investment cost. Although, this is heavily dependent on how much battery capacity is needed in the system. [58, 59]

Lead-acid batteries are a mature technology, inexpensive per wattage, and a secondary battery, meaning they are rechargeable. Compared to lithium and nickel batteries, lead-acid is less durable when deep cycled. A deep cycle is when a battery provides sustained power until discharged to more than 50 % or even up to 80 %. With each charge and discharge cycle, the battery capacity decreases. How much the capacity decreases depends on the depth of discharge, DOD, discharge duration, and how long the battery is left to discharge without being cycled. Additionally, operating temperature affects the battery capacity, as it decreases by 1 % when the operating temperature of the battery is below 20 °C. [60, 61]

A standard flooded lead-acid battery with rated values at 12V and 115 Ah, would usually have a measured terminal voltage from 12.7 V to 13.8 V when fully charged. If a new battery is fully charged, the State of charge, SOC, will be 100 %. The SOC of a battery is defined as the remaining charge left in a battery relative to its nominal capacity. This indicates how much charge remains in the battery and how efficient the battery is currently. A used battery will give a lower percentage SOC in a fully charged state than a new battery. Therefore, a lower measured voltage in a fully charged state will indicate that capacity is reduced and the battery is closer to reaching its life expectancy. The life expectancy of a battery will be reduced when the battery is overcharging, undercharging, or leaving the battery to self-discharge over a longer period of time. A 12-month time period is considered a long time for a battery left to discharge. [62–64]

When extended battery life is required, lead-acid batteries are prevented from going below 20 % of SOC, as lead-acid batteries normally are not operated at low SOC. For a 12 V 115 Ah lead-acid battery, the DOD will reduce the life expectancy by the number of cycles the battery can be recharged. An approximation of this is illustrated in Figure 3.6. If this type of battery is cycled down to 80 % DOD, which corresponds to 650 cycles, it would have a life expectancy of approximately 1.80 years if cycled 360 times per year. [15, 65]

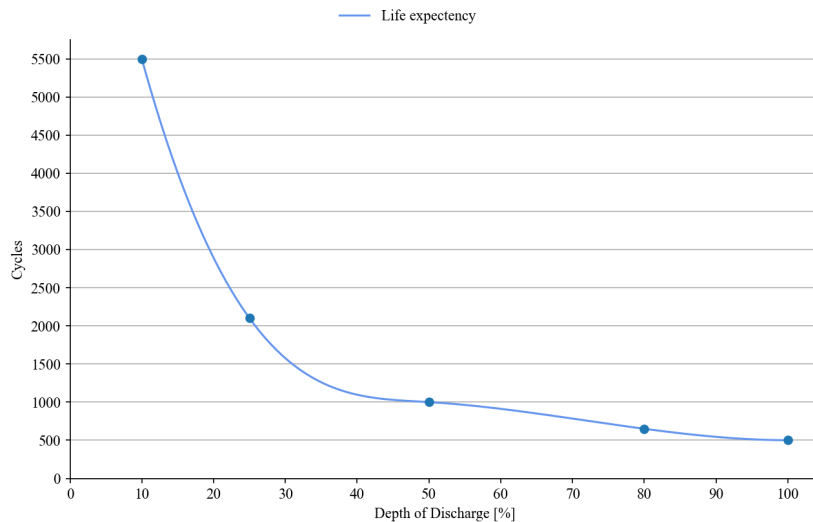


Figure 3.6: An approximation of the effect of DOD on life expectancy of a 12 V 115 Ah lead-acid battery.[65]

To prolong the battery life, restore lost capacity, and make the battery more efficient, an equalizing of the batteries should be performed. This is to remove lead sulfate remaining on the lead plates, which occurs when a lead-acid battery is discharged and recharged. Equalizing is vital to the performance of a battery, especially when used in a solar system. If a battery is kept discharged over time, it becomes more difficult to convert the lead sulfate into active materials again. [66]

For a solar system, it is necessary to choose a battery that can withstand deep charging and discharge without being damaged. This may lead to a SOC lower than 20 %. However, if only a few charging cycles are expected during the battery lifetime, a SOC below 20 % can be accepted.[15]

3.7 Thermal energy storage

The amount of thermal energy possible to store with sensible heat storage, Q_s given in J , is defined by specific heat, C_P given in $J/(kg \cdot K)$, of the medium, the mass of the storage material, m in Kg , and the variation in temperature. This is given in Equation 3.8, where, T_f , is final temperature and T_i , initial temperature given in K . [67]

$$Q_s = m \cdot (C_{p,f} \cdot T_f - C_{p,i} \cdot T_i) \quad (3.8)$$

By using Equation 3.9 the mass of the fluid can be calculated by multiplying density, ρ given in kg/m^3 , and volume, V , given in m^3 .

$$m = \rho \cdot V \quad (3.9)$$

The second law of thermodynamics states that it is impossible to transfer heat to a warmer object from a cooler. Respectively, an object warmer than the surroundings will continuously lose thermal energy. To maintain most of the thermal energy, heat loss must be minimized. Therefore, insulation should be implemented to reduce conduction losses and the air leakage caused by convection. This insulation aims at reducing the overall heat transfer coefficient, U , by adding a material with low thermal conductivity. The insulation can both prevent unwanted heat loss and heat gain. [68, 69]

The overall heat transfer coefficient, U , also referred to as the u-value, is given in Equation 3.10 and is measured in $W/(m^2 \cdot K)$. A low u-value is preferred as less heat is leaked from the system or material. The heat transfer rate defines this coefficient, q , given in W , temperature difference, ΔT in K and surface area A_s of the geometry evaluated measured in m^2 .

$$U = \frac{q}{\Delta T \cdot A_s} \quad (3.10)$$

3.8 Volume in tank

Parts of this section are copied from the preliminary project work *Small Scale PV Solar Cooker*. [14] When utilizing a heating element within a tank for heating, the volume inside needs to cover the heating element at all times to prevent burnout. The volume inside a cylindrical tank can be estimated based on the height, h , of the oil inside the tank and length, L . To control the volume inside the tank, the oil height is found by reading the level of a level pipe installed on tanks 2 and 3 in the three-tank system. Tank 1, however, has to be estimated by using a dipstick. Since the tank has cylindrical edges, an approximation of the length is estimated to be the cylindrical length and two times the length of half of the curved ends, as is illustrated in Figure 3.7.

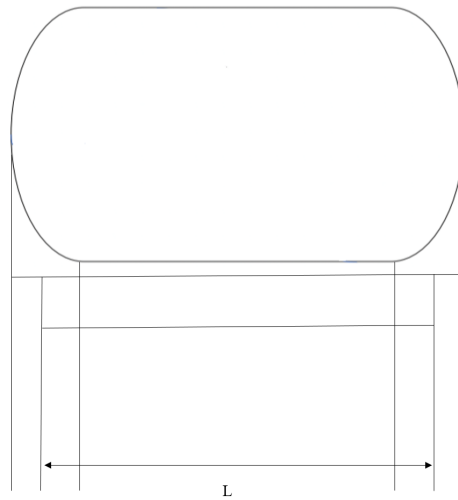
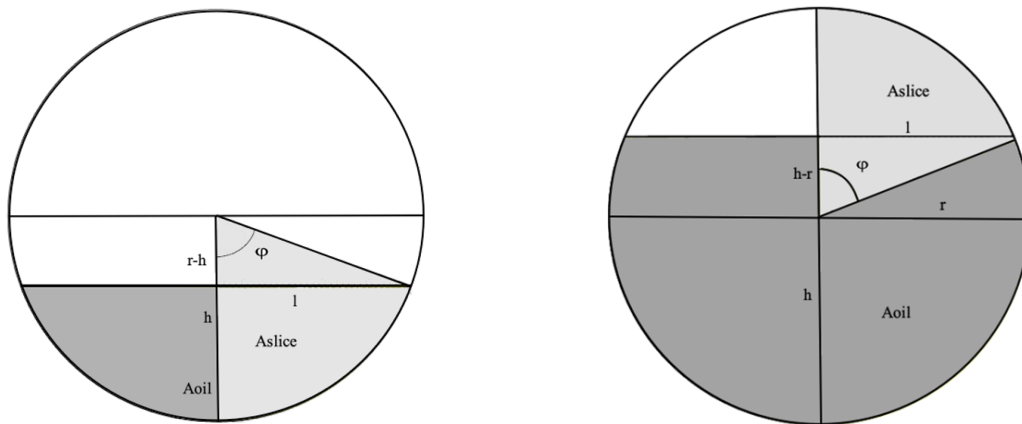


Figure 3.7: An approximation of the length, L , of the cylindrical tank, which is estimated to be the cylindrical length and two times the length of half of the curved ends.

The cross-sectional area needs to be calculated to calculate the volume inside the tank. This method for finding the cross-sectional area can be divided into two scenarios, where parameters for more than half full tank are given in Figure 3.8a and for less than half full tank given in Figure 3.8b. [12]



(a) For the scenario with less than half full tank.

(b) For the scenario with more than half full tank.

Figure 3.8: The parameters illustrated in order for the cross-sectional area to be calculated, furthermore used to find the volume of the oil inside the tank. [12]

For calculations regarding the half-full tank scenario, $h < r$, equations denoted by a are utilized, while equations considering less than half full tank, $h > r$, are denoted by b . Both sets of equations can be applied to the scenario where the tank is exactly half-full. The equation for finding the oil width, l , inside the tank are given in Equation 3.11a and 3.11b.

$$l = \sqrt{r^2 - (r - h)^2} \tag{3.11a}$$

$$l = \sqrt{r^2 - (h - r)^2} \quad (3.11b)$$

The angle, ϕ , between oil level and the line for an exact half full tank is given by Equation 3.12a and 3.12b. This equation is used to calculate the area of the slice, A_{slice} given in Equation 3.13, which is further used in 3.14a and 3.14b. From this the respective cross sectional area, A_{oil} , for either of the two scenarios can be calculated by Equation 3.15a and 3.15b.

$$\phi = \frac{\arccos(r - h)}{r} \quad (3.12a)$$

$$\phi = \frac{\arccos(r - h)}{r} \quad (3.12b)$$

$$A_{slice} = \pi \cdot r^2 \cdot \frac{\phi}{2\pi} \quad (3.13)$$

$$A = A_{Slice} - \frac{l \cdot (r - h)}{2} \quad (3.14a)$$

$$A = A_{Slice} - \frac{l \cdot (h - r)}{2} \quad (3.14b)$$

$$A_{oil} = 2A \quad (3.15a)$$

$$A_{oil} = 2\pi \cdot r^2 - 2 \cdot A \quad (3.15b)$$

After calculating the cross-sectional area and length, the total volume of the oil can be found by Equation 3.16. Further, this can be utilized to determine if the oil level is above the heating element.

$$V = A_{oil} \cdot L \quad (3.16)$$

In order to calculate the surface area of the oil within the tank, the perimeter of the oil needs to be found. Perimeter for the half-full tank scenario is given in Equation 3.17a and less than half-full tank scenario in Equation 3.17b

$$P_{oil} = 2\pi \cdot \frac{\alpha}{2\pi} \quad (3.17a)$$

$$P_{oil} = 2\pi - 2\pi \cdot \frac{\alpha}{2\pi} \quad (3.17b)$$

If evaluating a different geometrical shapes where the radius and length are known, as seen in Figure 3.9. The area of the oil can be calculated as given in Equation 3.18 and the volume can be found by Equation 3.16. Then the perimeter can be derived by Equation 3.19. Furthermore, the surface area of both geometrical shapes, as seen in Figure 3.7 and Figure 3.9, can be calculated with Equation 3.20.

$$A_{oil} = 2\pi \cdot r^2 \quad (3.18)$$

$$P_{oil} = 2\pi \cdot r \quad (3.19)$$

$$A_s = P_{oil} \cdot L + 2 \cdot A_{oil} \quad (3.20)$$

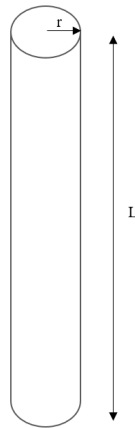


Figure 3.9: The cylindrical tank with length, L , and radius, r .

4 Experimental work

To utilize the remaining energy after the batteries are fully charged, the oil in tank 2 of the three-tank system could be used as heat storage. High temperatures could be maintained over time by diverting excess power to a sufficiently insulated tank and eventually reaching the operating temperature of the system at 230 °C. Utilization of excess energy could be achieved by connecting a controller to the batteries and the three-tank system.

Several experiments have been performed to determine which solar array configuration and controller combination provides the highest efficiency for the three-tank system. System performance is highly dependent on the solar conditions, as the heating element, HE, controller and solar array configuration have to be dimensioned after this. Not all experiments conducted are included; only the ones with the most optimal weather conditions.

Three different system solutions are demonstrated in a variation of six cases. The three system solutions consist of a battery system where excess power from a charge controller is directed to a heat battery, a direct system using PV power for direct heating of a storage, and a hybrid system that can accept power from PV and a wind generator. A battery system is demonstrated in case 1, direct heating is demonstrated in cases 4,5 and 6, and a hybrid solution in cases 3. Case 2 is a preliminary test of the wind turbine prior to case 3. An overview of the cases and the corresponding configurations is given in Table 4.1

Table 4.1: The configuration for each case, including specifications regarding controller, heating elements, power source and energy storage is given.

| Case | Controller | Load | Power source | Energy storage |
|------|------------|---------------------------|---|----------------------------|
| 1.1 | Tristar | 2x500 W 24 V HE in series | 3 PV panels in parallel | 2x12 V batteries in series |
| 1.2 | Tristar | 2x500 W 24 V HE in series | 3 PV panels in parallel | 2x12 V batteries in series |
| 1.3 | Tristar | 2x500 W 24 V HE in series | 3 PV panels in parallel | 2x12 V batteries in series |
| 2 | – | – W 24 V HE in series | 400 W wind turbine | 2x12 V batteries in series |
| 3 | Tristar | 2x500 W 24 V HE in series | 3 PV panels in parallel and 400 W wind turbine | 2x12 V batteries in series |
| 4 | Geysewise | 2x500 W 24 V HE in series | 3 PV panels in parallel | – |
| 5 | Homemade | 2x500 W 24 V HE in series | 6 PV panels in series | – |
| 6 | Geysewise | 1100 W PTC HE | Variable AC voltage source | – |

All experiments have been performed on days with good solar conditions and minimal clouds. However, as the work period extends over several months, the solar conditions have improved during the spring. The solar conditions of the experiments are hence, not equal for the different experiments. Since location is a decisive factor for the solar irradiation, a graph of the average solar irradiation per day over a whole year at the specific location is included. The average solar irradiation for Trondheim at the roof of the Thermal Laboratory is illustrated in Figure 4.1.

Measurements of the solar irradiation is retrieved through PVsyst, which is a program gathering meteorological data from several sources available on the web. In this thesis meteorological data from Metronorm 7.3 is utilized, where data is collected from 2 500 terrestrial stations and complemented by satellite. Available data is based on an average measurements taken between 1900 and 2015, as this was the data available in the program for the relevant location.

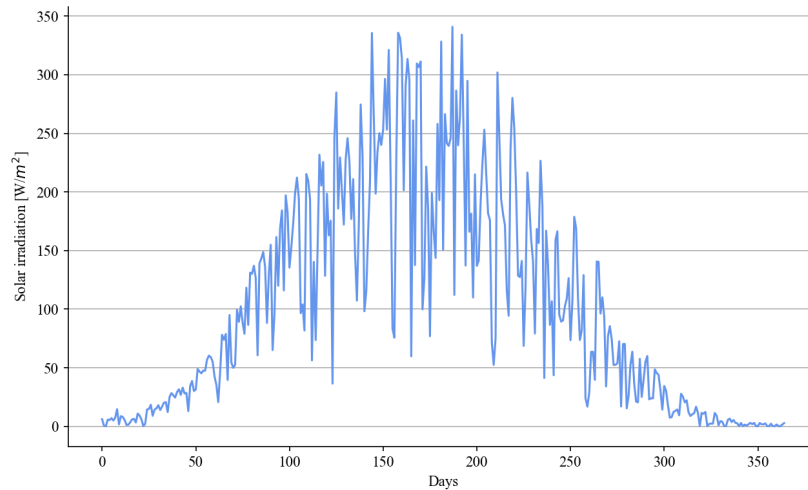


Figure 4.1: The average horizontal solar irradiation for 24 hours per day throughout a year at the roof of the Thermal Laboratory in Trondheim. The highest values occurs between day 150 and day 200. [70]

Since the main objective of the experiments was to demonstrate excess power from PV panels to high-temperature heat storage, the solar array serving as the power supply had to be correctly dimensioned. PV panels must produce a sufficient amount of power to charge the batteries and divert excess power to the load. Additionally, the power must not exceed the current rating of the controller or the nominal battery voltage. The PV panels used in the experimental work are six Solartek PVP26030 panels rated at 260 W; specifications are given in the Solartek manual linked in the Appendix A. The PV panels are mounted on the roof of the Thermal Laboratory at NTNU, as shown in Figure 4.2



Figure 4.2: Placement of PV panels on the roof of the Thermal Laboratory on the fourth floor.

Duratherm 630 was considered the best heat transferring fluid for the given system based on previous project work. Duratherm 630 is a thermal oil engineered for applications that require temperature stability up to 332 °C. With this oil, precise temperature control can be achieved, and it is an excellent alternative to high-temperature synthetic fluids at a fraction of the cost. Additionally, it has high performance, is environmentally friendly, and offers good protection against oxidation. The oil's smoke point is at 333 °C, and the flash point is 221 °C. The safety and technical data for Duratherm 630 are given in the Safety and Technical data sheets linked in the Appendix A.

The oil level of tank 2 must cover the heating elements to prevent burnout. To ensure that the heating elements were covered, a measured oil level of 13 cm from the bottom of the tank was required. Using the equations presented in section 3.8, this corresponds to an oil volume of 24.24 L. This oil volume was utilized in all cases performed on the three-tank system, except from case 6.

During the experimental work, information was provided about the outlet pipe. It was said that a pipe had been installed in the outlet, elevating the actual outlet to a higher level than the heating elements. This outlet pipe would prevent complete draining of the tank and would serve as a safety mechanism. Based on this information, a flushing of the heat storage tank was performed to conduct an experiment with a minimum oil level. This oil level was calculated to be 2.92 L.

The initial temperature of the oil is ambient temperature of approximately 21 °C for all experiments without preheating. Initial conditions for battery voltage, oil volume and oil temperature are given in Table 4.2. Starting at the respective initial temperature for each case and by utilizing the theory presented in section 3.7, the time required to reach the operating temperature of 230 °C for the initial oil volume can be calculated. The time needed to reach operating temperature at rated power for the different cases is also given in Table 4.2.

Table 4.2: Initial conditions regarding battery voltage, oil volume, oil temperature and theoretical time to reach 230 °C for all experiments. Theoretical time calculated is based on operating with the rated power of the heating elements.

| Case | Battery voltage | Oil volume | Oil temperature | Time to reach 230 °C |
|------|-----------------|------------|-----------------|----------------------|
| [-] | [V] | [L] | [°C] | at rated power |
| 1.1 | 26.10 | 24.24 | 20 | 4 h 31 min |
| 1.2 | 31.56 | 24.24 | 21 | 4 h 24 min |
| 1.3 | 26.94 | 2.92 | 22 | 32 min |
| 2 | 24.80 | – | – | – |
| 3 | – | – | – | – |
| 4 | – | 24.24 | 49 | 3 h 54 min |
| 4.2 | – | 24.24 | 22 | 4 h 30 min |
| 5 | – | 24.24 | 33 | 4 h 18 min |
| 6 | – | 7.07 | 22 | 1 h 11 min |

4.1 Data collection

All temperature measurements were collected by using k-type thermocouples connected to a PicoLogger. These thermocouples have an uncertainty of ± 2.2 °C.[71] A total of six thermocouples were placed in the three-tank system to measure the temperatures in the oil. Tanks 1 and 3 had one measuring point each, while three thermocouples were placed in tank 2. Placement of the thermocouples in tank 2 is shown in Figure 4.3, where one is placed close to the heating elements, one is at the outlet of the tank, and one is in the middle of the tank inserted through the ventilation pipe. Temperatures for case 6 were logged similarly.

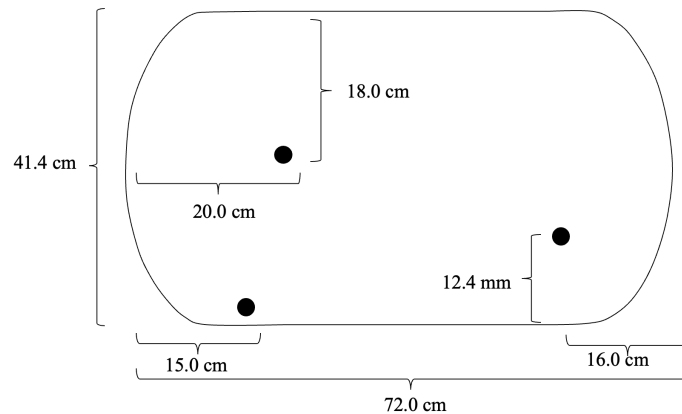


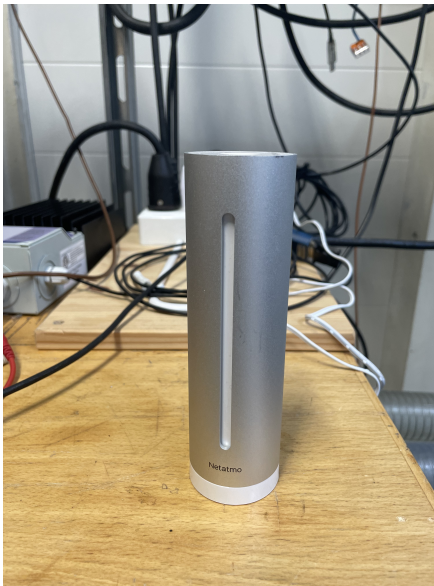
Figure 4.3: Placement of three thermocouples in tank 2 of the three-tank system. [12]

All data except the voltage and current from the solar array were stored using Labview programs developed by the electrical engineer Stein Kristian Skånøy at NTNU, with a log interval of 1 sec. Only the homemade controller, case 5, could measure the current from the solar array. Two multimeters were, hence, connected to manually measure the current in series and the voltage in parallel for the other controllers. As current and voltage were manually logged, the values are considered constant until the next measuring point. The logging intervals for each case are described in the respective methodology. In Figure 4.4 the setup of the multimeters is shown. The limiting current on the multimeters is 20 A; if this value is exceeded, the multimeters will be overheated and, at worst, melt.



Figure 4.4: Multimeters connected to the solar array, voltage is measured to the right and current to the left.

Two power meters were installed in the laboratory to log power, current, and voltage from the wind turbine. This was done to log AC and DC power from the wind turbine. Solar and wind data are collected from a weather station located on the roof of the fifth floor of the Thermal Laboratory. This causes uncertainty regarding the data, as the weather conditions at the weather station might differ from those at the experimental site. Due to this uncertainty, a local weather station was purchased and installed to measure local wind velocities. The local weather station from *Netatmo* consists of one main indoor unit, an outdoor unit and an additional wind measuring unit. The indoor and outdoor units are shown in Figure 4.5. This measuring device has a sampling time of six seconds, where data is sent to the main unit every fifth minute. Hence, each data point represents the average wind velocity for the past five minutes. [72]



(a) Indoor main unit



(b) Outdoor unit

Figure 4.5: Indoor and outdoor units of the local weather station.

The outdoor and indoor units are placed in a copy room on the fourth floor of the Thermal Laboratory. This is to make sure that these units have a strong signal to the wind measurement device placed on the pole of the wind turbine. As the Netatmo system transfers signals through WiFi signals, the units must be placed at locations with sufficient WiFi connections. The placement of the wind measuring unit is shown in Figure 4.6.



Figure 4.6: Location of the wind measuring unit, placed on the pole of the wind turbine.

4.2 Case 1: PV panels, batteries, and Tristar PWM controller

Based on findings from previous theses, the three-tank system needs to be demonstrated with PV panels, as this has never been successfully done. However, the system has been tested with artificial sunlight providing unsatisfactory results. The setup of the system of Case 1 is the same as the setup in the previous work, except for PV panels instead of artificial light.

4.2.1 Methodology

The system setup consisted of three PV panels, two 12 V batteries, two heating elements rated at 500 W 24 V, and a PWM controller. In section 3.4 the theory regarding the configuration of PV panels and heating elements is elaborated. Since the batteries, heating elements, and PWM controller were selected beforehand, the solar array had to be sized accordingly. The wiring diagram for this setup is illustrated in Figure 4.7.

Two 12 V 115 Ah lead-acid batteries connected in series were used as energy storage, resulting in a total nominal voltage of 24 V. Technical data for the batteries are given in the data sheet linked in Appendix A. As the controller is rated at 45 A, it was desirable to achieve as high as possible current within this limit. A safety limit of 1.5 was recommended by the manual reducing the maximum allowed current to 30 A. The operating manual for the controller is linked in the Appendix A. It was decided to conduct the experiment with three PV panels wired in parallel. The wiring scheme of the setup is illustrated in Figure 4.7.

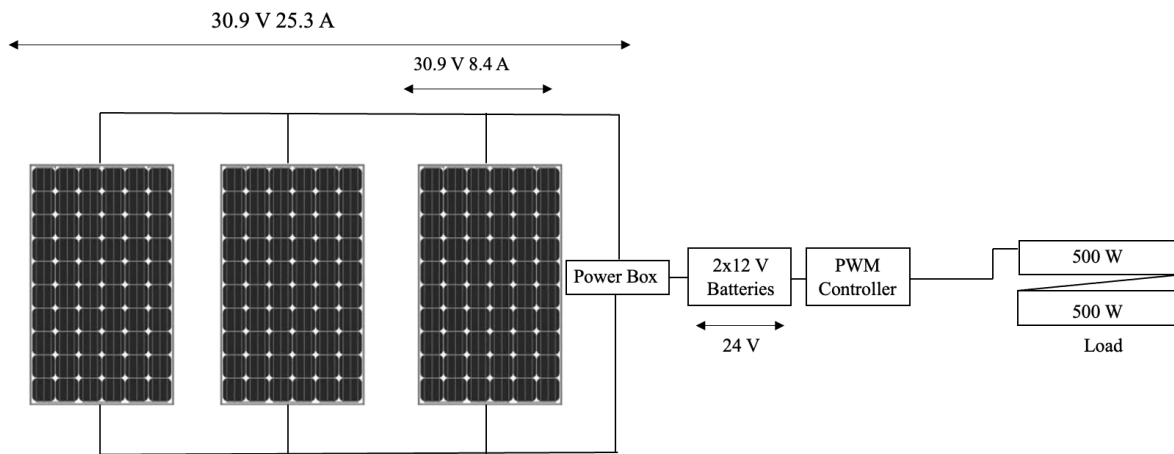


Figure 4.7: Wiring scheme of the setup with PV panels, two batteries, PWM controller and the heating elements inside the three-tank system.

The controller used in this experiment is a Tristar PWM controller with a current rating of 45 A, shown in Figure 4.9a. The controller is used in the operating mode diversion charge control and is connected according to the wiring scheme displayed in Figure 4.8. This operational mode will prioritize keeping the batteries fully charged and divert excess power to the load.

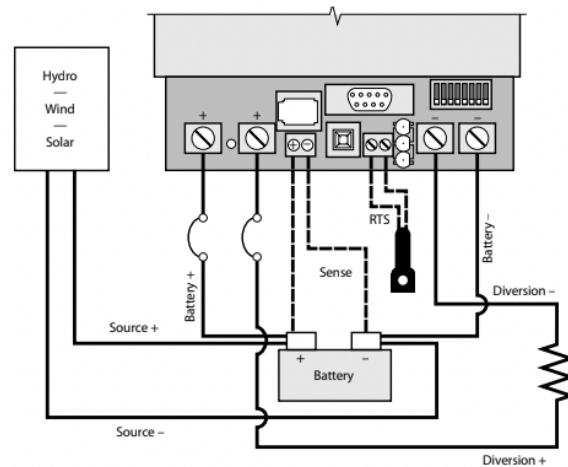


Figure 4.8: Wiring scheme for the controller in diversion mode, as displayed in the manual linked in Appendix A

The eight dual in-line packages, DIP, switches had to be adjusted to fit the system and intended purpose to set the controller in diversion mode. This was done according to the manual linked in Appendix A. First, switch 1 and 7 had to be turned on to use the controller in diversion mode. Switch 2 and 3 are used to set the battery voltage, where the combination of 2 on and 3 in off position corresponds to a battery voltage of 24 V.

Further, the following three switches are used to set the charging algorithm. The lowest battery charging voltage is selected by setting these switches in the off position. This value determines when the batteries are considered fully charged, and the controller will start diverting power to the excess load. The lowest available value of 27.6 V was chosen as the batteries were worn-out and had a low maximum SOC compared to a new battery.

Based on this, it was decided to fully charge the batteries in advance. If the experiment had been conducted without pre-charging the batteries, the charging period would most likely have exceeded the time of sunlight. Without pre-charging, the controller would not have diverted any power to the load and consequently not stored any heat in the storage tank. Finally, switch 8 was turned off as manual equalization was not desired. The PWM controller is shown in Figure 4.9a and the wiring and DIP switch settings in Figure 4.9b.



(a) Tristar PWM controller.



(b) Wiring of the controller, the DIP switches can be seen in the upper right corner.

In this experiment, the heating elements in tank 2 of the three-tank system serve as an external load receiving the excess energy from the solar array. The load must have the capacity to receive the total power from the solar array without exceeding the power and voltage rating of the heating elements. The installed heating elements are rated 500 W 24 V and are connected in series. This results in a power capacity of 1000 W, higher than the peak power production from the solar array of 780 W. An illustration of the experimental setup is given in Figure 4.10.

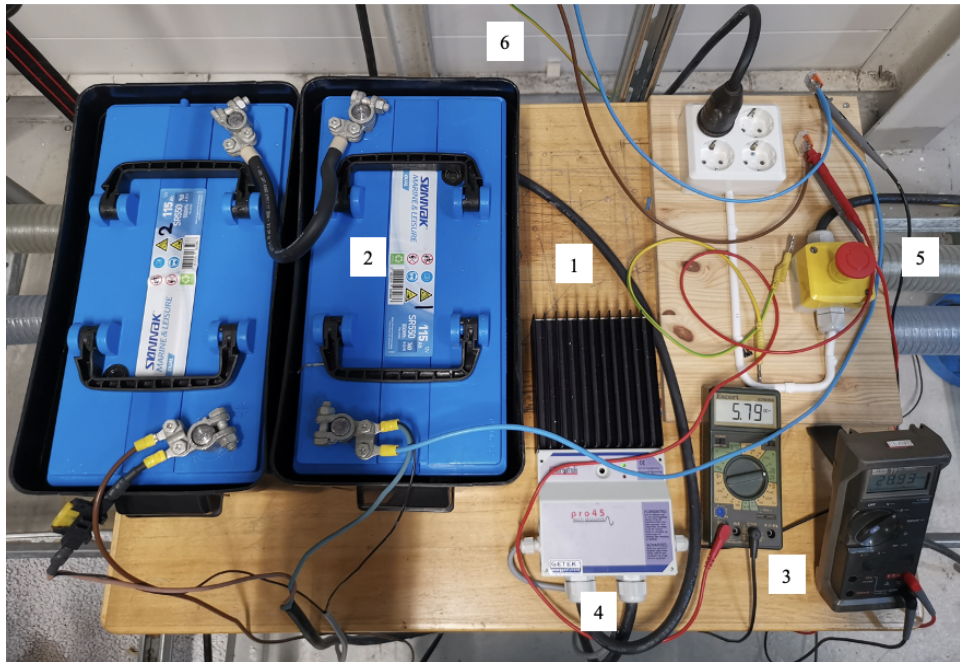


Figure 4.10: Indoor experimental setup for case 1

1. PWM controller.
2. Two 12 V batteries connected in series.
3. Multimeters measure current and voltage from the solar array.
4. Connection to the heating elements serving as load.
5. Emergency switch for power to the heating elements.
6. Connection to the solar array.

Temperatures were logged using a Picologger and the thermocouples placed in the three-tank system, as previously described. Voltage and current from the solar array were logged manually every tenth minute for cases 1.1 and 1.2, while case 1.3 was logged every fifth minute. Due to an unexpected interruption that shadowed the PV panels in case 1.1, the experiment had to be stopped before reaching the operating temperature. Consequently, this experiment was performed a second time with the same experimental setup and solar array configuration. Poor solar conditions resulted in low power during the experiments for case 1.1 and 1.2. It was, hence, decided to perform this experiment a third time. In this experiment AC power from the grid was used to demonstrate the opening of the bimetallic spring due to insufficient solar conditions. This was carried out by using a variable transformer, adjusted to supply voltage at 40 V.

4.2.2 Results 1.1

Figure 4.11 illustrates the relationship between solar irradiation and the current generated by the PV panels. As expected, the current fluctuates between 09.48 and 12.13 as a function of solar irradiation. Between 10.22 and 10.45, there is an interruption in the generated current. This is due to low solar irradiation, most likely caused by clouds.

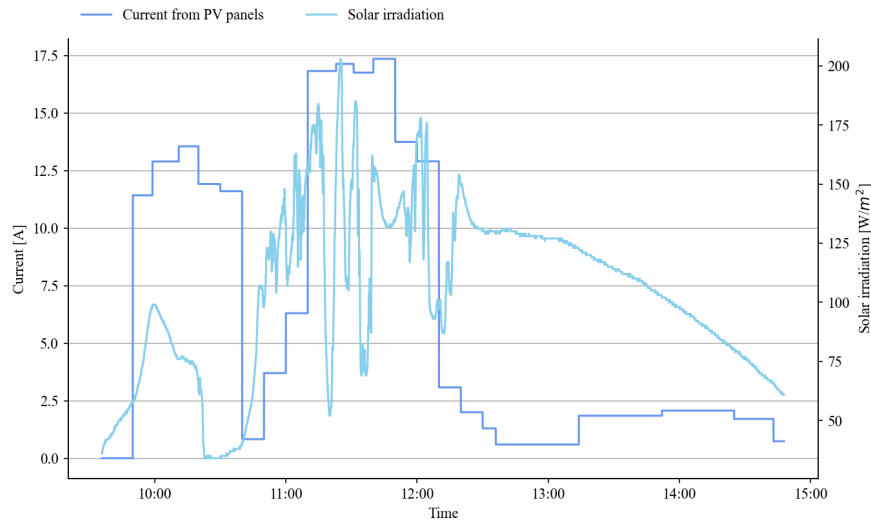


Figure 4.11: Solar irradiation during the experiment and the corresponding current from three PV panels.

The solar irradiation remains relatively high after 12.13, which is not consistent with the electricity generated by the PV panels as this is low after 12.13. However, this is due to unexpected roof construction work on the roof during the experiment, which cast a shadow on the PV panels. The solar irradiation measurements were not affected by construction work because the weather station is mounted in a different location on the roof.

The resulting voltage on the battery and load, which are the heating elements in tank 2 of the three-tank system, is shown in Figure 4.12. It can be seen that the voltage of the batteries starts at a high value because they were almost fully charged before the experiment started. From the figure, it can be seen that at 09.48, the controller starts to divert power to the heating elements after the batteries are fully charged. There is an unexpected interruption from 10.22 to 10.45 due to reduced solar irradiation because of clouds. The reduction after 12.13 was from construction work on the roof casting shadows on the PV panels, resulting in a significant decrease in voltage diverted to the load.

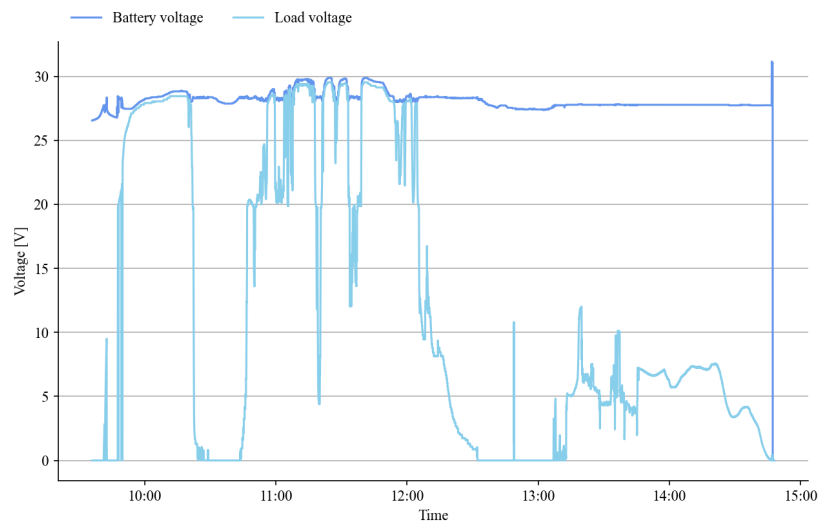


Figure 4.12: Voltage fed to the battery and to the load from the PV panels during the experiment.

The temperature development in tank 2 during the experiment is shown in Figure 4.13. The measurements are recorded with thermocouples placed at the top, middle, and outlet of tank 2. Furthermore, temperature at the top of the tank increases rapidly, but after 12.13, the temperature stagnates. It can be seen that the temperature at the top of the tank decreases first.

From Figure 4.12, it can be seen that the controller starts to divert the voltage to the heating elements at 09.48, resulting in a temperature increase accordingly. The interruptions starting at 12.13 are due to unanticipated construction work on the roof. Since the controller no longer diverts voltage from the PV panels, the temperature also stops rising. However, the temperatures remain stable at about 48 °C from 12.13 to the end of the experiment.

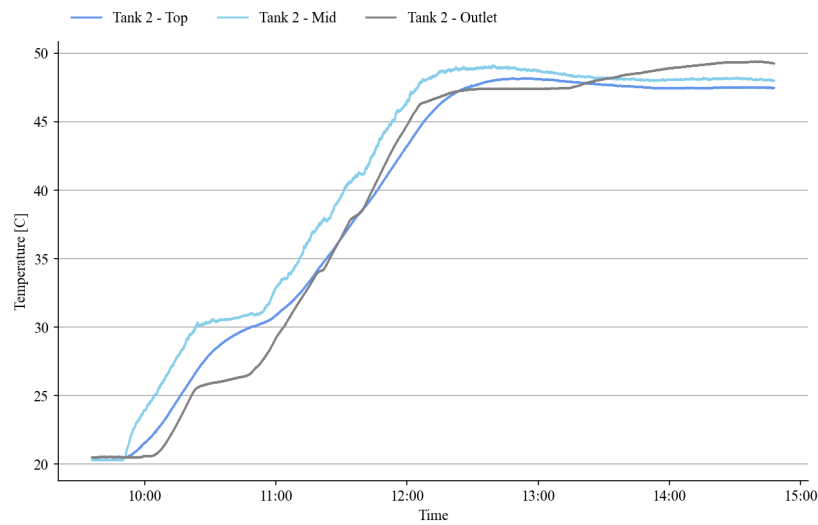


Figure 4.13: Temperature change inside tank 2, on top of the tank, middle and outlet.

In Figure 4.14 the measured current from the PV panels and the current diverted to the load are illustrated. As expected the current of the PV panels has an overall higher value than the current to the load. The current from the PV panels has a significantly higher value than the load current between 09.48 and 10.22 and 10.45 and 12.13.

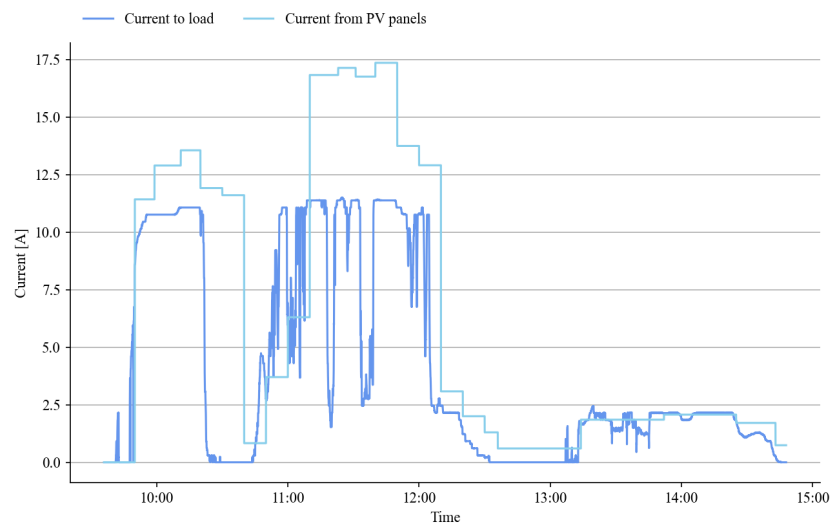


Figure 4.14: Produced current from the PV panels to the controller and current diverted to the load.

The IV-curve for case 1.1 is presented in Figure 4.15, where the experiment was performed with three PV panels connected in parallel. This graph is plotted from the IV-curve of the solar panels, given in Appendix B. The graph is based on solar irradiation of 200 W/m^2 , which is the closest value to the average solar irradiation of 104 W/m^2 from the test. It can be seen that the used heating elements at 2.54Ω are causing a low voltage, resulting in a low duty cycle.

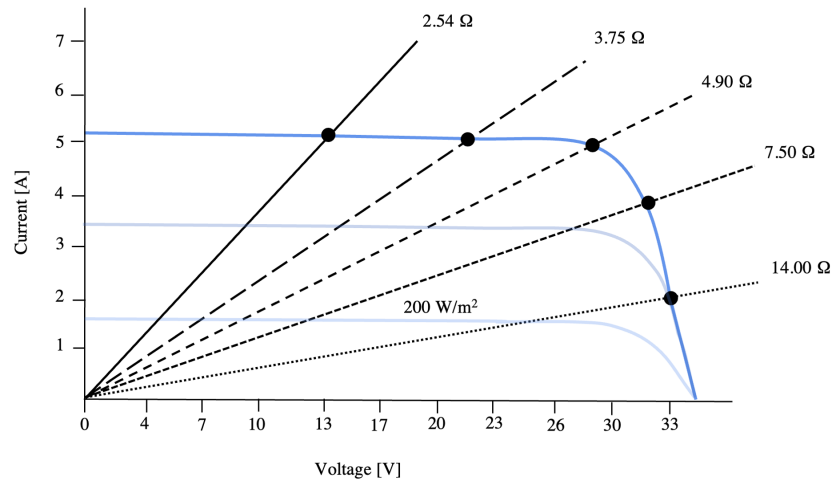


Figure 4.15: IV-curve for the PV configuration for case 1.1 with different heating elements, illustrating three PV panels in parallel at 200 W/m^2 .

4.2.3 Results 1.2

Since the previous test only reached $48 \text{ }^\circ\text{C}$, another test was conducted a month later when the roof construction work was completed, and the weather conditions had improved. Figure 4.16 illustrates the relationship between the solar irradiation and the current produced by the three PV panels. Solar irradiation was maintained at a high value of over 300 W/m^2 from the beginning of the experiment until around 15.15. Furthermore, the highest solar irradiation is measured from 12.00 to 13.00, and the lowest value is reached at 16.10.

The current produced by PV panels is stable at a high value of 16 A from the beginning until 14.15. After this, the value continuously declines until it reaches 0 A at 15.15. This pattern matches the high solar irradiation at the start of the experiment. By 14.15, the solar irradiation is still relatively high; however, the produced current decreases.

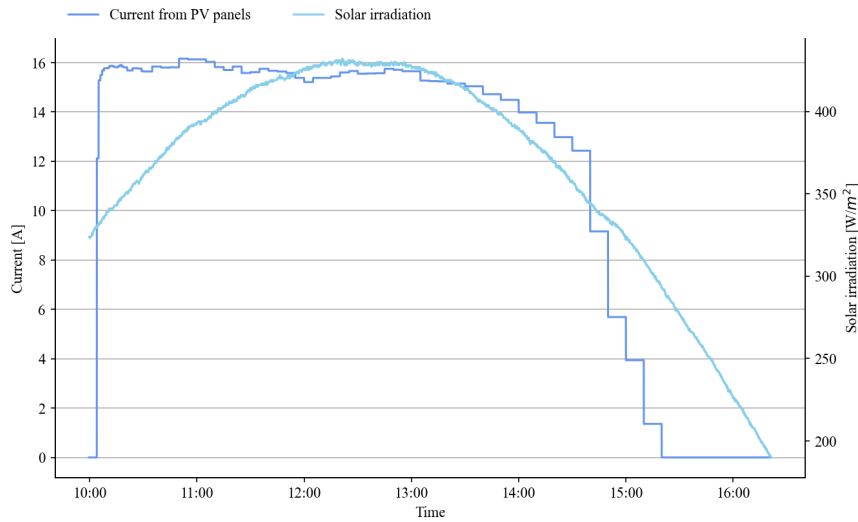


Figure 4.16: The solar irradiation and the corresponding current produced by the three PV panels.

The battery and load voltage during the test are given in Figure 4.17. The figure shows that the battery voltage starts at a very high value, as the batteries were fully charged before starting the experiment.

At approximately 14.40, the load voltage is significantly reduced, while the battery voltage is only reduced a small amount. The voltage drop is due to lower solar irradiation, as the sun has reduced intensity in the afternoon. In addition, the controller switched to equalizing mode for a short period of time, which could affect the power to load. Between 15.00 and 16.00, the load voltage increases and decreases sporadically. During this period, most of the voltage goes to the batteries to maintain the battery voltage, reducing the load voltage and consequently the power to the heating elements.

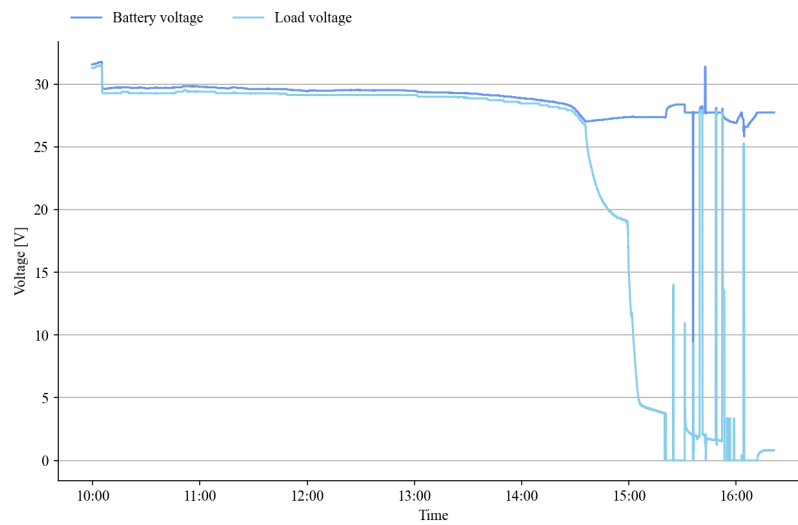


Figure 4.17: The voltage fed to the battery and voltage diverted to the load from the PV panels.

Figure 4.18 illustrates the three temperatures measured in tank 2 during the experiment. The top temperature drops at the start because there is a change in the polarity of the thermocouple. When the polarity was reversed, the temperature increased to roughly 50 °C, matching the temperature increase in the middle and outlet of tank 2. All three temperatures continued to increase until around 15.00.

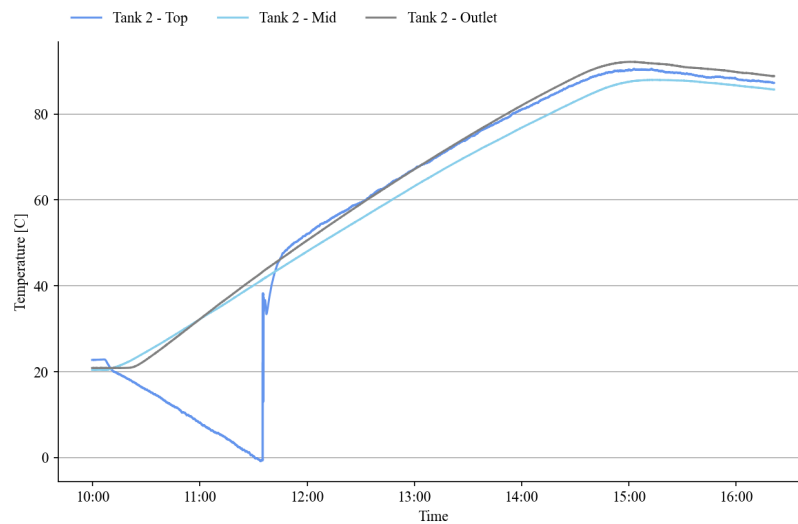


Figure 4.18: Temperature change at the top, middle and outlet in tank 2 during the experiment.

Both the current produced by the PV panels and the current directed to the load are shown in Figure 4.19. The current from the PV panels is initially at 16.0 A and is stable at this high value until around 13.30. Then the current gradually decreases to 0 A at 15.20.

The current directed to the load is lower than the current produced by PV panels, as some of the current is used to charge the batteries. From the start until roughly 14.40, the current directed to the load is 11.0 A, then progressively drops to 0 A at 15.10. After 15.10, the load current shows some fluctuations.

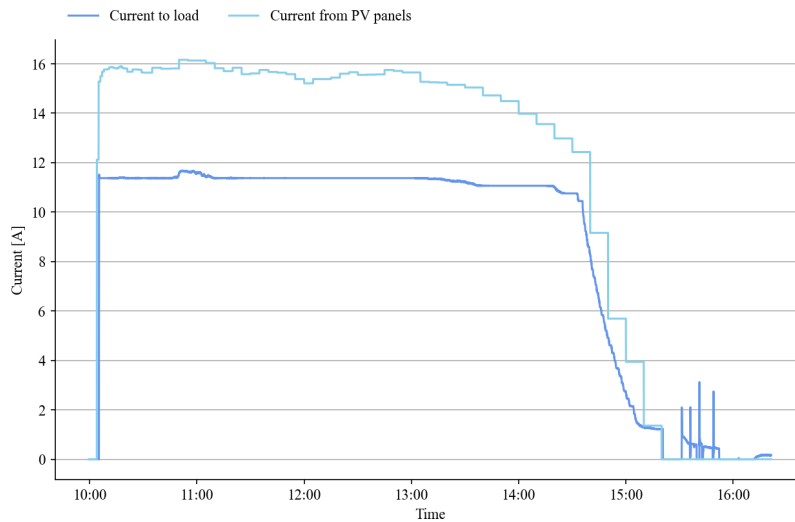


Figure 4.19: The current produced by the three PV panels and the current directed to the load.

Case 1.2 was performed with the same solar configuration as case 1.1. The IV-curve for this experiment are displayed in Figure 4.20 and is plotted from the IV-curve of the solar panels, given in Appendix B. As this experiment was performed later in the spring, the solar conditions had improved, resulting in average solar irradiation of 365 W/m^2 during the experiment. As a result, it can be seen from the graph that the heating elements of 2.54Ω were a good match to the PV configuration and solar array.

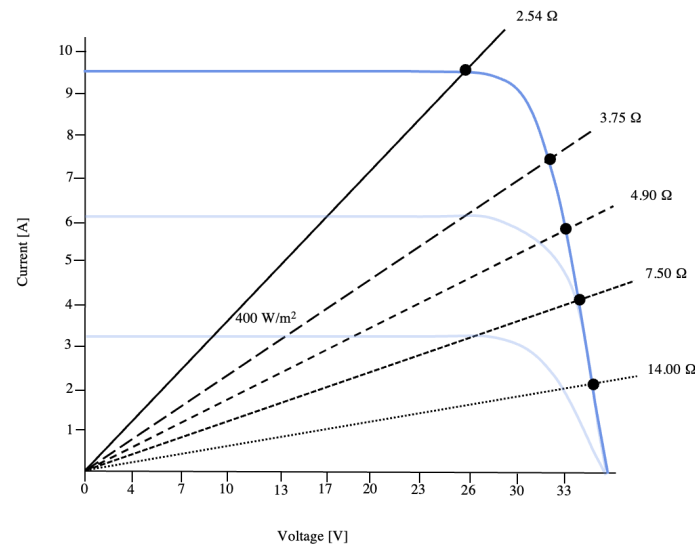


Figure 4.20: IV-curve for the PV configuration for case 1.2 with different heating elements, illustrating three PV panels in parallel at 400 W/m^2 .

4.2.4 Results 1.3

After receiving information from the supervising professor about the outlet pipe, this experiment was conducted with an oil level of 2.92 L, the lowest oil level possible in the tank. However, after this experiment, it was discovered that the information provided was wrong and that the outlet pipe did not cover the heating element. This knowledge was obtained from observing the results from case 1.3, studying drawings from previous work and a thorough investigation of the tank. The heating elements in case 1.3 are heating air instead of oil. However, the results of case 1.3 are still presented as the experiment contributed to a certainty about the information about the outlet pipe.

Figure 4.21 shows Solar irradiation and corresponding produced current from the PV panels for case 1.3. As seen from Figure 4.21, solar irradiation is strong throughout the experiment, despite some periods with clouds. In the two periods from 09.00 to 10.00 and from 13.00 to 14.30, solar irradiation is especially low, dropping to approximately 200 W/m^2 . The produced current corresponds well with solar irradiation, except for periods with short peaks or drops in solar irradiation. From 16.40 until the end of the experiment, the produced current drops to zero, despite a relatively strong solar irradiation. This happens because the PV panels and battery were disconnected and the power source was switched to AC power from the grid.

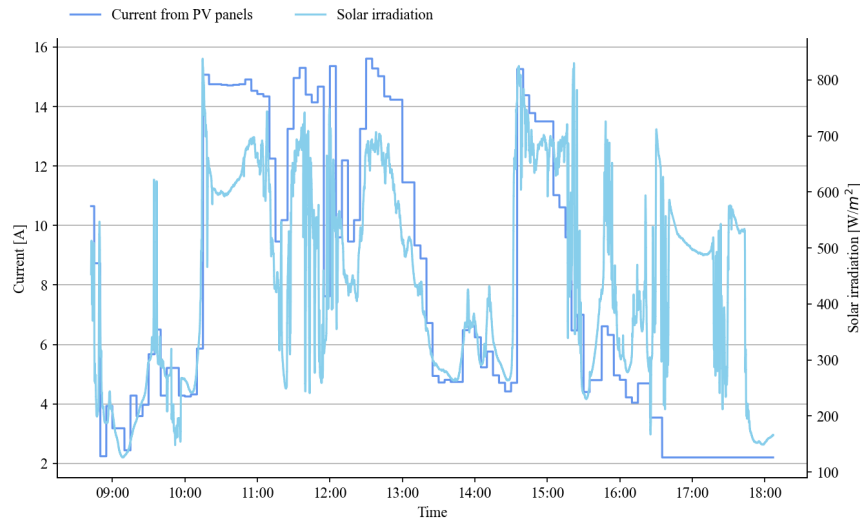


Figure 4.21: The solar irradiation and the corresponding current produced by three PV panels.

In Figure 4.22 the current produced by the PV panels and the load current are displayed. Measurements of current to load are stopped at 16.47 when the AC power from the grid was connected, as the Tristar, PV panels and batteries were disconnected at this point. It can be seen that the load current follows the same slope as the current from the PV panels. However, the load current has an occasionally lower amplitude, except between 09.00 and 10.30. Then the current to load has an unexpected higher value than the current produced from the PV panels. Strong solar irradiation allows the controller to operate at 100 % PWM for some periods. Then all power produced is directed to the load, except for some losses in the controller and wires.

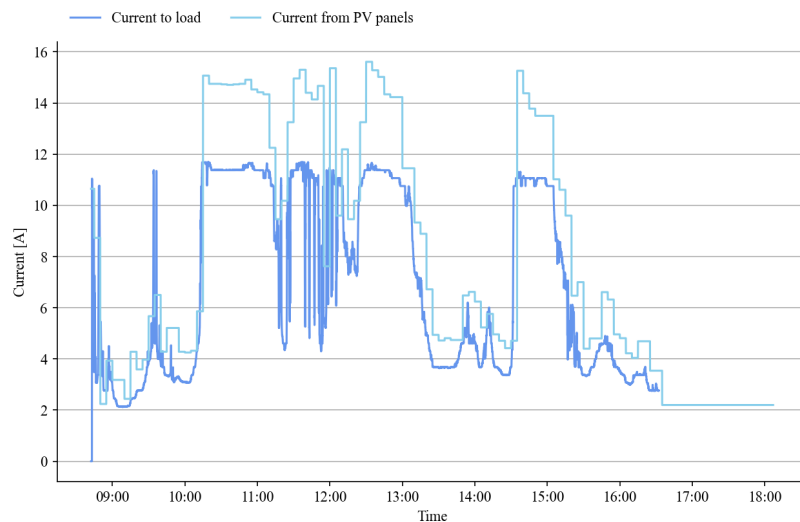


Figure 4.22: The current from PV panels to the controller and current diverted to the load.

Similar observations can be made for the load voltage and voltage from the PV panels illustrated in Figure 4.23. A stable value is measured for the battery voltage during the whole experiment, with some peaks around 10.30, 12.00 and 15.00. The Load voltage decreases after 15.00 due to lower power produced by the PV panels due to lower solar irradiation.

Since the load voltage starts to decrease after 15.00, less power is delivered to the batteries; thus, all the power produced is utilized to keep the battery voltage stable. The load voltage decreased until 16.47, when the PV panels and batteries were disconnected and the power source was switched to AC power from the grid. Therefore, the battery and load voltage measurements were stopped at 16.47.

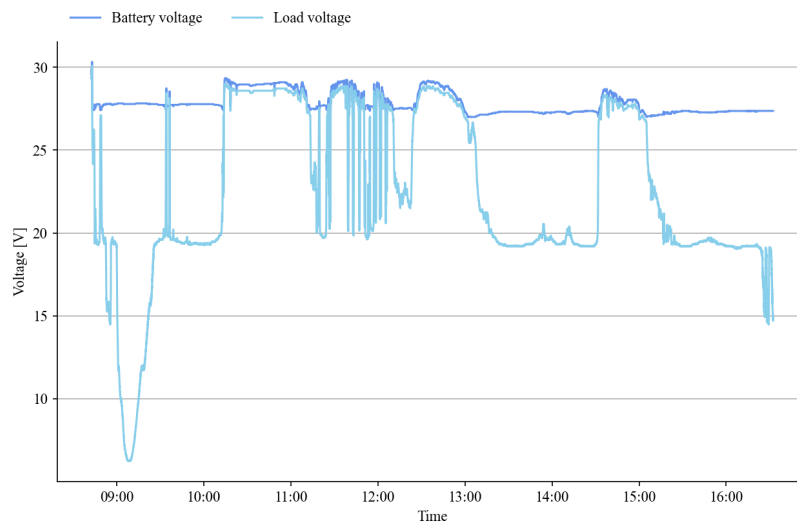


Figure 4.23: The voltage fed to the battery and to the load, from the PV panels. The graph only show values until 16.40 when the power source was switched to AC power from the grid directly connected to the heating elements.

A decision was made to change the power source to AC at the end of the experiment. This was to demonstrate the function of the bimetallic spring at the operating temperature of 230 °C. As seen from Figure 4.24, the temperature in the tank started to decrease after 15.00, which implied that the operating temperature would not be reached with solar power. Additionally, this was in the afternoon with a gradually decreasing solar irradiation.

The switch to AC power is reflected in the figure with a sudden temperature increase at approximately 16.40. The top and outlet temperature increase rapidly until the temperature approaches 200 °C, which slightly reduces the slope. This illustrates the opening of the bimetallic spring, where the oil at ambient temperature is flowing into tank 2 from tank 1. The bimetallic spring opened at approximately 18.04 for an average temperature within tank 2 of 204 °C. This increased the oil volume by 1.6 L to 25.6 L at the end of the experiment.

The temperature in the middle of the tank has an unexpected temperature reduction for a short period when the AC power from the grid is connected around 16.40. This reduction can be seen in Figure 4.24. Further, it increases steadily until the AC power is switched off at around 18.00, where it has an unexpected rapid increase in temperature.

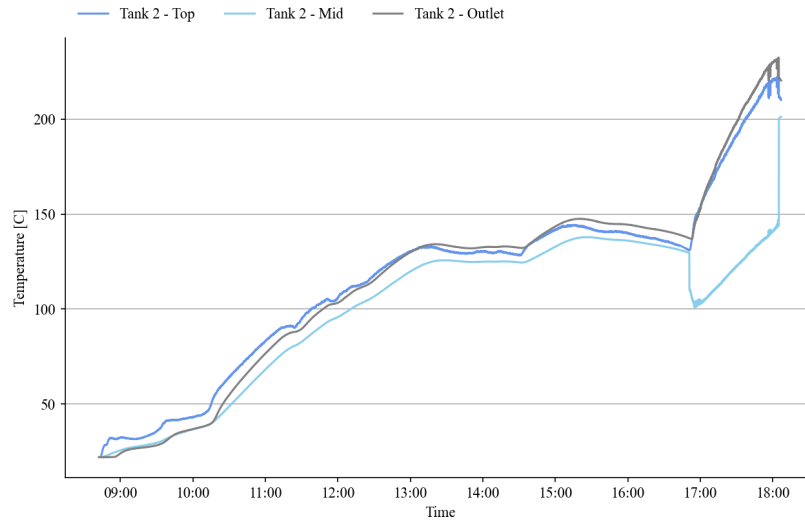


Figure 4.24: The temperature change inside the top of the tank, middle and outlet of tank 2.

Figure 4.25 illustrates the IV-curve of the solar configuration for this experiment. The experiment was carried out with three parallel poled PV panels, with an average solar irradiation of 438 W/m^2 . The IV-curve in the figure represents solar irradiation of 400 W/m^2 , which is the value in the data sheet closest to the actual solar irradiation. As the actual measured solar irradiation is higher than in the figure, the intersection between the used heating elements of 2.54Ω and the IV curve will be slightly shifted to the right. Then the intersection may be closer to the optimal operating point of the IV-curve.

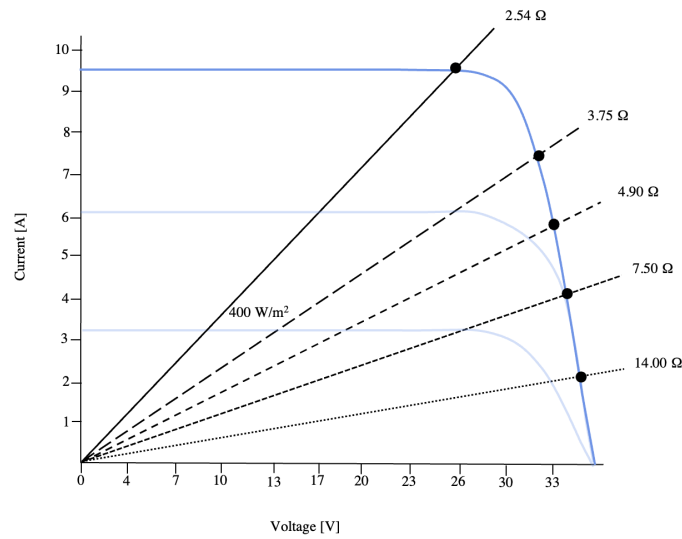


Figure 4.25: IV-curve for the PV configuration for case 1.3 with different heating elements, illustrating three PV panels in parallel at 400 W/m^2 .

4.2.5 Discussion

The results of case 1.1 are characterized by an overall low solar irradiation of 104 W/m^2 . Despite the low solar irradiation, there were almost no clouds which caused the temperature to increase rapidly in the beginning. The temperature stagnated when unexpected construction work at 12.13 cast a shadow on the PV panels. However, if construction work had not interrupted the experiment, the temperature could have reached a higher temperature. As solar irradiation is good from 11.00 until 13.00 and the most rapid increase in temperature is between 11.00 and 12.00 before being interrupted, the temperature might have increased at the same pace with the same solar conditions until 13.00.

It can be seen from the IV-curve displayed in Figure 4.15 that higher solar irradiation would be a better match for the installed heating elements, causing the system to operate more efficiently. The IV-curve is given for an average solar irradiation of 200 W/m^2 ; thus, the heating elements are an even worse mismatch than illustrated as the average solar irradiation actually was 104 W/m^2 .

Due to the low solar irradiation and construction work, it was decided to perform a similar test later in the spring when the solar irradiation had increased. During this test, the solar irradiation was significantly increased, with an average of 365 W/m^2 . As seen from the resulting IV-curve in Figure 4.20, the heating elements are a much better match. From the temperature data for case 1.1 and case 1.2, it can be seen that the high solar irradiation has a significant impact on the temperature, as oil volume is kept at the same level. The temperature in case 1.1 increases approximately $28 \text{ }^\circ\text{C}$ in 2.5 hours from an ambient temperature of $20 \text{ }^\circ\text{C}$. Compared to the temperature in case 1.2, which has increased almost $40 \text{ }^\circ\text{C}$ from an ambient temperature of $21 \text{ }^\circ\text{C}$ in the same time.

Although the IV-curve for case 1.2 is better suited than case 1.1, the IV curve is based on 400 W/m^2 , while the measured average is 365 W/m^2 . Therefore, the IV-curve seems closer to the most optimum power point than it is. This gives the impression of a better fitting of the elements than what it may be in reality. However, in case 1.3, the IV-curve is also based on 400 W/m^2 . At the same time, the average solar irradiation actually was 438 W/m^2 , shifting the resistance of the heating elements and three PV panels in parallel to the right further closer to the optimum point. This better compliance of the heating elements and the higher average solar irradiation could have contributed to the higher temperature achieved in the tank during case 1.3 than in case 1.2. However, the main cause may be the lower oil level.

Case 1.3 was performed with wrong information regarding the outlet pipe. The oil level for this experiment was too low to cover the heating elements, leading to the heating of air instead of oil. This explains the rapid increase in temperature within tank 2 compared to case 1.1 and case 1.2.

Since the heating elements were exposed to air, which could cause burnout, they might have been damaged. On the other hand, by investigating the results of case 1.3, the voltage and current stays within normal operating range. Therefore, the heating elements may not have taken any damage after being heated in the air.

In case 1.3, the temperature in the middle of tank 2 had an unexpected drop in temperature when switching to AC power at around 16.40. After investigating the setup and results from the experiments, it was discovered that there was insufficient electric grounding in the circuit during the connection to AC power. This may be the reason the thermocouple measured temperature in the middle of the tank decreases, as it may have been disturbed by the lack of proper grounding.

For case 1.3 in Figure 4.22, the current to load between 09.00 and 10.30 has an occasionally higher current than the current produced from the PV panels. This was unexpected and may be due to the current measurement from the PV panels was taken manually; therefore, they will have some uncertainty. The current peak to load corresponds well with the rapid increase in solar irradiation for these periods. In addition, the current to load and solar irradiation is measured with a rapid interval of 1 s through the Labview program. Then the current from PV panels may have been higher in the same interval if measured every 1 s.

The highest current produced by the PV panels is observed in case 1.1, with a value of 17.4 A for the short interval from 11.40 to 11.50. This is the experiment with the lowest solar irradiation at this point for all three cases. However, the high current may be because the angle of gradient is optimal in this interval for case 1.1 compared to case 1.2 and 1.3.

Case 1.2 has the best solar conditions of all three cases and is good until around 15.30, as seen from Figure 4.16. At 15.15, the current produced by the PV panels drops down to 0 A, even though the solar irradiation is still above 300 W/m^2 . This may be due to the solar irradiation measuring device being located in another place on the roof than the PV panels. Therefore, an object could be shadowing the panels as buildings and technical equipment are located on the roof of the Thermal Laboratory.

4.3 Case 2: Wind turbine and batteries

To maximize the power output to the heating elements and achieve efficient system operation, is it beneficial to operate the three-tank system as a hybrid solution with multiple power sources. Wind power has been considered the most advantageous secondary power source based on low costs and easy installation. It was, hence, decided to install and connect a wind turbine to the existing setup.

4.3.1 Methodology

Numerous wind turbines have been evaluated based on different criteria; the considered models and respective specifications are given in Appendix C. The wind turbines have been evaluated based on power, voltage, compatible regulators, price and availability. Additionally, cut-in speed has been considered in the final decision.

The SunWind turbine has a maximum PV capacity of 160 W and a current limitation of 10 A. This made the turbine unsuitable for the three-tank system, as each PV panel is rated at 260 W. All of the remaining turbines met the technical requirements. However, the Leading Edge turbine was not available by Norwegian suppliers. Hence it was an ineligible choice.

The SilentWind turbine was expensive and could not be confirmed to work with the Tristar controller. This turbine would require a new controller, causing an additional cost to the already price. Therefore, the turbine was considered unsuitable. The AirNordic turbine could be delivered within 2 to 3 business days to a merchant in Trondheim, which was very beneficial regarding the time limitations of the project. Based on the mentioned specifications, the AirNordic wind turbine was considered the best option. Even though the turbines from Primus Windpower and Rutland fulfilled the requirements, the stock status could not be confirmed by the supplier leading to an unreliable delivery time.

Figure 4.26 shows the placement of the AirNordic wind turbine on top of the technical building on the roof of the Thermal Laboratory at NTNU. This location was chosen due to the easy access and proximity to the PV panels and the original weather station.



Figure 4.26: Location and mounting of the wind turbine on top of the technical building on the roof of the Thermal Laboratory.

Before the system could be tested as a hybrid solution, the wind turbine had to be tested separately to ensure that the setup was working correctly. This test consisted of a wind turbine with an included control unit connected to two 12 V 115 Ah batteries. The control unit had to be included to keep the wind turbine from exceeding the cut-out speed and regulate the voltage from the generator. Additionally, the control unit breaks the wind turbine when the battery is fully charged. This test is referred to as case 2, and the experimental setup is illustrated in Figure 4.27.

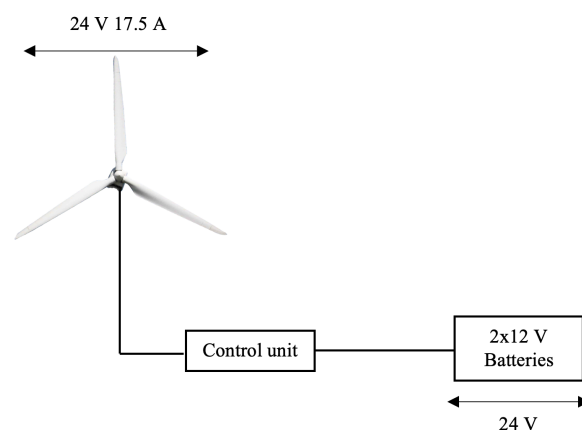


Figure 4.27: Schematic illustration of the experimental setup for case 2.

Prior to the test, the batteries were discharged to 12.40 V each. This was done to ensure that the controller did not brake the turbine during the experiment. The same original weather station logged the wind speed as the solar irradiation. A power meter and a converter were installed to log the power from the wind turbine. This made it possible to digitally log both AC and DC power from the wind turbine. Digitally logging the power enabled the opportunity to log continuously for 24 hours. The indoor setup of the experiment is shown in Figure 4.28.



Figure 4.28: The indoor experimental setup for case 2.

1. Wind control unit and AC power meter.
2. Connection to a wind turbine.
3. Batteries.
4. Converter and DC power meter.
5. Computer for logging wind velocity, power voltage and current.

4.3.2 Results

Figure 4.29 shows wind speed and corresponding power production from the wind turbine from 12.00 to 21.00 on 14.05.22. Wind velocity and power production were logged over several days; however, only the period with power production is included due to poor wind conditions. The figure displays frequent fluctuations in the wind velocity, reaching a maximum of 12.1 m/s at 14.06. Two periods with a lower overall wind velocity can be observed, around 13.30 and 18.00.

Power production occurs sporadically in a short period, as seen from the distinct peaks in the figure. The highest power production occurs at 14.07, where 186 W is produced at wind velocities ranging from 4.8 m/s to 7.1 m/s. It is the wind gust that most likely causes the prominent peak at 14.06. The period with the highest power production is from 14.00 to 14.30. In this period, the wind velocities range from 1.0 m/s to 12.1 m/s, with an average wind velocity of 4.0 m/s. Despite the relatively low average wind velocity, the highest measured wind velocities occur in this interval, including wind gusts of 10.0 m/s, 11.0 m/s, and 12.0 m/s. This indicates a significant coherence between periods with high power production and the highest measured wind velocities. The period with the second-highest power production occurs at 17.05. In this period, 103 W is produced, with wind velocities ranging from 6.8 m/s to 7.0 m/s.

From the figure, it can be seen that the cut-in speed of the wind turbine is 4.6 m/s, as this is the lowest wind velocity where power is produced. Despite this, it is observed that there are higher wind velocities without power production, with the highest measured wind velocity without power production being 9.1 m/s.

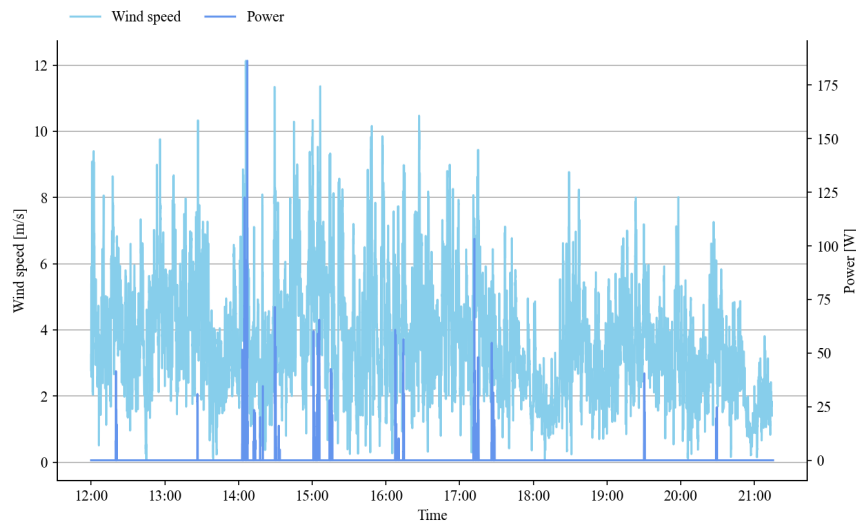


Figure 4.29: Illustration of the power from the control unit of the wind turbine to the batteries, and the wind velocity from 12.00 to 21.00 on 14.05.22.

The corresponding voltage and current from the wind turbine are illustrated in Figure 4.30. In periods without power production, the turbine voltage is kept approximately constant at 21.5 V. Current is produced when the turbine starts to rotate, and the voltage drops accordingly. Periods with produced current correspond with the power production, illustrated in Figure 4.29. The batteries had an initial voltage of 24.80 V, which increased to 24.84 V at the end of the experiment.

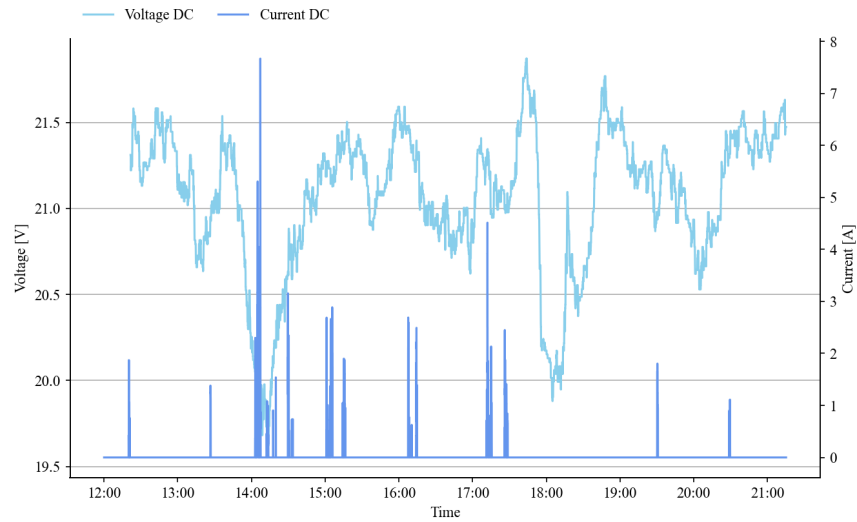


Figure 4.30: Produced voltage and current from the wind turbine in the period 12.00 to 21.00 on 14.05.22.

Figure 4.31 shows the measured wind velocity from both the local Netatmo wind measuring device and the original weather station on the roof of the fifth floor of the Thermal Laboratory from 23.14 24.05.22 to 14.52 25.05.22. Due to the poor WiFi signal from the Netatmo weather station, this interval is the only period with continuous measurements. It is observed that the measurements from the local device are overall higher than the measurements from the distant measurements. Both data sets follow the same trend, with three periods of significantly higher wind velocities. For the local measurements, the peaks occur at around 00.30, 05.30 and 09.30. Compared to the distant measurements, the peaks occur at around 01.00, 05.00 and 12.00. The highest measured value for the local device is 24.0 m/s, logged at 05.22. For the original weather station, the highest value is 11.8 m/s, occurring at 12.29.

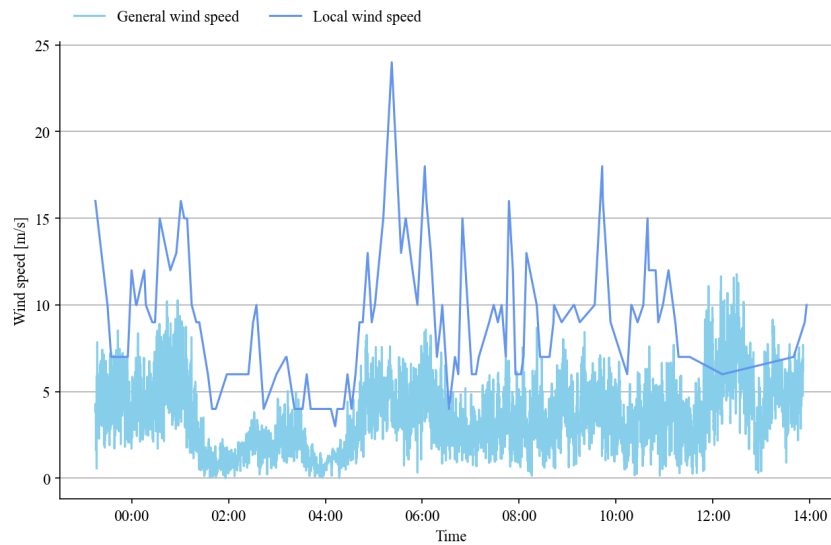


Figure 4.31: Measured wind velocity from 23.14 24.05.22 to 14.52 25.05.22 from the local Netatmo wind measuring device and the original weather station on the roof of the fifth floor on the Thermal Laboratory.

4.3.3 Discussion

According to the findings presented, a continuous wind velocity of approximately 5.0 m/s is needed for the wind turbine to produce power. This is a considerable deviation from the cut-in speed of 2.0 m/s given in the manual. The apparent high cut-in speed could be caused by multiple factors, the most prominent being the location of the wind measuring device.

As the original weather station is mounted on a significantly higher location, the measured wind velocity is possibly higher than the actual wind velocity at the wind turbine. Therefore, a local wind measuring device was installed at the pole of the wind turbine to compare with the measurements of the original weather stations. However, this device had a poor WiFi signal, causing a weak connection to the indoor unit. This is probably a consequence of the device being mounted too far away from the associated Netatmo weather station units. As the signals are transferred by WiFi, the dysfunction might be caused by poor WiFi signals on the roof. This is, however, questionable as the locations were within the range of 100 m given in the manual.

Local wind measurements showed an overall higher wind velocity than the wind measurement from the original weather station. This higher value might indicate an error in the local measuring device, as the wind velocity on the roof was low. The local wind velocity is unlikely to be higher than the distant original weather station, as this measuring device has a higher altitude. Although not proven, it is conceivable that surrounding buildings are shadowing the wind to the turbine. It is, hence, unlikely that the local wind velocity is higher than the distant measurements. Based on this, the measurements from the original weather station are considered to be more accurate. Additionally, this original weather station has a significantly higher sampling time, making the measuring device more accurate when exposed to frequent fluctuations.

Due to low power production caused by poor wind conditions, it should be considered to change the location of the wind turbine. This could, however, be difficult, as the current location was chosen based on practical reasons and construction work on the roof. The turbine has to be connected to the three-tank system, making the length of the cable a limiting factor.

As previously mentioned, mounting delays and poor wind conditions limited the time to test the wind turbine. As a result, not all planned experiments involving the wind turbine have been conducted. Among these are a test of the three-tank system as a hybrid solution. To perform an experiment with both solar and wind, the weather conditions must be ideal with sufficient wind and solar. Additionally, the wind turbine should be tested at high wind velocities connected to a fully charged battery to demonstrate the braking mechanism of the turbine. The excess energy could be transferred to the heat storage tank if the turbine does not break.

4.4 Case 3: PV panels, wind turbine, batteries, and Tristar PWM controller

As a supplement to the power produced by the PV panels, a wind turbine could be included as a secondary power source. By including the wind turbine, this solution could obtain more flexibility for periods with low or no solar irradiation, for example, during the night. This system setup aims to demonstrate the system as a hybrid solution.

4.4.1 Methodology

The wind turbine has a rating of 24 V and 400 W, which delivers a maximum of 17.5 A to the controller. Since the PWM controller has a maximum allowed source current of 30 A, the amount of connected PV panels is limited. The results of the separate wind turbine test in Case 2 disclosed that a low amount of power was generated. Furthermore, the weather forecast had predicted similar wind conditions as in case 2. Thus, it was assumed that a low power production was produced from the wind turbine. Therefore, a number of three photovoltaic panels was chosen, corresponding to a maximum current of 25.3 A delivered to the controller. This setup is shown in Figure 4.32. The current delivered from the wind turbine and PV panels summed up is 12.8 A over the 30 A rating of the controller.

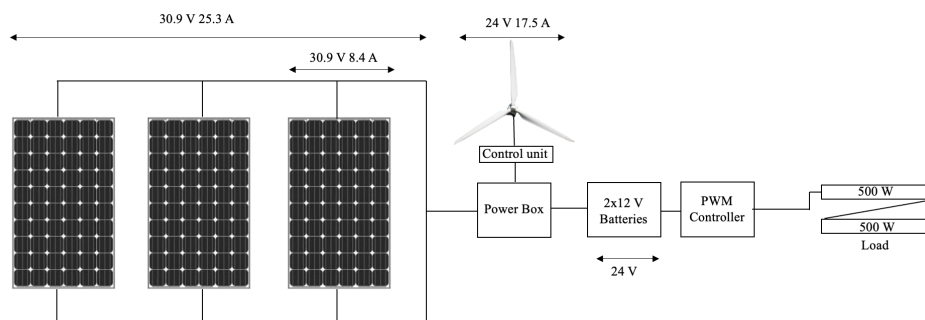


Figure 4.32: Schematic illustration of experimental setup for case 3. This case have not been performed due to insufficient weather conditions.

The experiment was planned to be conducted several times in May, but the weather was a restricting factor. The weather forecast had predicted good wind conditions, and the solar conditions were overall good in May, even though there were predicted clouds. As a result of case 2, the wind turbine needed approximately 5.0 m/s to spin and produce power, despite the design cut-in speed of 2.0 m/s. It was only one day in May with sufficient wind speed, and on this day, the wind turbine without PV panels was tested. Unfortunately, the setup with wind and PV panels was not tested due to limited time caused by a late mounting of the wind turbine on the roof.

4.4.2 Results and discussion

This experiment has not been performed due to poor weather conditions and an unexpected mounting delay due to construction work on the roof. To perform this experiment, there must be a sufficient amount of both sun and wind at the same time. The ideal scenario would have been to start the experiment with almost fully charged batteries so that the batteries are fully charged by the solar and wind turbine, before the turbine breaks and the excess solar power is diverted to the heat storage tank.

In system solutions including a battery, it can be beneficial with an additional power source. This makes it possible to charge the batteries when the system is not used, for instance, during the night. Even more important is to keep the batteries fully charged if used to power smaller household appliances so that charging the batteries does not compromise the use for cooking. A limitation is that the wind turbine does not produce power when the batteries are fully charged. Despite this, it can be seen from the results that the solar irradiation starts to decrease around 14.00. The results from the wind turbine experiment given in Figure 4.29 revealed that the most prominent power production occurred at approximately this time of the day. Consequently, installing a wind turbine could be beneficial to charge the battery when the solar irradiation is low.

The benefit of an additional power source will depend greatly on local weather conditions. A system like this might be less beneficial in areas with stronger solar conditions and more extended periods of sunlight, such as Tanzania. An additional power source also increases the complexity and demand for maintenance, which is undesirable due to limited availability of materials and higher costs. Despite that, an additional power source could be advantageous in Norway or other low-irradiation areas. Low solar irradiation increases the number of solar panels to cover demand, making the available area a limiting factor. In addition, the availability of materials is less of an issue in Norway.

4.5 Case 4: PV panels and Geysewise MPPT controller

The system is tested with an MPPT controller, as this operates more efficiently than the PWM controller. This setup demonstrate the concept of a direct system for heating a storage.

4.5.1 Methodology

The controller is from the South African supplier *Geysewise* and is called the Geyser Eco MPPT. This controller is designed to transfer solar energy to heat. Geysewise specializes in PV water heating systems and PTC heating elements. However, the experience of using this system to heat high-temperature fluids is limited.

In this setup, the input power from the source is limited as the controller has a current rating of 20 A and is not compatible with wind power. However, the results from case 1 disclosed that the current did not exceed 17.5 A with three PV panels wired in parallel on a day with high solar irradiation. Therefore, it was determined to perform the experiment with three parallel wired PV panels, despite the current limit of 20 A. This configuration of the solar array gives a total current of 25.3 A and an array voltage of 30.9 V, as illustrated in Figure 4.33.

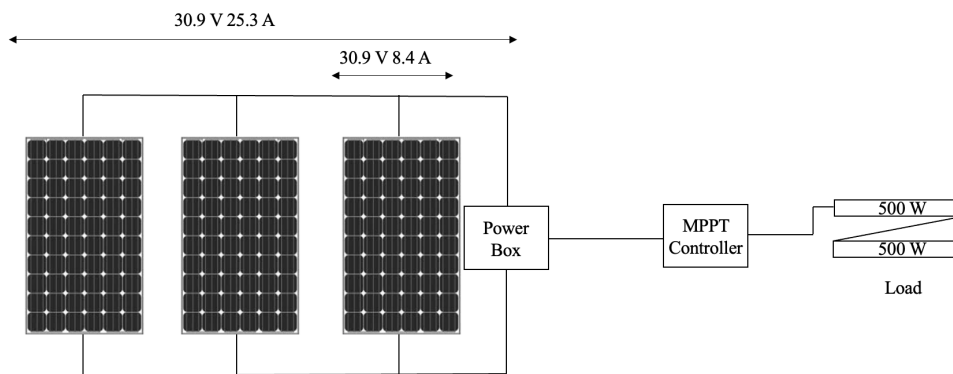


Figure 4.33: Schematic illustration of the experimental setup for case 4.

Case 1 revealed that the battery struggled to maintain a high voltage, which limited the power diversion to the load. Based on this, it was decided to test the MPPT controller in a battery-less setup, meaning that all power from the PV panels is sent directly to the heating elements in the storage tank. As the controller is designed for systems without battery storage, this setup was expected to provide efficient operation and heating. The function of the controller is to regulate the voltage from the solar array to operate in the range of the heating element ratings. As seen in Figure 4.34, the MPPT controller is connected directly to the load. The 48 V MPPT controller is used for this experiment, as this fits the rating installed heating elements.

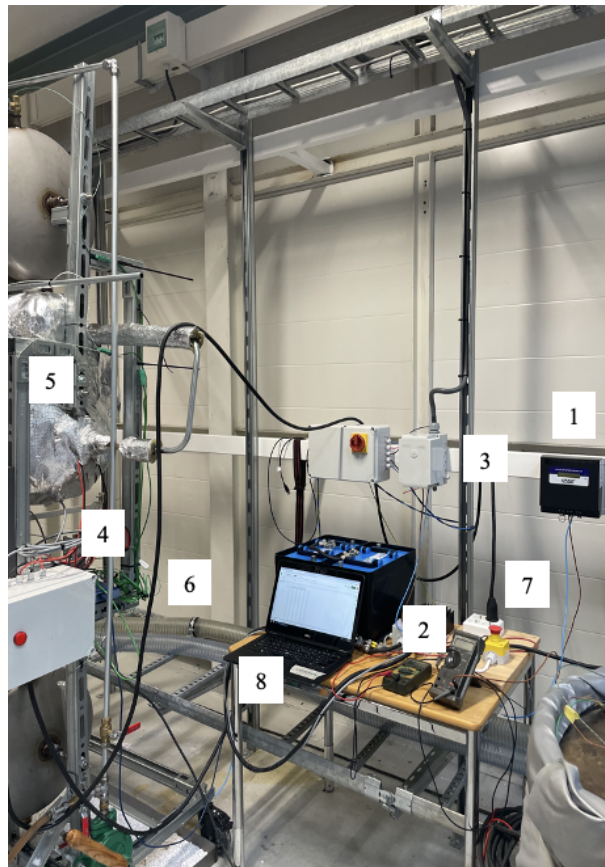


Figure 4.34: Indoor experimental setup for case 4.

1. Geyserswise 48 V MPPT controller.
2. Multimeters to measure current and voltage from the solar array.
3. Connection to the solar array.
4. Connection to heating elements.
5. Heat storage tank with Duratherm 630.
6. Thermocouples and Picologger.
7. Fuse for heating elements.
8. Computer for logging temperatures and solar irradiation.

As previously described, the voltage and current from the solar array were measured manually using two multimeters. Voltage, current, and power out of the controller were read on the controller display. For the first 20 minutes of the experiment, the values were logged every minute. For the next 40 minutes, the values were logged every fifth minute. Further on, values were logged every tenth minute until the end of the experiment.

This setup was tested again in May after testing the PWM controller with batteries. Case 1.3 did not reach operating temperature without using AC power from the grid, even though solar conditions had improved. It was, hence, decided to test the MPPT controller again, as this setup was considered more likely to reach operating temperature with PV as the only power source. If this case does not reach the temperature, AC power from the grid could be connected to demonstrate the function of the bimetallic valve. Logging of current and voltage in and out of the controller was performed manually every five minutes for this experiment.

4.5.2 Results 4.1

Temperatures in tank 2 at the top, middle, and outlet are measured and illustrated in Figure 4.35, in addition to solar irradiation. At the beginning of the experiment, the temperature was 50 °C at the outlet and 48 °C at the top and middle. This high start temperature is the remaining heat from the case 1.2 experiment, performed a day in advance. The temperature in the tank increases consistently from the beginning to around 12.00, where the temperature has a reduced gradient. All three temperatures continue to rise until they reach their maximum point at 13.30; at this point the temperature is 103 °C at the outlet, 100 °C at the top, and 98 °C at the middle. After reaching the maximum value, the temperatures gradually decreased until the end of the experiment at 15.20.

Measurements of solar irradiation correlate well with the temperature gradient. The solar irradiation begins at 200 W/m^2 and increases until 11.15 before it drops to just below 200 W/m^2 . This is reflected in the temperature measurements, as seen by the reduced slope of the temperature increase. Further, the solar irradiation has a smaller peak to just above 300 W/m^2 before dropping down again between 11.30 to 12.00. Furthermore, the solar irradiation continues to rise until 13.00, before gradually decreasing until the end of the experiment.

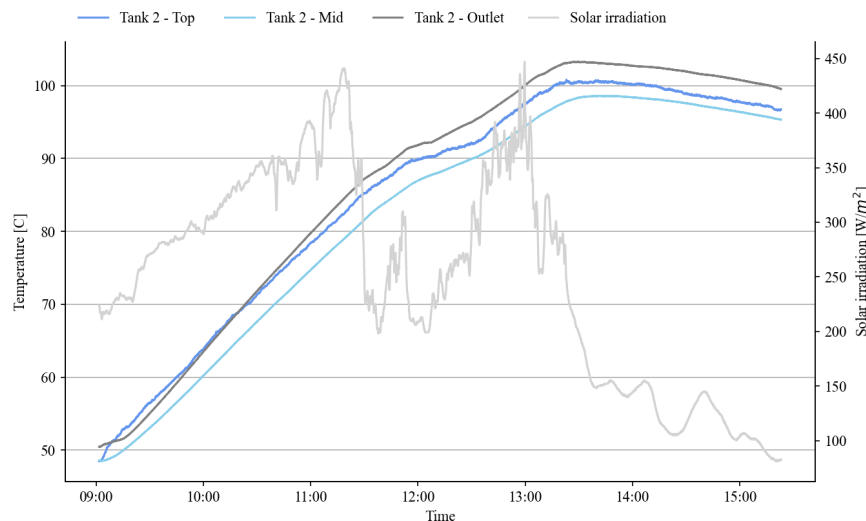


Figure 4.35: Temperature at the top, middle and outlet of tank 2, in addition to the solar irradiation during the experiment.

As expected, the voltage into the controller has a higher value than the voltage out of the controller, as illustrated in Figure 4.36. Consequently, the current from the PV panels to the controller is lower than the current out of the controller. The difference between input and output of the voltage is kept stable from 09.00 to 11.30 as well as the current. After 11.30, input voltage and current are reduced.

The highest difference between the input and output voltage is around 30 V at the end of the experiment, at 15.10. This is when the controller regulates the voltage the most. Regarding the current output and input, the highest difference is approximately 20.0 A, occurring at 13.15. The data shows that the output voltage and current difference are maintained, with an approximately constant difference throughout the experiment.

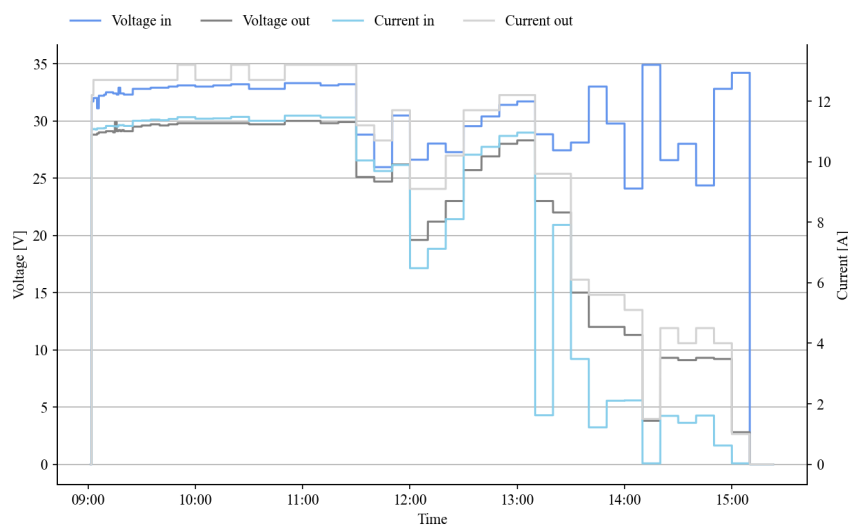


Figure 4.36: Voltage and current measured by the multimeters from the PV panels to the controller. In addition to the current and voltage from the controller to the heating element, measured by the controller.

Figure 4.37 shows the solar irradiation and the respective current produced by the PV panels. The current produced by the PV panels reflects the value of the solar irradiation measured relatively well. When the solar irradiation reaches the peak point of 450 W/m^2 at 13.00, the current produced is approximately 12.0 A. The peak point of the current produced by the PV panels is 13 A, occurring at 09.50, 10.20, and 10.50. It can be seen that this is at a different time than the peak point for solar irradiation. For the peaks from 09.00 to 11.00, the solar irradiation is 200 W/m^2 , before increasing at 11.00 to over 300 W/m^2 .

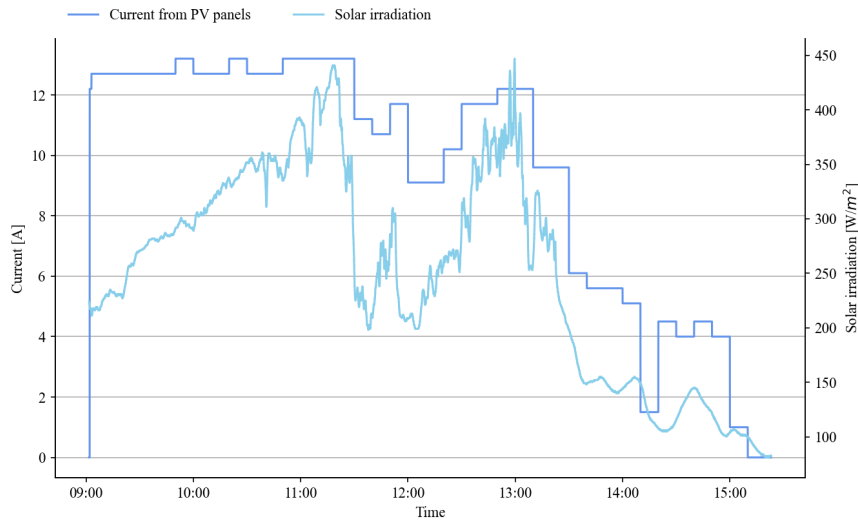


Figure 4.37: The solar irradiation and the current produced by the three PV panels.

As previously described, the solar configuration of case 4 consisted of three PV panels in parallel. The IV-curve given in Figure 4.38 is based on the solar irradiation of 200 W/m^2 from the IV-curve of the solar panels given in Appendix B. However, the average solar irradiation during the experiment was 250 W/m^2 . The higher average indicates that the actual current produced during the experiment is assumed to be more optimal than this graph indicates.

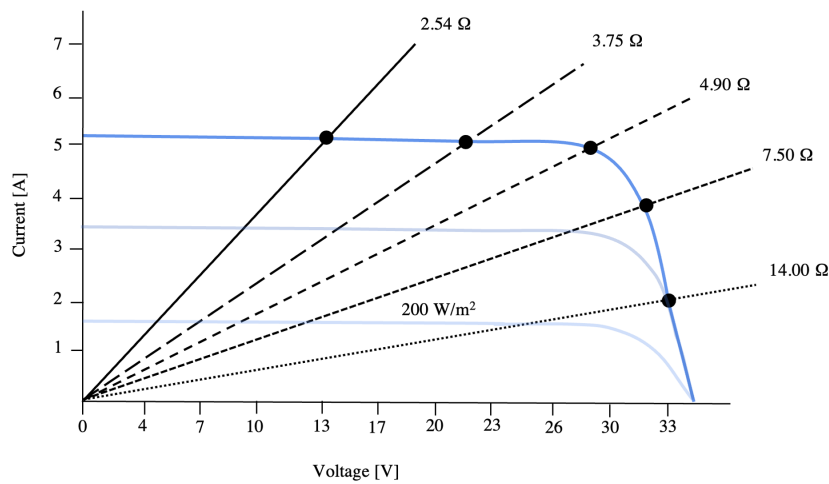


Figure 4.38: IV-curve for the PV configuration for case 4.1 with different heating elements, illustrating three PV panels in parallel at 200 W/m^2 .

4.5.3 Results 4.2

This setup was tested a second time in May with better solar conditions. In Figure 4.39 the temperature development at the top, middle, and outlet can be seen with solar irradiation. Temperatures steadily increased from 22 °C to 92 °C, from 09.19 to 13.28. At 13.28 is the solar irradiation at its highest. Between 13.00 and 14.00, the temperature stagnates and decreases from 92.05 to 91 °C at the top. This is due to clouds; hence, the lower solar irradiation. Therefore, AC power from the grid is connected at 14.00 to reach 230 °C and demonstrate the opening of the bimetallic valve. The temperature did not reach 230 °C until 17.56. However, the bimetallic spring did not open until 18.01, when the temperature was 232 °C at the top of the tank. Then the temperature at the top and outlet shows a slight decrease in temperature. Regarding the temperature in the middle of the tank, some unexpected rapid change in temperature is observed at 14.00, 17.36, and 18.01.

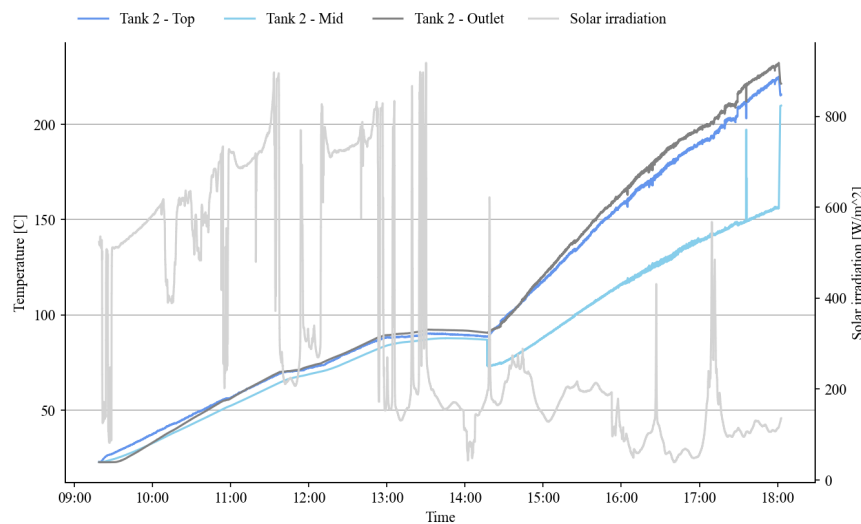


Figure 4.39: The temperature at the top, middle and outlet of tank 2, in addition to the solar irradiation. The power source was switched to AC power from the grid at 14.00 to reach the operating temperature.

Voltage and current in and out of the controller are illustrated in Figure 4.40. During the experiment, the voltage in and out of the controller is stable between 25.0 V and 30.0 V for high solar irradiation. On the contrary, the current out of the controller is around 13.0 A for high solar irradiation. The current to the controller is around 11 A for high solar irradiation and drops to between 4.0 A and 6.0 A for poorer conditions. When solar irradiation is high between 09.19 and 12.00, the difference between input and output voltage and current is lower. At 14.00, when the AC power from the grid is connected, the regulator is disconnected. Thus the values are 0 A from there on and out.

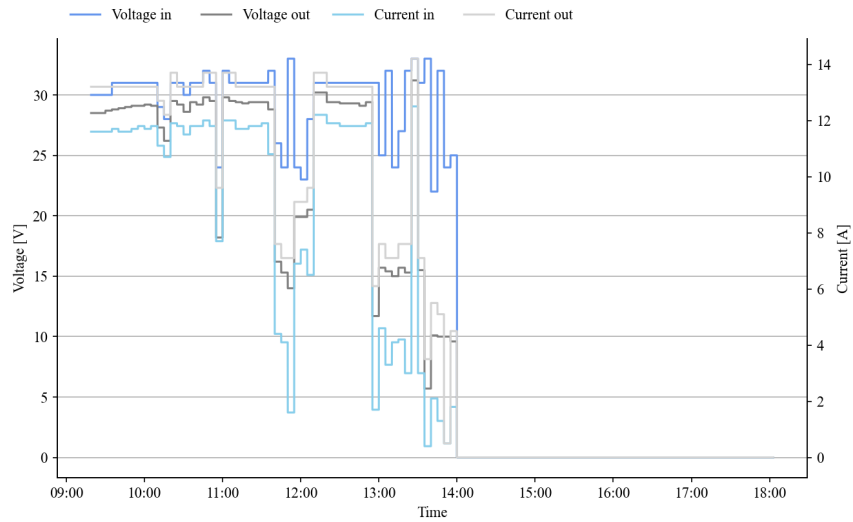


Figure 4.40: Voltage and current measured by the multimeters from the PV panels to the controller. In addition to the current and voltage from the controller to the heating element, measured by the controller. At around 14.00 AC power from the grid was connected and values were no longer logged.

The highest peak in solar irradiation is at 13.30 with a value of 918 W/m^2 with a corresponding current of 14.2 A. This is given in Figure 4.41. The solar irradiation is highest from 09.19 to 13.30 before decreasing, and the produced current is reduced accordingly. There are some peaks after 14.00 when switching to AC power from the grid. However, only for shorter periods.

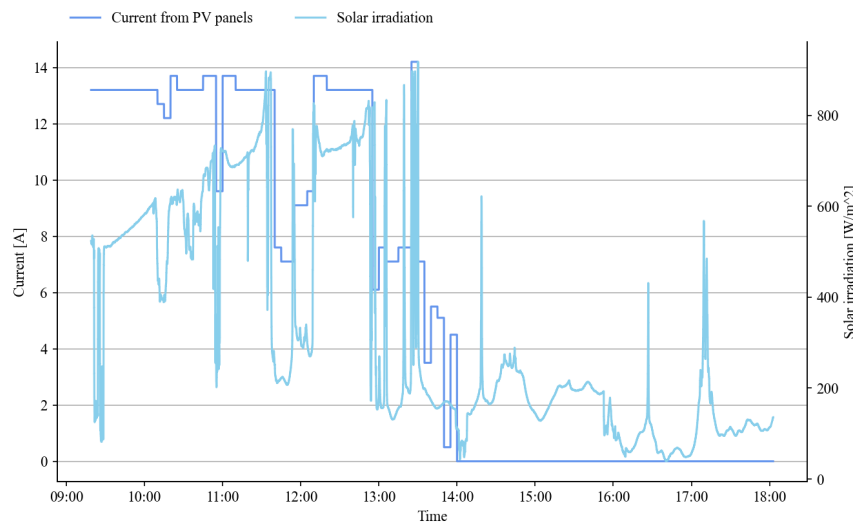


Figure 4.41: The solar irradiation and the current produced by the PV panels.

The solar configuration is the same as in case 4.1. However, the average solar irradiation for this experiment is 334 W/m^2 . Therefore, the IV-curve is based on solar irradiation of 400 W/m^2 , given in Figure 4.42. This makes the heating elements a good fit for the system setup, even though the average solar irradiation is slightly lower than the one illustrated. The current and voltage measured out of the controller are close to the optimal operating point, as seen in the IV-curve in Figure 4.40.

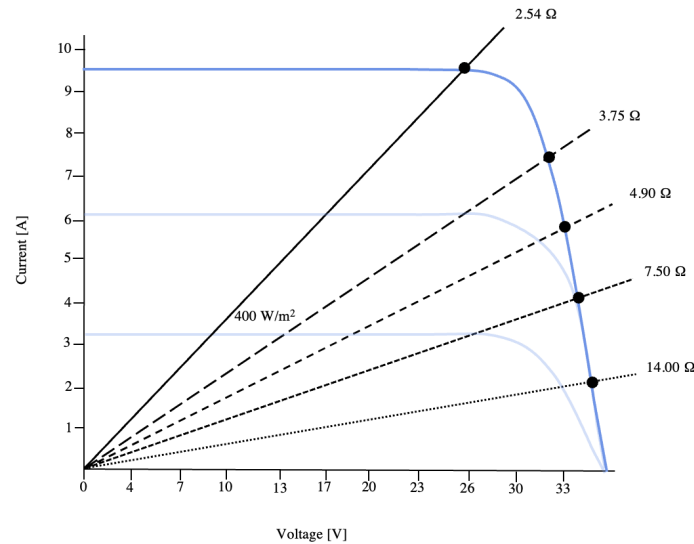


Figure 4.42: IV-curve for the PV configuration for case 4.2 with different heating elements, illustrating three PV panels in parallel at 400 W/m^2 .

4.5.4 Discussion

The experimental setup for cases 4.1 and 4.2 consisted of three PV panels wired in parallel, the 48 V Geyserswise MPPT controller, and the two heating elements wired in series installed in the three-tank system. The first experiment, case 4.1, was performed on a day with high solar irradiation; however, the weather shifted during the experiment with only short periods of high solar irradiation around 11.00 and 13.00. Therefore, the experiment was conducted again in May with better solar conditions. The second experiment is referred to as case 4.2.

As seen from the results of both experiments, given in Figure 4.36 and Figure 4.40 the voltage and current depend on solar irradiation. It can be seen that the current decreased significantly as the sun faded. The voltage also experienced a small decrease but was relatively stable at around 30 V for high solar irradiation during both experiments. The controller regulates the voltage down and increases the current, which is expected as the controller uses buck regulation. However, it can be seen that the regulation by the controller is larger when the solar irradiation decreases. This may be due to the low current value after 13.00 for cases 4.1 and 4.2, which is even further from the optimal operating point for the heating elements.

Based on the temperature measurements, the oil was heated efficiently in Case 4.1, as the temperature increased from 50 °C to 95 °C in two hours. The temperature increases with the same slope as the solar irradiation increases during the morning. For this reason, it is conceivable that the temperature could have reached the operating temperature of 230 °C if the solar irradiation had not started to decrease at 11.00.

On the other hand, case 4.2 did not reach operating temperature with better solar conditions for a longer duration. Case 4.2 only increased from around 22 °C to 91 °C in approximately 3 h and 40 min due to a decreased solar irradiation between 13.00 and 14.00. The longest time registered for solar irradiation without shadowing the panels in this thesis is in case 1.2, where solar irradiation is high until 1530. The corresponding current is reduced to approximately 0 A around 15.00. Therefore, the operating temperature may not have been reached despite a longer duration in case 4.2

This setup could have been tested with the 72 V Geysewise MPPT controller, as the oil was heated efficiently under good solar conditions. However, it was decided not to perform a second test with the 72 V controller. The results of case 5 revealed that the heating elements did not operate efficiently at voltages higher than the rated value.

Despite the positive temperature increase in the tank, the IV curve for this setup reveals that the controller was not operating in the optimal range in case 4.1. The heating elements used have low resistance, and a higher temperature may have been reached with heating elements of 4.90 Ω . On the other hand, the used heating elements would have been better if the solar conditions had not decreased. If the solar conditions had not decreased after 13.00, the average solar irradiation would have increased, shifting the intersection between heating elements and the IV-curve closer to the optimal point of operation.

For case 4.2, the average solar irradiation was higher, even though the solar irradiation decreased after 13.00 also for this experiment. Due to the high solar irradiation, the IV-curve in Figure 4.42 revealed that the controller worked closer to the optimal range for this case. This may be why the temperature has a higher temperature increase from 22 °C to 91 °C, compared to 50 °C to 95 °C in case 4.1. However, the most deciding factor for the temperature increase is most likely the higher solar irradiation.

4.6 Case 5: PV panels and homemade MPPT controller

To investigate the behavior of the three-tank system at a high voltage, the system was tested with a homemade MPPT controller. The controller is made by the former NTNU student Odin Hoff Gardå and is a buck controller, closer described in section 3.3.

4.6.1 Methodology

This setup consisted of an MPPT controller, six PV panels connected in series, and two heating elements placed in the three-tank system. The system setup is illustrated in Figure 4.43. The homemade controller has a low current rating but can handle high voltages. It is, hence, chosen to perform this experiment with all six available PV panels connected in series.

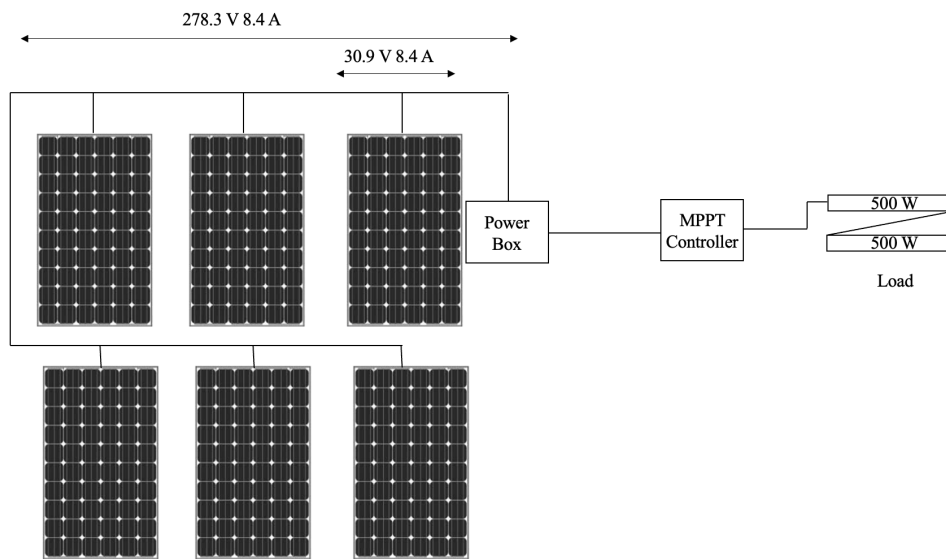


Figure 4.43: Schematic illustration of the experimental setup for case 5.

Low efficiency is expected when performing a test on the three-tank system with this configuration of the solar array. This is due to the low resistance of the heating elements, which makes them unable to reduce the voltage sufficiently. It was, however, chosen to perform the test with the already installed heating elements due to practical reasons and time limitations. In this experiment, all data were logged by a Labview program specifically created for this controller, with a sampling time of 1 second. An illustration of the system setup is given in Figure 4.44.

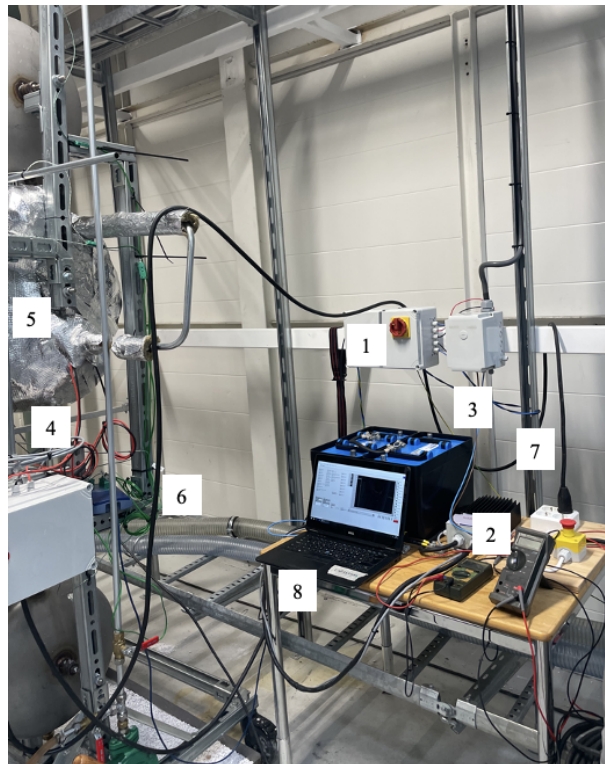


Figure 4.44: Indoor experimental setup for case 5.

1. Homemade MPPT controller.
2. Multimeters to measure current and voltage from the solar array.
3. Connection to the solar array.
4. Connection to heating elements.
5. Heat storage tank with Duratherm 630.
6. Thermocouples and Picologger.
7. Fuse for heating elements.
8. Computer for logging temperatures and solar irradiation.

4.6.2 Results

The controller was tested only for a short period, as the heatsink temperature reached 90 °C at 13.15, and the controller had to be turned off to prevent damage. In Figure 4.45 the heatsink temperature and solar irradiation are shown. During the entire experiment, the solar irradiation had a high value of over 350 W/m^2 , with a maximum value of 550 W/m^2 at 13.07.

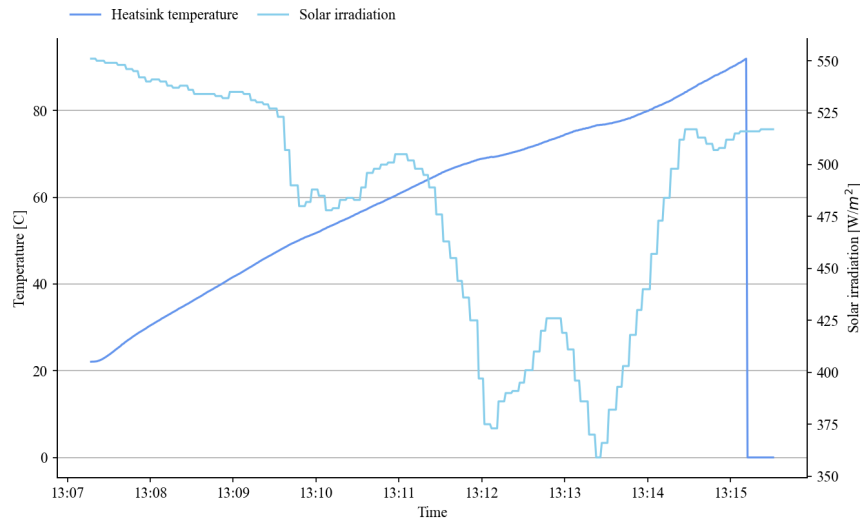


Figure 4.45: The heatsink temperature inside the controller and the respective solar irradiation.

The temperatures in tank 2 had a slightly higher start temperature than the ambient temperature. The slightly increased temperature was due to a short test before starting the experiment to see if the controller was working. This resulted in a higher initial temperature of around 28 °C at the top, 24 °C at the outlet, and 27 °C in the middle. The temperatures in tank 2 and the solar irradiation are given in Figure 4.46. During the experiment, the solar irradiation had a high value of over 350 W/m². Furthermore, the temperature at the top of the tank had the steepest gradient and reached a maximum of around 36 °C. The temperature in the middle of the tank was the second highest, reaching 29 °C, while the outlet only reached 26 °C.

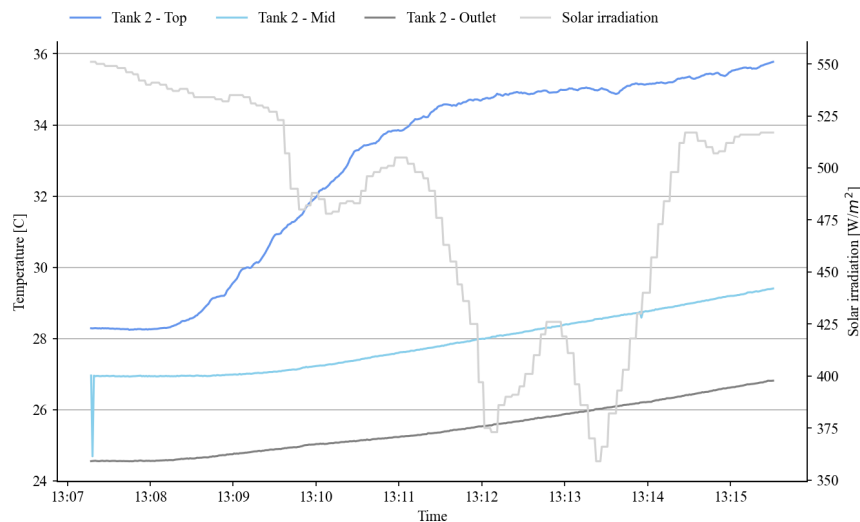


Figure 4.46: The measured temperatures inside tank 2 at top, middle and outlet of the tank, in addition to the solar irradiation.

The current and voltage produced by the six PV panels are shown in Figure 4.47. During the experiment, the voltage had an overall high value of around 160.0 V, reaching a maximum value of 217.0 V at the beginning. Furthermore, the current had a low value of around 2.5 A, peaking at 3.4 A at 13.08.

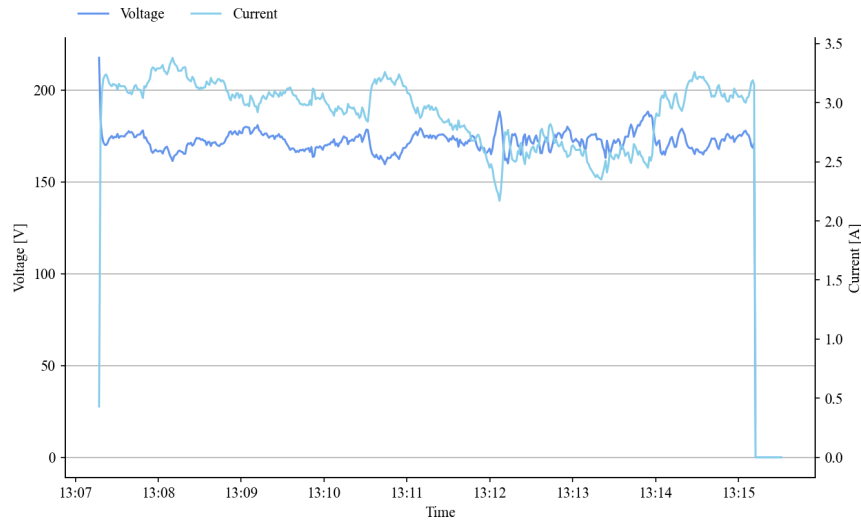


Figure 4.47: The voltage and current produced by the six PV panels during the experiment.

Figure 4.48 shows the power produced by the six PV panels and the percentage of this power diverted to tank 2 by the controller. The produced power was around 500 W during the experiment, which is relatively high. While the produced current is low, the high voltage contributes to the high power. The low PWM percentage indicates a low amount of power being diverted to the heating element.

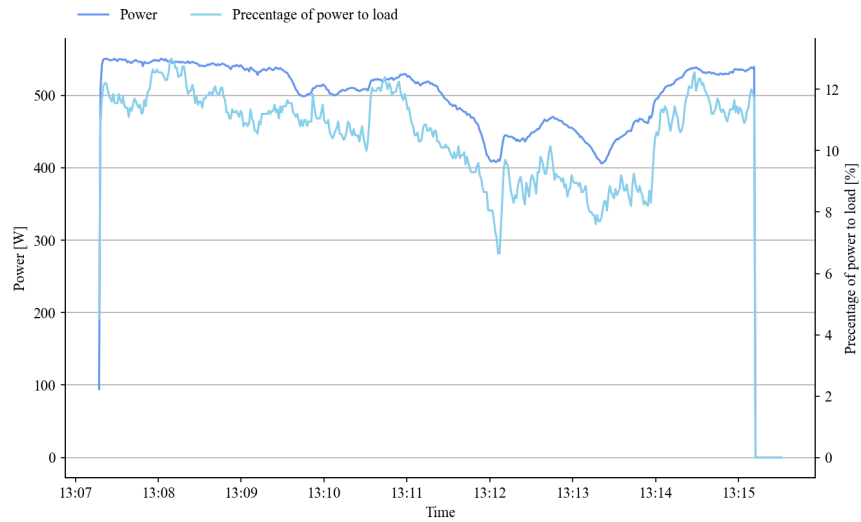


Figure 4.48: The power produced by the six PV panels connected in series and the percentage of this power diverted to tank 2 by the controller.

As case 5 was performed with six PV panels in series, the heating elements at 2.54Ω provided poor regulation, as seen from the intersection between the plotted resistance and the IV-curve in Figure 4.49. This test was performed during good solar conditions with an average of 384 W/m^2 . The IV-curve is given for an average solar irradiation of 400 W/m^2 , which implies that the regulation is weaker under the actual test conditions.

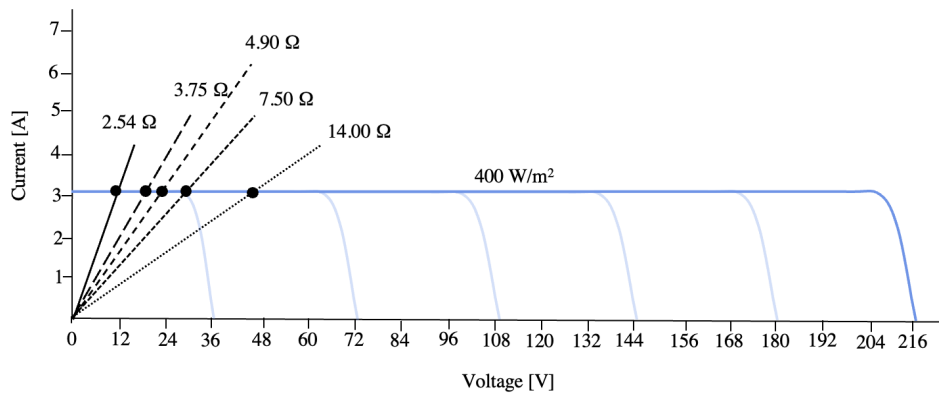


Figure 4.49: IV-curve for the PV configuration for case 5 with different heating elements, illustrating six PV panels in series at 400 W/m^2 .

4.6.3 Discussion

The experiment of case 5 was performed on a day with relatively good solar conditions at the end of March, with only a few clouds between 13.12 and 13.13, as seen in Figure 4.45. This experiment was, however, ended after only eight minutes due to the rapidly increasing high heatsink temperature. Despite this, the oil temperature increased quickly, which could have resulted in a high end temperature if the experiment had not been ended.

Based on the current and voltage rating of the controller, the solar array configuration for this experiment consisted of six PV panels wired in series. This configuration produced a high voltage and a relatively low current from the PV panels, as seen in Figure 4.47. However, the panels produced much power due to the good solar conditions and high voltage. Despite this, it can be seen from the low percentage power to the load in Figure 4.48, that only a small share of the produced power was sent to the heating elements. The percentage of power to the load is stable at around 11 %, reaching a maximum of approximately 13 %. This share should optimally be 100 %, as no batteries were connected to the system. Consequently, a low percentage of power to the load indicates that the main share of the power is accumulated in the controller. This is, hence, most likely the cause of the rapidly increasing heatsink temperature.

The considerably poor result is, however, not unexpected. It can be seen from Figure 4.49 the IV-curve for this experiment, that the resistance in the heating elements used is too low. The resistance plot intersects with the IV curve at approximately 12.0 V, which is noticeably low. The intersection at such a low voltage causes poor regulation. This is because the used controller is a buck controller that optimally should operate at a voltage of approximately 210.0 V. Therefore, a higher resistance should have been used to most likely achieve a better regulation with this controller.

Another method to obtain good results with this controller could be to use fewer PV panels wired in series. This would require heating elements with lower resistance to reach the optimal operating point. This would, however, result in lower power production due to fewer panels. Although, this could be a good method to test the performance of the controller.

4.7 Case 6: PTC heating element and Geysewise MPPT controller

In contrast to the previous cases, this setup was not tested on the three-tank system. This experiment aimed at testing the positive temperature co-efficient, PTC, heating elements and MPPT controller to investigate the behavior of the PTC elements at high temperatures, as illustrated in Figure 4.50.

4.7.1 Methodology

The setup consists of the 72 V Geysers Eco MPPT controller connected to a heating element. The Heating element is submerged in oil in a steel cylinder. The two PTC heating elements rated at 900 W and 1100 W are from the same manufacturer as the controller, *Geysewise*. In contrast to conventional heating elements, the power output of PTC elements is not constant.

PTC heating elements are made of ceramic chips with temperature-limiting characteristics. As the temperature of the surrounding fluid increases and the chips reach a given design temperature, the internal resistance of the chips increases rapidly. This reduces the heat output of the elements, following Equation 3.4 solved for power.



(a) Setup with a 900 W heating element as the load.

(b) Setup with a 1100 W heating element as the load.

Figure 4.50: Schematic illustration of the setup with a heating element and a MPPT controller.

It was decided only to test the 1100 W element, as both elements are self-regulating and designed for similar use. PTC elements are self-regulating with a variable temperature-dependent internal resistance. These elements are designed to increase the internal resistance such that the temperature of the surrounding fluid does not exceed a given design temperature. This makes these elements ideal for heating fluids kept at a constant temperature, such as domestic hot water.

For these particular heating elements, the design temperature was unknown. However, the maximum rated temperature was 230 °C. To ensure efficient operation, this temperature should be equal to or higher than the operating temperature of 230 °C for the three-tank system. It was, hence, necessary to experimentally determine the design temperature before implementing it into the system. A cut-out thermostat at 75 °C was included for the controller, however, this was disconnected as the aim of the experiment was to reach 230 °C. To test the heating element and controller, six PV panels were connected. The PV panels were wired in two sets of three panels in parallel, connected in series.

Table 4.3: Electrical ratings of the heating element and controller. The manual for the controller and heating element is linked in Appendix A

| | Power [W] | Voltage [V] | Maximum output current [A] |
|---------------------|-----------|-------------|----------------------------|
| PTC Heating element | 1100 | 72.0 | 15.3 |
| MPPT controller | 1800 | 72.0 | 20.0 |

The values in the table are based on the table for low irradiance areas from the user manual, linked in Appendix A. It can be seen that the solar irradiance for African areas is considerably higher than the Norwegian average of 1.9 kWh/m² to 2.7 kWh/m² per day according to section 3.2.2. Based on this, it was decided to connect six PV panels to increase the power without exceeding the voltage rating. Although the current rating is exceeded with this solar configuration, the prior experiments revealed that the PV panels did not produce current corresponding to operation at maximum power. The wiring of the PV panels is illustrated in Figure 4.51.

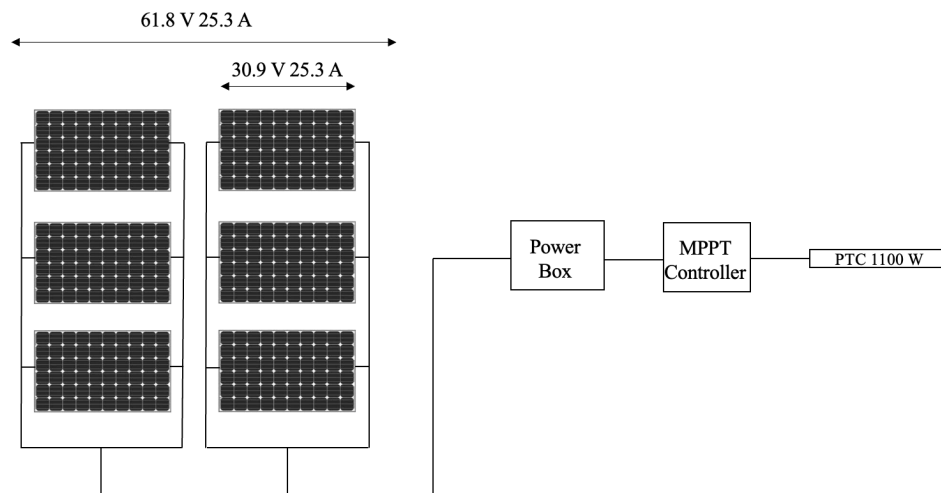


Figure 4.51: Schematic illustration of the experimental setup of case 6, using the 1100 W PTC heating element.

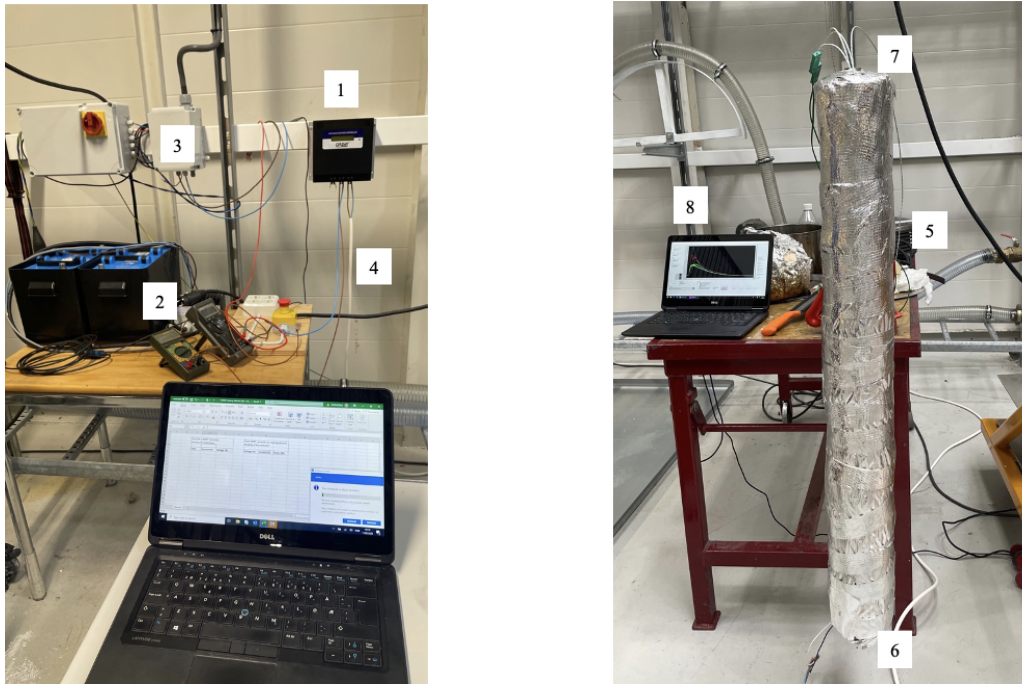
To test the heating element, a separate test rig was built, illustrated in Figure 4.52. This was to investigate the performance before considering implementation in the three-tank system. As the element is too long for the existing three-tank system, the heat storage tank would have to be replaced before installation of the PTC element.

The test rig consisted of an 114.0 cm long steel cylinder with an outer radius of 5.2 cm, attached to a table using a clamp. The cylinder was sized according to a minimum height of 90.0 cm to cover the element and the heating of oil from 21 °C to 230 °C at the desired time of 30 minutes. Design decisions are based on the calculations given in Appendix D.



Figure 4.52: The test rig without insulation, mounted on a table using a clamp.

The heating element was screwed in place at the bottom of the cylinder to easily ensure that the heating element was covered with oil during the experiment. To ensure atmospheric pressure in the cylinder, an opening was created at the top of the to prevent an increase in pressure. The cylinder was insulated with a low cost material for safety measures, as the steel cylinder will get hot during the experiment. Figure 4.53 shows the experimental setup.



(a) Controller and multimeters for voltage and current measurements, in addition to a computer for logging.

(b) Test rig with thermocouples, the heating element is inserted in the bottom of the cylinder.

Figure 4.53: Experimental setup for case 6.

1. MPPT 72 V controller.
2. Multimeters for measuring current and voltage from the solar array.
3. Connection to the solar array.
4. Connection to the heating element.
5. Test rig filled with Duratherm 630.
6. PTC heating element.
7. Thermocouples for temperature measurements.
8. Computer for logging temperatures and solar irradiation.

The temperature was measured by five thermocouples placed in the cylinder, shown in Figure 4.54. The first 10 minutes of the experiment voltage and current from the solar array were logged every minute, from there, the data was logged every fifth minute, and at the end data was logged every tenth minute. Current, voltage, and power from the controller were read from the controller display and logged in the same time intervals as the current and voltage from the solar array.

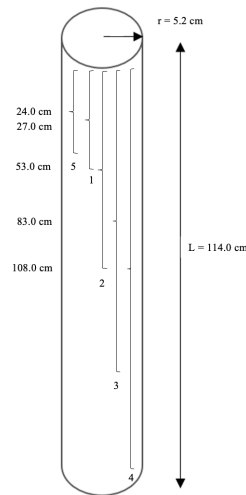


Figure 4.54: Placement of the five thermocouples in the cylinder test rig for case 6.

4.7.2 Results

The solar irradiation, the surface temperature of the heating element, and the average temperature in the oil during the experiment are illustrated in Figure 4.55. The average temperature was estimated based on a mean average of the four oil temperatures inside the cylinder measured by the thermocouples. From the graph, the temperature of the heating element rises steeply from $22 \text{ }^\circ\text{C}$ at 10.15 and reaches about $70 \text{ }^\circ\text{C}$ at 10.30. Then the temperature gradually increases until it reaches $160 \text{ }^\circ\text{C}$ at 11.45. The corresponding average temperature in the oil has a steeper rise at the beginning from $22 \text{ }^\circ\text{C}$ until about $80 \text{ }^\circ\text{C}$ at 11.00. From this point, the temperature has a lower incline until it reaches $150 \text{ }^\circ\text{C}$ at about 11.45. Before both temperatures stabilize and rise by only a few degrees until the end at 14.40.

Solar irradiation has an initial value of 267 W/m^2 . Around 12.30, the solar irradiation gradually decreases as the sun goes down, with some interruptions. These interruptions are probably due to clouds shadowing the PV panels and do not affect the average or heating element temperature, as it continues to rise during these periods.

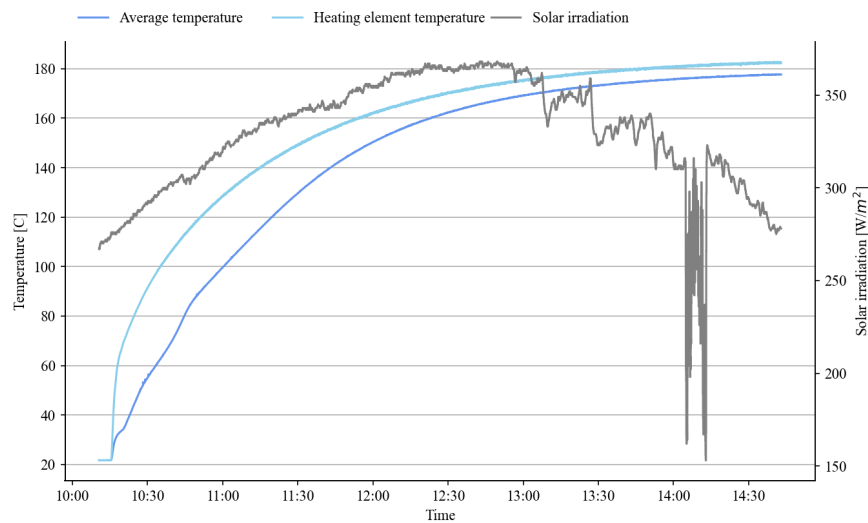


Figure 4.55: Temperature on top of the heating element, average oil temperature in the cylinder and the solar irradiance during the experiment for case 6.

Figure 4.56 displays the average temperature of the oil and the respective resistance of the heating element. The resistance of the heating element is calculated from the manually logged values for current and voltage from the controller. The average temperature was estimated using the average of the five thermocouples. The internal resistance of the heating element starts at 6.0Ω and increases slightly with temperature until 11.00. Furthermore, resistance increases from 7.0Ω to 26.0Ω in larger increments with each measuring point, depending on the temperature. At 13.45, the resistance has reached 26.0Ω with an oil temperature of $177 \text{ }^\circ\text{C}$. The temperature does not increase further during the experiment because of the high resistance.

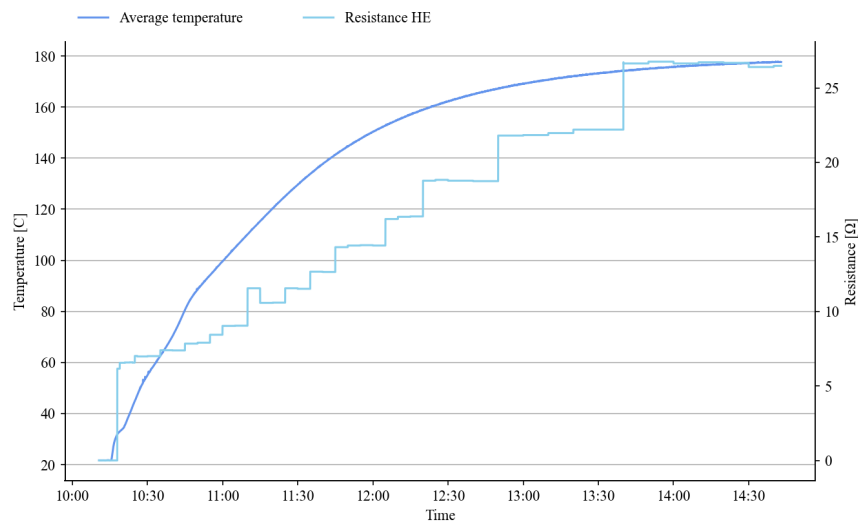


Figure 4.56: Internal resistance of the self regulating PTC heating element, and the oil temperature. The resistance is calculated from voltage and current measurements.

The voltage and current generated by the PV panels and the current and voltage values going from the controller to the heating element are shown in Figure 4.57. The voltage fed into the controller from the PV panels is constant at about 70.0 V throughout the experiment. In addition, the controller regulates the output voltage down to 62.0 V and is stable at this value for the rest of the experiment. As the voltages are approximately constant, the current is reduced as a result of the continuously increasing resistance of the heating element.

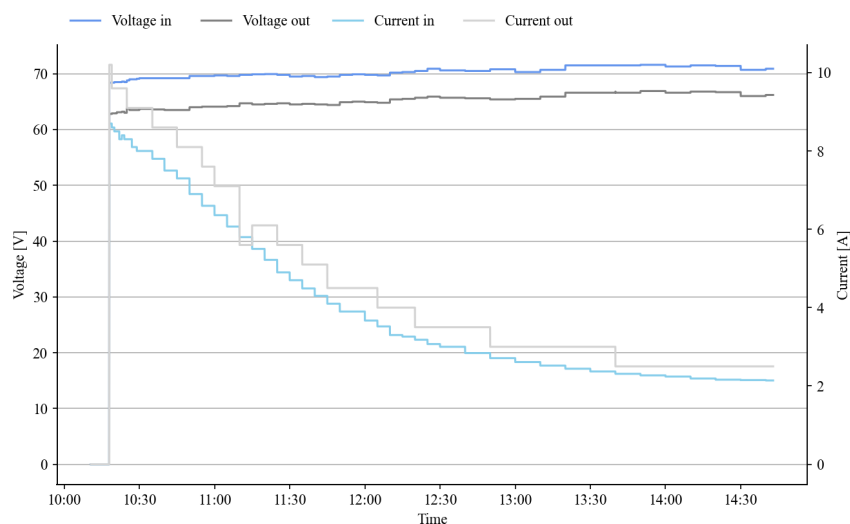


Figure 4.57: Input voltage and current from the PV panels to the controller, measured by the multimeters. In addition to the output voltage and current from the controller to the heating element.

The current flowing into the controller starts at 8.7 A but slowly decreases from the beginning of the experiment. After passing through the controller, the output current is increased to a higher value. As the resistance of the heating element continues to increase with temperature, both the current flowing into and out of the controller continues to decrease until about 13.40. The difference between the input and output current is 0.5 A. A small deviation can be seen between 11.15 and 11.30, where the output current of the controller is lower than the input current. This error is also reflected in the resistance in Figure 4.56. The reason for the sudden current drop is unknown. However, it could be a reading error or a glitch in the controller.

The solar configuration recommended in the controller manual was used in the test, consisting of two sets of three PV panels connected in parallel, connected in series. As the average solar irradiation during the experiment was 329 W/m^2 , the IV-curve is based on a solar irradiation of 400 W/m^2 given in Appendix B. In this experiment a self-regulating heating element was used, resulting in a gradually increasing internal resistance.

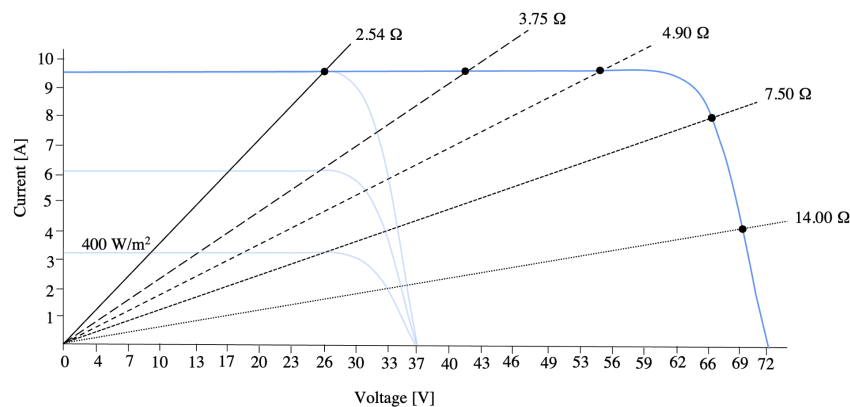


Figure 4.58: IV-curve for the PV configuration for case 6 with different heating elements, illustrating two sets of three PV panels in parallel connected in series at 400 W/m^2 .

4.7.3 Discussion

The experiment regarding case 6 was performed on a day with good solar conditions. However, the experiment was performed in March, which is the reason for the relatively low solar irradiance. The oil temperature had a step increase at the beginning of the experiment. This is most likely a result of the solar irradiance increasing during the morning. As this test was performed with a self-regulating heating element, the step temperature increase is most likely due to the low initial internal resistance. The results disclose that the oil temperature stagnates when the internal resistance reaches a value of 26.6Ω .

During the experiment, it was revealed that the slope of the surface temperature followed the same trend as the oil temperature. This was an unexpected result, as the heating element is designed to keep a constant fluid temperature, assuming a constant surface temperature. The continuous increase could be that the cut-out thermostat at 75 °C was disconnected as the aim of the experiment was to achieve an oil temperature of 230 °C. This seems unlikely as the surface temperature shows a steep increase from the beginning of the experiment, which does not flat out before the temperature is approximately 160 °C.

The results revealed a gradually increasing internal resistance as the temperature of the surrounding fluid increased. When the temperature exceeded 170 °C, the temperature and internal resistance stagnated. It can be assumed that the resistance has reached a level where the resulting current is too low to increase the temperature further. As a result of this, the experiment was ended.

If continuing the experiment, it can be assumed that the internal resistance would have continued to increase, consequently reducing the current to a level where the oil temperature would have started to decrease. This is based on the voltage and current measurements seen in Figure 4.57, where the output current reached a value of 2.5 A, while the input current was 2.15 A at the end of the experiment. It can also be seen that the voltage is kept relatively constant during the experiment and is regulated down a few volts by the controller. The low power indicates that the power from the PV panels is not utilized due to the high internal resistance of the heating element.

For this reason, it can be discussed whether the combination of a self-regulating PTC element and an MPPT controller results in optimal power utilization. The results of this experiment indicate that the internal resistance of the elements prevents the controller from optimizing the power produced by the photovoltaic panels.

From the corresponding IV-curve in Figure 4.58 it can be seen that the optimal resistance of the heating element to the corresponding solar conditions is approximately 6 Ω . At the beginning of the experiment, this resistance is reached at an oil temperature of just below 65 °C. Accordingly, it is indicated that this is the temperature at which the system operates the most efficiently. According to the *Geyserwise* manual linked in Appendix A, Trondheim is defined as a low irradiation area. As the solar array is dimensioned after this manual, it is conceivable that 65 °C is the design temperature of the heating element. Moreover, it can be argued that 65 °C is the design temperature of the element, as it is designed for heating domestic hot water, which is commonly kept around this temperature.

The oil temperature never reaches the operating temperature of 230 °C, as the temperature stagnates at approximately 180 °C. Based on the results, this is caused by the internal resistance reaching a level where the current is too low to increase the temperature of the oil, despite the experiment being conducted on a day with high solar irradiation. This reveals that the total power from the PV panels is not utilized. As a result, it is demonstrated that the system does not operate efficiently at high temperatures and performs best at an oil temperature of around 65 °C. This was a somewhat expected result, as the maximum temperature of the heating element is 230 °C, which indicates that this is not the optimal operating point.

4.8 Cooldown

Poor insulation was mentioned as a disadvantage of the system that had to be improved. The heat storage tank is insulated with two layers of Fyrewrap. However, this was proven insufficient in prior experimental work. Before starting experimental work on this master thesis, the insulation was improved with an additional layer around the heating elements and perforations in the tank. Despite these improvements, significant heat losses were observed during the experiments.

4.8.1 Methodology

Due to the observed heat loss, it was decided to log the cooldown process for tank 2 in the three-tank system. The cooldown of the three-tank system was recorded from the operating temperature of approximately 230 °C to the ambient temperature of around 23 °C. Based on the cooling process, an u-value for the the heat storage tank can be calculated. This value is calculated based on Equation 3.10 and 3.20, from the theory presented in section 3.7 and 3.8.

4.8.2 Results

Figure 4.59 shows thermal images of the three-tank at the operating temperature of 230 °C, from a front and side view. The images uncover heat leakage in the system, shown in the yellow areas of the pictures. It can be seen that the primary heat losses are at the top of the tank, the insertion point of the thermocouple in the ventilation pipe, and around the heating elements. It was also observed smoke from the insertion point in the ventilation pipe. The yellow area at the bottom of Figure 4.59b is caused by the heat accumulated in the fuse box.

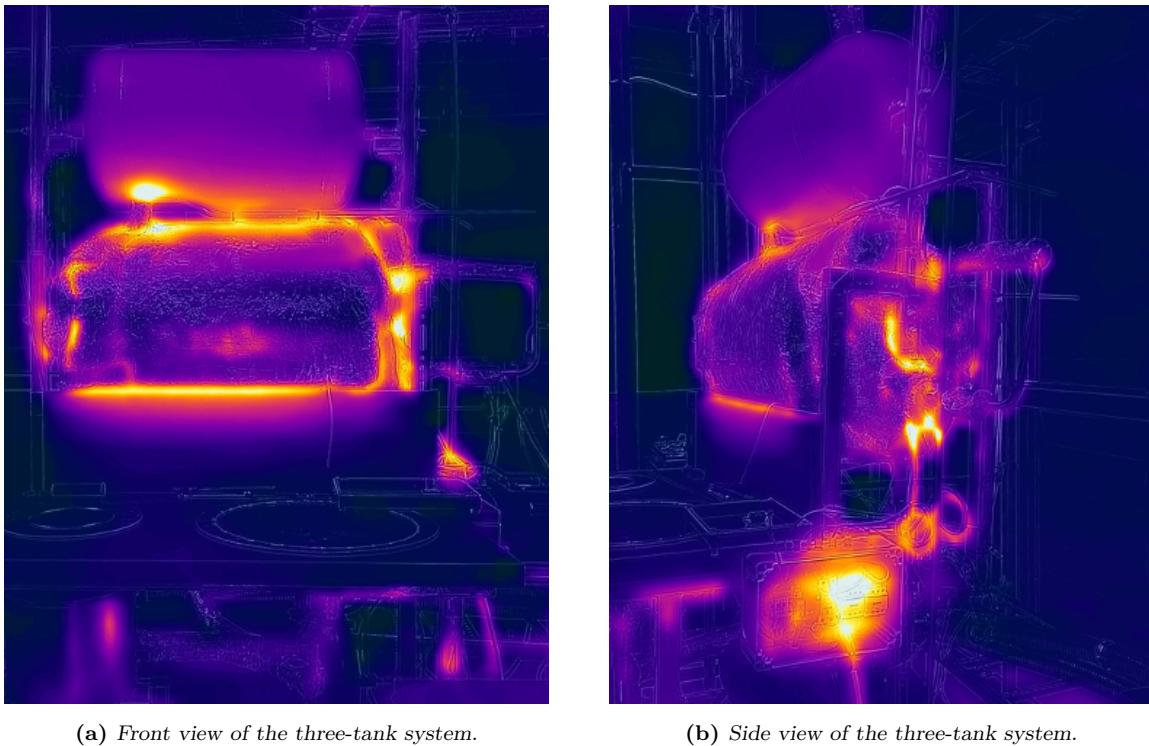


Figure 4.59: Thermal images of the three-tank system at operating temperature. The yellow areas indicate heat loss in the tank

In Figure 4.60 the cooldown from 230 °C to approximately ambient temperature of 23 °C of the three-tank system is displayed. The cooling process is logged for 88 h and 55 min from 26.05 to 30.05 and is presented by an average temperature of the oil during cooling. This average is estimated from the average of the thermocouples in the middle, top, and outlet of tank 2. There is an unexpected rapid drop in temperature after 12.00 on Friday 27.05, as the logging of temperature was stopped at 04.08 in the morning and not started again until 13.07 on Saturday 28.05. This was due to an error message in the LabView program, which paused the logging. Therefore, the stippled line presents an assumed cooldown curve for the period with missing values.

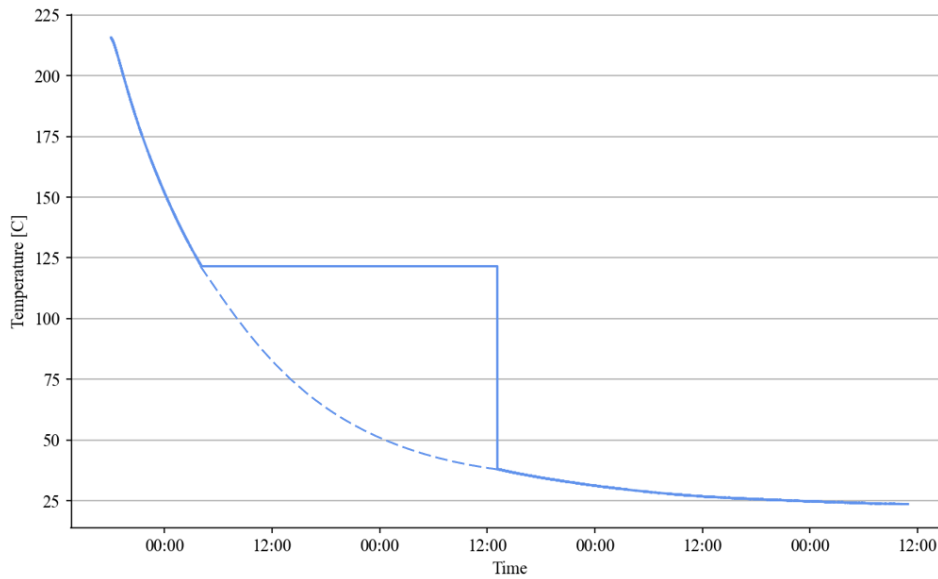


Figure 4.60: Average temperature of the oil during cooling, estimated from the average of the thermocouple in the middle, top and outlet of tank 2. Measurements are logged for 88h h and 55 min. Due to an error message in Labview, the logging was stopped after 12.00 the second day. Assumed values for the cooling process is presented in a stippled line.

The calculations regarding the u -value of tank 2 in the three-tank system are based on an oil volume of 24.24 L. A cooldown period of 10 hours is chosen to calculate the u -value, as this is the assumed time that the oil is stored during the night. This is also the period from the end of the experiment to the error in the Labview program occurred. Moreover, the period corresponds to a cooldown from the highest achieved average temperature of 216 °C to 122 °C. The presented u -value is an average of the calculated u -values for each temperature step in this interval, according to the calculations presented in Appendix E. The resulting average u -value is thus, calculated to $3.7 \text{ W/m}^2\text{K}$.

4.8.3 Discussion

The results revealed significant heat losses due to insufficient insulation. Despite using a high quality insulation and further improvements, a high heat loss is observed. Insulation needs further improvement, especially at the top and bottom and around the ventilation pipe and heating elements. The insertion point of the thermocouple is most likely a significant source of heat loss, as the thermal images showed heat loss specifically around this point and not the entire ventilation pipe. The insertion point is sealed with silicone gel; however, this may be damaged after several tests and movement of the thermocouple. Therefore, it is possible that improving the leakage could reduce the heat loss of the tank.

Just as necessary is the insulation of the top and bottom of the tank. Despite using high-quality insulation, the high heat loss indicates that the system may need to be professionally insulated to reduce the heat loss to a satisfactory level. This will, however, increase the costs and value of the system. Implementation of such a system in Tanzania could be an issue, as valuable components are at risk of theft, and the availability of high-quality insulation is presumably limited. Even if the warmer climate in Tanzania might reduce heat loss, the system still needs adequate insulation to ensure safety and efficient operation of the system. One of the main advantages of the three-tank system compared to other off-grid cooking solutions is the possibility of storing excess energy from the power source in a thermal storage. It is, hence, essential that the heat storage can store energy in high-temperature oil when the demand is low.

Logging the cooldown process and calculation of the u-value for the three-tank system revealed that the tank could not store high-temperature oil and maintain high temperatures during the night. This is a severe issue that must be improved to operate the system efficiently. As the system could not store high-temperature oil at night, it was impossible to test it by preheating the oil a day in advance. A test with preheat could have made it possible to reach the operating temperature with solar power as the only power source.

5 Summary

In this section, the primary results of each experiment are presented together with the respective weather conditions. As the experiments are performed over an extended period, the weather conditions differ, which significantly impacts the power produced by the solar array. This can be seen from the data presented in Table 5.1.

Table 5.1: Summary of the primary results from each case. This includes the average solar irradiation, wind velocity, power to load, and the respective date of the experiment.

| Case | Average solar irradiation | Average wind velocity | Average power to load | Date |
|------|---------------------------|-----------------------|-----------------------|---------------|
| [-] | [W/m ²] | [m/s] | [W] | [-] |
| 1.1 | 104 | – | 96 | 03.02.22 |
| 1.2 | 365 | – | 241 | 21.03.22 |
| 1.3 | 438 | – | 168 | 19.05.22 |
| 2 | – | 2.97 | – | 14.05.22 |
| 3 | – | – | – | Not performed |
| 4.1 | 250 | – | 244 | 22.03.22 |
| 4.2 | 334 | – | 292 | 26.05.22 |
| 5 | 384 | – | 51 | 29.03.22 |
| 6 | 329 | – | 284 | 11.03.22 |

The highest temperature achieved in each experiment, together with the duration of the experiment, is given in Table 5.2. The theoretical time to heat the oil from the initial measured temperature to the operating temperature of 230 °C is also presented, calculated from the theory presented in Section 3.7 based on the average power to the load. The duration of each experiment depends on weather conditions, as each experiment ended when the solar irradiation or oil temperature started to decrease, with the exceptions of case 1.1, case 1.3, case 4.2 and case 6.

Case 1.1 was ended due to unexpected construction work on the PV panels, and case 6 ended when the internal resistance of the heating element reached a level where the oil temperature did not increase. While cases 1.3 and 4.2 ended after reaching the operating temperature of 230 °C, using AC power from the grid to heat the remaining temperature step. However, the duration of these two experiments only includes the time the PV panels were connected, though these two cases have a longer duration.

Regarding experiment 1.3, the average power to load is based on solar power, where AC power from the grid is omitted. However, in case 1.3 the operating temperature should theoretically be reached with the average power to load only powered by the PV panels. Since the average power is utilized in the calculations, the power is constant at 168 W, although in reality, it is high in the middle of the day and very low early in the morning and afternoon.

Table 5.2: Results of all experiments with respect to the highest temperature achieved, duration of the experiment, and theoretical time to reach 230 °C at average power from the experiment. The highest temperature achieved is for oil heated only by PV panels. Regarding cases 1.3 and 4.2, only the time PV panels were connected is taken into account for the duration of experiment, although AC power was connected and the total duration of the experiments were longer.

| Case | Highest achieved temperature | Duration of experiment | Theoretical time to reach 230 °C |
|------|------------------------------|------------------------|----------------------------------|
| [-] | [°C] | [h] | [h] |
| 1.1 | 49 | 5h 7 min | 47 h 7 min |
| 1.2 | 92 | 6 h 16 min | 18 h 20 min |
| 1.3 | 148 | 7 h 55 min | 3 h 14 min |
| 2 | – | 9 h 15 min | – |
| 3 | – | – | – |
| 4.1 | 103 | 6h 23 min | 15 h 59 min |
| 4.2 | 92 | 4 h 19 min | 13 h 30 min |
| 5 | 36 | 8 min 30 sec | 84 h 6 min |
| 6 | 178 | 4 h 32 min | 4 h 31 min |

6 Discussion

When only taking the cases performed on three-tank system with an oil volume of 24.24 L into account, the highest achieved temperature for the heat storage tank was 103 °C. This temperature was reached in case 4.1, as seen from Table 5.2. However, the start temperature of this experiment was 49 °C due to an experiment of case 1.2 a day in advance. Consequently, case 4.2 is the experiment with the highest temperature gradient, increasing from 22 °C to 92 °C in around 4 hours. This may be due to the high average solar irradiation combined with a good match of the heating elements to the controller. Case 4.2 is closely followed by case 1.2, which reached a temperature of 92 °C from 21 °C, though over a longer period. Case 1.2 had better solar conditions as there were no clouds that day, compared to case 4.2, which ended at 14.00 due to clouds. However, the solar irradiation is lower as case 1.2 was performed in February. Therefore, it is likely that case 4.2 could have reached an even higher temperature if the experiment had been performed on a day with no clouds.

Based on the system setup, it is likely that case 4.2 would achieve the highest temperature. Case 4 is performed without a battery and with an MPPT controller. This controller can divert more power over a shorter period than the PWM controller used in case 1.2, as it does not have to reduce the PV voltage down to the battery voltage. In addition, case 1.2 includes a battery which reduces the amount of power being sent to the load. Independent of the solar conditions, the setups without a battery should achieve high temperatures in the tank faster than the setups where a battery is included due to the power required to maintain the battery voltage.

The different setups and solar irradiation for the specific day have a substantial impact on how well the heating elements suit the system. As seen in figure Figure 4.20 and Figure 4.42, the heating elements were a good fit for both case 1.2 and 4.2. Nevertheless, case 1.2 has the advantage of a higher average solar irradiation closer to the optimal operating point in the IV-curve, giving it better potential to divert high average power to the heating elements.

The used batteries are old and left to discharge for several months every year since most master projects are performed in the spring. Therefore, they need to be equalized to prolong their useful life. This might be the reason for the low amount of power to the load in case 1.2, as the controller switched to equalizing mode during the experiment. In addition, the batteries not being sufficiently charged before starting the experiment could have been an influencing factor.

Case 1.1 and case 1.2 both have a long calculated time to reach the operating temperature due to the batteries. When experiments are performed with old and worn-out batteries, more power is needed to maintain the battery charging voltage, which significantly impacts the amount of power that is diverted to the load. This issue could be resolved by changing the setting of the lowest battery charging voltage in the controller. This value determines when the batteries are considered fully charged and accordingly at what battery voltage power is diverted to load. However, this setting is set at the lowest possible value of the Tristar controller. Purchasing new batteries could, hence, have been better. On the other hand, this would have been an additional cost that may not be required for demonstrating and testing the setup.

As expected, case 6 achieves the highest oil temperature of all cases and has the second highest average power diverted to the heating element. However, the solar configuration for this case consisted of six PV panels, compared to three PV panels in cases 1.1, 1.2, 1.3, case 4.1 and 4.2. This gave the setup a basis to utilize the relatively low solar irradiation, which had a lower average value than most of the other cases. Additionally, the rig also had a low oil level. However, this setup could have reached a significantly higher temperature if a regular heating element had been used. The rapidly increasing internal resistance of the PTC element was a limiting factor, as the operating temperature of the system exceeded the design temperature of the heating element. It seems that case 6 should have reached 230 °C within the duration of the experiment, regarding the calculation of the theoretical time to reach 230 °C. However, this calculated value is based on an average power to load, without considering the gradually increasing internal resistance of the heating element.

Case 5 had the highest average solar irradiation of the cases performed with 24.24 L of oil but the lowest average power to heating elements. The high average solar irradiation is most likely a consequence of the short duration of the experiment. The low average power may be the controller not managing to reduce the high voltage to an optimal operating point. As seen from the corresponding IV-curve in Figure 4.49 the heating elements are not a good match to the solar configuration, which causes poor regulation from the controller and a very low duty cycle.

The theoretical time for case 5 to reach 230 °C is the longest for all the cases. If the duration of this case had lasted longer with the high solar irradiation, it might have increased the average power to the load. However, since the average power diverted to the load is very low compared to the other cases, this may not be the result. The rapidly increasing heatsink temperature indicates that most of the power is accumulated in the controller, causing overheating after only a couple of minutes.

It can be seen from Table 5.1 that the closer the experiments are performed to the summer, the higher the solar irradiation is. This observation corresponds to the yearly average solar irradiation per day given in Figure 4.1. The exception is case 4, where the solar irradiation is higher for the experiment the day in advance. This is, however, due to clouds. If the conditions had been ideal, the solar irradiation would most likely have been similar to the day in advance.

Based on this, performing all experiments closer to summer would most likely provide better results. The findings revealed considerable differences in the solar irradiation, which significantly impacted the oil temperature. Furthermore, from January until the end of May, there have been few days with a clear sky. The weather conditions in Trondheim have been a limiting factor for the experimental work. It is essential to have solid solar irradiation for several hours to reach the operating temperature. Therefore, experiments have been performed on clear days in the winter months and on days where clouds have occurred. This was necessary for the thesis to progress and stay within the time limit.

Although none of the cases reached the operating temperature with PV panels as the only power source, a more efficient operation might be achieved with some modifications. By investigation of the cooldown, thermal imaging, and calculation of the u-value, large heat losses were identified. The experiments also revealed that the tank struggles to maintain high temperatures and that much of the power from the PV panels are used to maintain the temperature without further increasing it. By improving insulation, the tank should be able to store heat and maintain high temperatures. However, this should be done by professionals, as previous attempts have failed to provide sufficient insulation.

This is essential for use in low irradiation areas, such as Norway, as the area of use most likely would be at remote cabins. If this system is installed, the tank must be able to store and accumulate heat over time, as a long time might elapse between use. This is essential as the results disclosed that the system could not reach the operating temperature under the given solar conditions in one day. Investigation of the cooldown revealed that almost all the heat produced in one day is lost during the night. This implies that the system cannot accumulate heat over time without further improvement of the insulation.

As seen from the IV-curve the installed heating elements did not match all solar configurations. This was also probably contributing to the relatively low oil temperatures achieved. A thorough investigation of different heating elements and local solar conditions could improve efficiency. According to the results, the installed heating elements have low resistance, which causes poor regulation of the controllers because of the low solar irradiation in many of the experiments. If heating elements that match the solar configuration, controller rating, and solar conditions are selected, the controller would be able to regulate the power properly and accordingly increase the operational efficiency. This has, however, not been tested as this would require the installation of new heating elements. As a result of the limited time and only a few days with sufficient solar conditions, this was not included in the experimental work.

The findings regarding the implementation of a wind turbine revealed minimal power production and limited potential for the implementation of a wind turbine as a secondary power source. This could be a consequence of poor wind conditions at the turbine location. The wind turbine was ordered in February to have enough time for installation and testing. However, due to HSSE causes, the lab employees had to install the turbine. The turbine needed a steel pole and mounting before it could be installed on the roof of the Thermal Laboratory, which could only be welded by the laboratory staff. An additional delay occurred as the turbine could not be mounted until an external company had finished their work. This work took longer than expected and was not completed until April, which significantly reduced the time to test the wind turbine.

Even in good wind conditions, the control unit of the wind turbine is a limiting factor, as the turbine breaks when the batteries are fully charged. This prevents the turbine from diverting excess power to the storage tank, which is one of the main benefits of the three-tank system. However, low power production indicates that a wind turbine is not feasible as a secondary power source under the given conditions. On the contrary, a wind turbine might serve as a secondary power source if the conditions are good. Such a solution could be advantageous in cabins when solar irradiation is low, and power needs to be stored for a long time. Although, implementing a wind turbine would require a battery, which contributed to lower power according to the findings.

Based on these findings, implementing a wind turbine in Tanzania would not be feasible, as expansion of solar capacity would be a better solution to increase capacity. Limiting solar conditions in Trondheim and Norway would most likely not be an issue in Tanzania, as solar irradiation and solar hours are evenly higher throughout the year. To implement such a system in Tanzania, the availability of materials, costs, and complexity are limiting factors. The system is more prone to theft by including a battery, as this increases the value. Additionally, the oil is considered valuable, which makes the drainage and theft of oil a possible issue.

On this basis, a battery-less solution is considered more beneficial for implementation in Tanzania. However, a limitation of this system is the complexity. It requires some knowledge and technical insight to operate the system due to the many components and valve openings. This makes implementation even harder, as new methods often are met with some resistance from the local population. Implementing a large-scale three-tank system for use in institutional canteens could, hence, be a better solution. This would most likely require less training of operators and reduce the risk of theft. In addition, it may contribute to a faster development of the solution.

7 Conclusion

This master thesis is a continuation of previous work regarding the three-tank system and the work towards a storage solution for solar cookers. The overall aim of the project is to develop a sustainable cooking solution for implementation in Tanzania. Based on this, the objective of the master thesis has been to demonstrate the concept of PV to high-temperature heat storage.

This concept was demonstrated, however, the poor solar conditions limited the period of experimental work. Consequently, the operating temperature was never reached with PV panels as the only power source. Based on the findings, this is due to a too low resistance of the installed heating elements. The heating elements did not match the solar conditions, causing poor regulation by the controllers. New heating elements were not installed due to limited time and resources at the lab. It is, however, anticipated that conducting the experiments with heating elements with suitable resistance would provide higher efficiency. A separate test of the PTC heating element revealed that the elements are not suitable for the system due to the low design temperature.

Through experimental work the *Geysewise* MPPT controller was proven suitable for the three-tank system. This created a valuable basis for the future implementation of the system. Based on an average solar irradiation in Trondheim of 200 W/m^2 on a sunny day, the 48 V MPPT controller should be combined with three 260 W PV panels in parallel and heating elements with a resistance of 4.9Ω to achieve optimal regulation.

Implementation of a wind turbine in the system provided a minimal capacity increase, as it produced a low amount of power. This was a consequence of poor wind conditions during the project work and the unfavourable placement of the turbine. The turbine produced power after sunset, making the turbine suitable as a secondary power source. However, the power produced is too low to benefit the system. Implementing a wind turbine in Tanzania would not be feasible, as expanding the solar capacity is considered more beneficial.

Since the oil and valuable parts of the system are prone to theft in Tanzania, it is considered more feasible to implement the existing system in Norwegian cabins. The high demand for maintenance, the availability of materials and costs are also challenges that must be solved before the system can be implemented in Tanzania. A solution including a battery would, hence, not be applicable for households in Tanzania due to the high costs. Accordingly, the implementation of a battery-less system on a larger scale would be most advantageous for the further development of the system in Tanzania.

Regardless of where the system is used, heat loss must be reduced. The results revealed that the tank struggled to maintain high temperatures, making it unable to reach the operating temperature. This is especially important if the system is implemented in cabins, where heat accumulates over time. If this challenge is overcome, the system holds great potential for utilization of excess energy in off-grid solar systems.

8 Further Work

During the period of the experimental work regarding this master thesis, weather conditions have been a limiting factor. Due to this, all of the planned tests have not been performed. Particularly a test of the three-tank system with both wind and solar power should be performed to examine the efficiency and potential of the system with multiple power sources. Before testing the system as a hybrid solution, the Netatmo weather station should be calibrated to investigate and define the uncertainty. This could be done by mounting it beside the remote weather station and comparing the data.

Based on the presented findings, the installed heating elements are not a good fit for the examined system setup with the current weather conditions. If further experimental work is performed on the three-tank system at NTNU, the heating elements should be changed. The presented IV-curves revealed that heating elements with a higher resistance would be a better match for the local weather conditions.

As changing the heating elements in the three-tank system is a time-consuming task, the setup could be tested with external heating elements or with elements installed in other off-grid cooking systems developed at NTNU. Such a test would provide valuable insight regarding the operation of the three-tank system and other similar cooking solutions.

Before the three-tank system could be implemented in either Tanzania or colder climates, the insulation must be improved. The findings in this master thesis disclosed that the system could not maintain high temperatures over time, which is a prerequisite for implementing the system. The insulation should be refurbished by an insulation company to ensure better performance, as students have tried to improve the current insulation without success.

References

- [1] The World Bank. *Access to electricity (% of population) - Tanzania*. 2022. URL: https://data.worldbank.org/indicator/EG.ELC.ACCS.ZS?locations=TZ&name_desc=false Accessed on: 04/26/2022.
- [2] IEA. *Tanzania Energy Outlook*. URL: <https://www.iea.org/articles/tanzania-energy-outlook> Accessed on: 04/26/2022.
- [3] N. Doggart et al. “The influence of energy policy on charcoal consumption in urban households in Tanzania”. In: (2020). URL: <https://www.sciencedirect.com/science/article/pii/S0973082620302556> Accessed on: 04/03/2022.
- [4] M. Mangula, J. Kuzilwa, and I. Legonda. “Energy Sources for Cooking and the Determinants of its Choices in Rural Areas of Tanzani”. In: (2019). URL: <https://ticd.ac.tz/wp-content/uploads/2020/10/ENERGY-SOURCE.pdf> Accessed on: 03/08/2022.
- [5] WHO. *Household air pollution and health*. 2021. URL: <https://www.who.int/news-room/fact-sheets/detail/household-air-pollution-and-health> Accessed on: 04/23/2022.
- [6] Q. Heist. *Deforestation in Tanzania Threatens the Future of Forests*. URL: <https://projectgaia.com/deforestation-in-tanzania-threatens-the-future-of-forests/> Accessed on: 02/01/2022.
- [7] WWF. *Deforestation and Forest Degradatio*. 2022. URL: <https://www.worldwildlife.org/threats/deforestation-and-forest-degradation> Accessed on: 04/23/2022.
- [8] A. Dean. *Deforestation and the carbon cycle*. 2019. URL: <https://www.climatecouncil.org.au/deforestation/> Accessed on: 01/30/2022.
- [9] SmartSolar Tanzania. *Solar Power Potential Tanzania*. URL: <http://www.smartsolar-tanzania.com/solar-sector-information/solar-power-potential-tanzania/> Accessed on: 02/25/2022.
- [10] WHO. *Access to clean fuels and technologies for cooking, rural (% of rural population) - Tanzania*. URL: <https://data.worldbank.org/indicator/EG.CFT.ACCS.RU.ZS?locations=TZ> Accessed on: 04/20/2022.
- [11] U.S Department of Energy. *Off-Grid or Stand-Alone Renewable Energy Systems*. URL: <https://www.energy.gov/energysaver/grid-or-stand-alone-renewable-energy-systems> Accessed on: 04/17/2022.
- [12] O.K.S.Fjelsdæter and V.S.Stordal. “Photovoltaic Solar Cooker with Heat Storage”. Master Thesis. NTNU, 2020. URL: <https://ntnuopen.ntnu.no/ntnu-xmlui/handle/11250/2779654>.
- [13] S. Thaule, M. Koledrup, and K. Gustafson. “Excess solar, wind, and hydro power to charge heat storage for cooking”. Master thesis. NTNU, 2019. URL: <https://ntnuopen.ntnu.no/ntnu-xmlui/handle/11250/2621469>.
- [14] K. Berg and A. A. Vik. “Small Scale PV Solar Cooker”. Unpublished work. Dec. 2021.
- [15] S. A. Kalogirou. *Solar Energy Engineering*. 2nd ed. Academic Press, 2014. URL: <https://www.sciencedirect.com/science/article/pii/B9780123972705000091#t0020> Accessed on: 07/03/2022.

- [16] Dr. L. E. Chaar. *Power Electronics Handbook*. 3rd ed. Butterworth Heinemann, 2011. URL: <https://www.sciencedirect.com/science/article/pii/B9780123820365000276> Accessed on: 03/30/2022.
- [17] T. Matuska and B. Sourek. “Performance Analysis of Photovoltaic Water Heating System”. In: (2017). URL: https://www.researchgate.net/publication/317053567_Performance_Analysis_of_Photovoltaic_Water_Heating_System Accessed on: 03/08/2022.
- [18] T. Watkins et al. “Insulated Solar Electric Cooking – Tomorrow’s healthy affordable stoves?” In: (2017). URL: <https://www.sciencedirect.com/science/article/pii/S2352728516300653> Accessed on: 04/03/2022.
- [19] A. Perrett. “An Investigation Into the Potential of DC Solar-Powered Cook Stoves with Tanzanian Food Vendors”. In: (2020). URL: <https://mecs.org.uk/wp-content/uploads/2020/12/MECS-Working-Paper-DC-Solar-Cooking-in-Mwanza-Sep-20.pdf>.
- [20] S. Batchelor et al. “Solar e-Cooking: A Proposition for Solar Home System Integrated Clean Cooking”. In: (2018). URL: <https://www.mdpi.com/1996-1073/11/11/2933/html> Accessed on: 03/08/2022.
- [21] J. Barton. *Exploring methods to divert excess solar power for water heating*. URL: <https://mecs.org.uk/blog/exploring-methods-to-divert-excess-solar-power-for-water-heating/> Accessed on: 01/23/2021.
- [22] N. Hoseck. *Wind and Solar Hybrid Systems For Off Grid Power: What You Need To Know*. URL: <https://www.primalsurvivor.net/wind-solar-hybrid-system/> Accessed on: 05/06/2022.
- [23] Byggehytte. *Noen erfaringer med Vindgenerator*. 2015. URL: <https://byggehytte.no/index.php?topic=1585.0> Accessed on: 03/04/2022.
- [24] H. R. Olsen. “Mulighetsstudie: Bruk av distribuert fornybar energiproduksjon på norske turisthytter”. Master thesis. NMBU, 2013. URL: <https://nmbu.brage.unit.no/nmbu-xmloi/handle/11250/188957?locale-attribute=no>.
- [25] Byggehytte. *Råd for valg av laderegulator med dump/shunt load regulator*. 2021. URL: <https://byggehytte.no/index.php?topic=3014.0> Accessed on: 02/20/2022.
- [26] C. B. Lwiwa. “Analysis of the Cooking Energy Demands for Urban Institutions in Tanzania”. Unpublished work. May 2022.
- [27] DBK Industrial. *PTC Heating Technology*. URL: <https://www.dbk-group.co.uk/ptc-heating> Accessed on: 02/11/2022.
- [28] DBK Industrial. *PTC Heating Technology*. URL: <https://www.dbk-group.co.uk/wire-heating> Accessed on: 05/06/2022.
- [29] DBK Industrial. *FAQ*. URL: <https://www.dbk-group.co.uk/faq-technologies> Accessed on: 05/06/2022.
- [30] DBK Industrial. *PTC thermistors as heating elements*. URL: https://www.tdk-electronics.tdk.com/inf/55/db/PTC/PTC_Heating_B59102_R102.pdf Accessed on: 05/06/2022.
- [31] Orbic Solar. *PTC and PV Heating Water*. URL: <https://www.orbicsolar.com/ptc-pv-water-heating/> Accessed on: 05/06/2022.
- [32] Xtend Elements. *Heat up test*. URL: <https://xtendelements.co.za/heat-up-test/> Accessed on: 05/06/2022.

- [33] 4x4 community. *Using a DC powered PTC element to heat water (successfully)*. URL: <https://xtendelements.co.za/heat-up-test/> Accessed on: 05/06/2022.
- [34] Powerforum. *Heating water from PV system*. URL: <https://powerforum.co.za/topic/3031-heating-water-from-pv-system/> Accessed on: 05/06/2022.
- [35] U.S Department of Energy. *Off-Grid or Stand-Alone Renewable Energy Systems*. URL: <https://www.energy.gov/energysaver/grid-or-stand-alone-renewable-energy-systems> Accessed on: 03/30/2022.
- [36] U.S Energy Information Administration. *What is energy? Sources of energy*. URL: <https://www.eia.gov/energyexplained/what-is-energy/sources-of-energy.php> Accessed on: 02/23/2022.
- [37] Our World in Data. *Electricity Mix*. URL: <https://ourworldindata.org/electricity-mix> Accessed on: 02/23/2022.
- [38] Hive Power. *Grid Stability Issues With Renewable Energy Sources, How They Can Be Solved*. URL: <https://hivepower.tech/grid-stability-issues-with-renewable-energy-how-they-can-be-solved/> Accessed on: 02/23/2022.
- [39] National Geographic Encyclopedia. *Wind Energy*. URL: <https://www.nationalgeographic.org/encyclopedia/wind-energy/> Accessed on: 02/18/2022.
- [40] U.S Department of Energy. *How a Wind Turbine Works - Text Version*. URL: <https://www.energy.gov/eere/wind/how-wind-turbine-works-text-version> Accessed on: 02/18/2022.
- [41] J. F. Manwell. *Wind Energy Explained: Theory, Design and Application*. 2nd ed. Wiley, 2009. URL: http://ee.tlu.edu.vn/Portals/0/2018/NLG/Sach_Tieng_Anh.pdf Accessed on: 02/18/2022.
- [42] M. Doble and A. K. Kruthiventi. "Alternate Energy Sources". In: (2022). URL: <https://www.sciencedirect.com/topics/earth-and-planetary-sciences/solar-energy> Accessed on: 02/24/2022.
- [43] Fortum. *Solar power - unlimited source of energy*. URL: <https://www.fortum.com/about-us/our-company/our-energy-production/solar-power-unlimited-source-energy> Accessed on: 02/24/2022.
- [44] Solenergiklyngen. *Om solenergi*. URL: <https://www.solenergiklyngen.no/omsolenergi/> Accessed on: 02/25/2022.
- [45] Norsk solcelleforening. *Solceller*. 2019. URL: <https://www.solenergi.no/solstrm> Accessed on: 02/24/2022.
- [46] Statkraft. *Renewable: Balancing with batteries*. URL: <https://www.statkraft.com/newsroom/news-and-stories/archive/2018/renewable-balancing-with-batteries/> Accessed on: 02/25/2022.
- [47] A. Skaaland, M. Rieke, K. Wallevik, and A. G. Imenes. "Potential and Challenges for Building Integrated Photovoltaics in the Agder Region". In: (2019). URL: https://www.researchgate.net/figure/Daily-mean-solar-energy-received-by-a-horizontal-surface-in-Norway-2-in-January-left_fig4_268487729 Accessed on: 02/24/2022.
- [48] H. Karoliussen. "TFNE1001 Fornybar Energi Grunnkurs - Solenergi". In: (2018).

- [49] Morningstar. *What is a solar charge controller?* URL: <https://www.morningstarcorp.com/faq/what-is-solar-charge-controller/> Accessed on: 02/22/2020.
- [50] Alencon Systems, LLC. *What Does a PV Charge Controller Do? How Can You Use One?* URL: https://alenconsystems.com/learning/pv-charge/?fbclid=IwAR1LSQbUI9CuD_qqqqtNCPwjNN5fuexKR1QSZoY2vK9s0PnyqPVbEFy4fMI Accessed on: 02/22/2020.
- [51] Clean energy review. *MPPT Solar Charge Controllers Explained.* URL: <https://www.cleaneenergyreviews.info/blog/mppt-solar-charge-controllers?fbclid=IwAR25BMQXi0EE7cMbiWsCcc9Dfw-UmC2VZUsH3ZTjGfwjDwReVsktYH1i5mY> Accessed on: 02/22/2020.
- [52] Morningstar. *What are the Different Types of Solar Charge Controllers?* URL: <https://www.morningstarcorp.com/faq/what-are-the-different-types-of-solar-charge-controllers/> Accessed on: 02/22/2020.
- [53] SunWize. *Solar Charge Controller Types.* URL: <https://www.sunwize.com/tech-notes/solar-charge-controller-types/> Accessed on: 02/14/2022.
- [54] Scientek. *The role and working principle of the MPPT charge controller.* URL: <https://www.scientekpower.com/news/516.html> Accessed on: 02/14/2022.
- [55] V. Xuem and L. Shu. "Different Control Mode for Synchronization Buck or Boost Topology by Using C2000 MCU". In: (2013). URL: https://www.ti.com/lit/an/sprabt6/sprabt6.pdf?ts=1654341277452&ref_url=https%253A%252F%252Fwww.google.com%252F.
- [56] Leading Edge. *How diversion charge controllers and dump loads work.* URL: <https://www.leadingedgepower.com/news/2013/how-diversion-charge-controllers-and-dump-loads-work.html> Accessed on: 02/14/2022.
- [57] University of Calgary. *Intermittent electricity.* URL: https://energyeducation.ca/encyclopedia/Intermittent_electricity Accessed on: 03/01/2022.
- [58] A. Suratsawadee, S. Sukruedee, C. Sirisamphanwong, and N. Ketjoy. *Comparison the Economic Analysis of the Battery between Lithium-ion and Lead-acid in PV Stand-alone Application.* Science direct, 2014. URL: <https://www.sciencedirect.com/science/article/pii/S1876610214010297> Accessed on: 04/26/2022.
- [59] Max fritid engros AS. *SR550 Dual Fritidsbatteri 115 Ah.* URL: <https://www.maxfritid.no/produkter/elektrisk/batteri/fritidsbatteri/batteri-fritid-dual-115ah-exide-sonnak-sr-550/> Accessed on: 04/26/2022.
- [60] C. B. Honsberg and S. G. Bowden. *Lead Acid Batteries.* URL: <https://www.pveducation.org/pvcdrom/batteries/lead-acid-batteries> Accessed on: 03/07/2022.
- [61] Battery University. *How does the Lead Acid Battery Work?* URL: <https://batteryuniversity.com/article/bu-201-how-does-the-lead-acid-battery-work> Accessed on: 03/07/2022.
- [62] Electronics-notes. *How Do Lead Acid Batteries Work.* URL: https://www.electronics-notes.com/articles/electronic_components/battery-technology/how-do-lead-acid-batteries-work-technology.php Accessed on: 03/07/2022.
- [63] Powersonic. *How to charge a lead acid battery.* URL: <https://www.power-sonic.com/blog/how-to-charge-a-lead-acid-battery/> Accessed on: 03/07/2022.
- [64] Battery University. *BU-903: How to Measure State-of-charge.* URL: <https://batteryuniversity.com/article/bu-403-charging-lead-acid> Accessed on: 03/07/2022.

- [65] K. Mongird, V. Viswanathan, J. Alam, C. Vartanian, V. Sprengle, and R. Baxter. “2020 Grid Energy Storage Technology Cost and Performance Assessment”. In: (2020). URL: <https://www.pnnl.gov/sites/default/files/media/file/Final%20-%20ESGC%20Cost%20Performance%20Report%2012-11-2020.pdf>.
- [66] BatteriesInAFlash. *DEEP CYCLE BATTERY FAQ*. 2022. URL: <https://www.batteriesinaflash.com/deep-cycle-battery-faq> Accessed on: 04/27/2022.
- [67] M. Hasanuzzaman and N. A. Rahim. “Energy storage technologies - Energy for Sustainable Development”. In: (2021). URL: <https://www.sciencedirect.com/topics/engineering/sensible-heat-storage> Accessed on: 02/11/2022.
- [68] Lumen Learning. *The Second Law of Thermodynamics*. URL: <https://courses.lumenlearning.com/boundless-physics/chapter/the-second-law-of-thermodynamics/> Accessed on: 11/30/2021.
- [69] N. Connor. *What is Heat Loss – Definition*. URL: <https://www.thermal-engineering.org/what-is-heat-loss-definition/> Accessed on: 01/30/2022.
- [70] PVsyst. *METEO DATA SOURCE*. URL: <https://www.pvsyst.com/meteo-data-source/> Accessed on: 05/05/2022.
- [71] Thermometrics. *TYPE K THERMOCOUPLE*. 2012. URL: <https://www.thermometricscorp.com/thertypk> Accessed on: 03/25/2022.
- [72] Lumen Learning. *Ha oversikt over klimamålingene på smarttelefonen*. URL: <https://www.netatmo.com/no-no/weather/weatherstation> Accessed on: 06/05/2022.

A Manuals and Data Sheets

Table A.1: Manuals and data sheets for the components used for the experimental work.

| Product | Name | Downloaded from: | Date downloaded |
|---|--|----------------------------------|-----------------|
| PV panels | Solartek solcellepaneler | Getek.no/SOLARTEKstandard | 04.02.22 |
| Duratherm 630 safety data | Safety Data Sheet (SDS) | Durathermfluids.com/safetydata | 04.02.22 |
| Duratherm 630 Technical data | Duratherm 630 | Duratherm.com/productdata | 04.02.22 |
| Tristar PWM controller | Installation, Operation and Maintenance Manual | Morningstarcorp.com/Tristar | 19.01.22 |
| Lead-acid batteries | Brosjyre - Marine & Fritidsbatterier | Exidegroup.com/Sønnak-Marine | 15.03.22 |
| Geyserville controller and PTC elements | PV System installers guide | Geyserville.com/PV-system-manual | 04.02.22 |

B PV panel configurations with heating elements

In this appendix the IV-curve of the utilized PV panels is displayed, which is based on information from the Solartek manual linked in Appendix A. Heating elements rated at 24 V with different resistances are plotted in the same graph to illustrate which element that would provide the highest efficiency of the system in each case as this is dependent on both solar irradiation and configuration of the solar array.

All tests except case 6 are performed with two 500 W 24 V heating elements connected in series, resulting in a total resistance of 2.54 Ω. This is due to practical reasons and time limitation, as these elements already are installed in the three-tank system. Figure B.1 shows the IV-curve for a single panel for different solar conditions. Heating elements with different resistances are plotted in the same graph, using values given in Table B.1.

Table B.1: Resistance calculations

| Solar irradiation [W/m^2] | Voltage [V] | Current [A] | Resistance ($R=U/I$) [Ω] |
|-------------------------------|-------------|-------------|-------------------------------------|
| – | 24 | 9.45 | 2.54 |
| 800 | 24 | 6.40 | 3.75 |
| 600 | 24 | 4.90 | 4.90 |
| 400 | 24 | 3.20 | 7.50 |
| 200 | 24 | 1.70 | 14.10 |

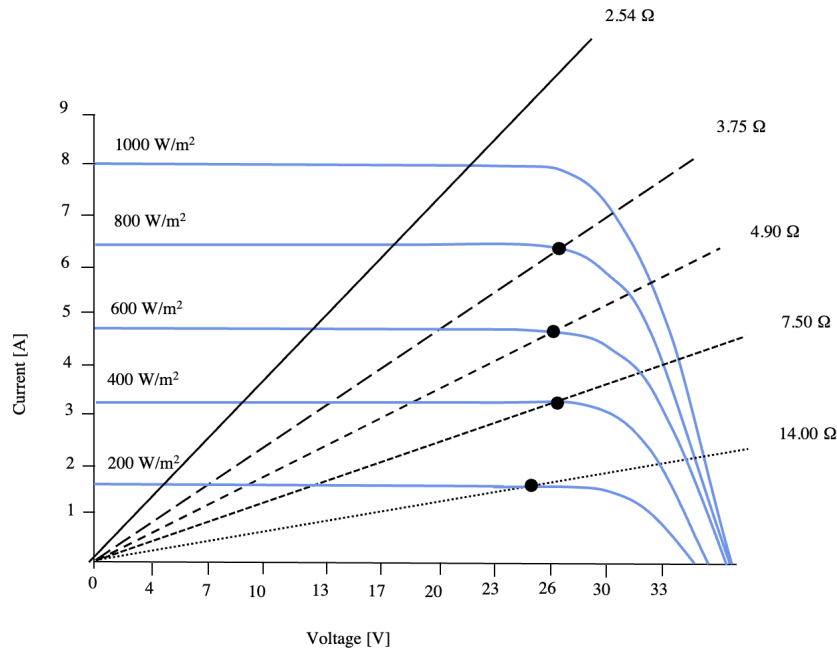


Figure B.1: IV-curve for a Solartek PV panel with different heating elements and solar irradiation.

C Wind turbines

Table C.1: Specifications of evaluated Wind turbines. Compatibility is here defined as the ability to operate with the Tristar controller, with or without a separate control unit for the wind turbine.

| Product | Producer | Power [W] | Voltage [V] | Cut-in speed [m/s] | Compatible regulator | Price [NOK] | Available at |
|---------------------|------------------|-----------|-------------|--------------------|------------------------------|-------------|---------------------|
| [-] | [-] | [W] | [V] | [m/s] | [-] | [NOK] | [-] |
| AirNordic 400W 24V | AirNordic | 400 | 24 | 2 | Tristar hybrid | 10 999 | Hyttetorget.no |
| SilentWind 400W 24V | SilentWind | 400 | 24 | 2 | MPPT | 19 932 | Hoydebutikken.no |
| SunWind 24V X400 | SunWind | 400 | 24 | 2.5 | Hybrid regulator included | 9 499 | Sparelys.no |
| Air-30 Land 24V | Primus Windpower | 400 | 24 | 3.58 | Tristar hybrid | 11 000 | Alternativenergi.no |
| LE-450 Vindturbin | Leading Edge | 450 | 24 | 3 | Tristar hybrid | 14 999 | Vannhandel.no |
| Rutland 1200T | Rutland | 483 | 24 | 3 | Rutland hybrid MPPT included | 14 500 | Alternativenergi.no |

D Design of test rig

The 1100 W PTC heating element is 90 cm long; thus, a cylinder-shaped steel pipe must be designed to safely perform a capacity test. A scenario where the oil is heated from 21 °C, T_i , to 230 °C, T_F , in 30 minutes at 1.1 kW was taken as the starting point for the calculations. Then the amount of oil needed to reach 230 °C under the given conditions is determined by Equation 3.8, derived in Equation D.1. The heating capacity and density were found from the technical data sheet for Duratherm 630 linked in Appendix A.

$$m = \frac{Q_s}{(C_{p,f} \cdot T_f - C_{p,i} \cdot T_i)} = 2.62 \text{ kg} = 3500 \text{ cm}^3 \quad (\text{D.1})$$

From this volume by using Equation 3.16, the minimum required diameter of the cylinder was calculated and derived in Equation D.2. The height of 90 cm was used, in order to cover the length of the heating element, $h_{element}$.

$$d = \sqrt{\frac{V_{oil}}{\pi \cdot h_{element}}} \cdot 2 = 7 \text{ cm} \quad (\text{D.2})$$

This diameter was used to evaluate the design diameter of the cylinder. To have a safety margin, an inner diameter of 10 cm and an outer diameter of 10.4 cm were chosen. To determine the height of the cylinder, the volume of oil required at an initial temperature of 21 °C, needed to be calculated. The volume of the heating element itself was subtracted when calculating the initial oil volume at V_{21} . Where the radius of the heating element was 0.075 cm and the height was 90 cm. To calculate this volume Equation 3.16 was utilized and derived in Equation D.3.

$$V_{21} = (A_{cylinder} - A_{element}) \cdot h_{21} = 7066 \text{ cm}^3 = 7.066 \cdot 10^{-3} = 7.066 \text{ L} \quad (\text{D.3})$$

Amount mass of oil needed at 21 °C is calculated by Equation 3.9. This is given in Equation D.4.

$$m = V_{21} \cdot \rho_{21} = 6.11 \text{ kg} \quad (\text{D.4})$$

To account for the expansion of oil when heated to 230 °C, the volume at this temperature needed to be found. A calculation of volume at 230 °C is given in Equation D.5.

$$V_{240} = \frac{m}{\rho_{230}} = 8.45 \text{ L} \quad (\text{D.5})$$

The height of the oil at this volume could be calculated to determine the minimum height of the cylinder to account for expansion. This calculation was derived in Equation D.6.

$$h_{240} = \frac{V}{(A_{cylinder} - A_{element})} = 107.6cm \quad (D.6)$$

From this, the minimum cylinder height of 107.6 cm is required. However, a height of 114 cm was chosen to have a safety margin. According to Equation D.7 and the selected geometry of the designed cylinder, an expansion of 17.6 cm is observed.

$$h_{expansion} = h_{240} - h_{21} = 17.6cm \quad (D.7)$$

E Python script for calculation of u-value

```

1 import pandas as pd
2 import matplotlib.pyplot as plt
3 import numpy as np
4 import math #For mathematical functions
5
6 excell = r'C:\Experiment\26.05.22 sol mppt\cooldown.xlsx' #Importing excel values ...
       of the cooldown for a period of 10 hours
7 Cooldown = pd.read_excel(excell,1,skiprows=[i for i in ...
       range(1,24123)],skipfooter=126887)
8 time = Cooldown['Time']
9 Tm = Cooldown['Average temp']
10
11 h_oil= 0.130; #measured from glass cylinder
12 r_tank=0.207; #standard radius of tank 2
13 l_tank= 0.67; #standard length of tank 2
14
15 #Calculations from formulas in 3.7 Thermal energy storage and 3.8 Volume in tank
16 l=math.sqrt(r_tank**2-(h_oil-r_tank)**2); alpha=math.acos((h_oil-r_tank)/r_tank);
17 A_slice=math.pi*(r_tank**2)*(alpha/(2*math.pi))
18 A=A_slice-l*(h_oil-r_tank)/2;
19 A_oil=(2*math.pi*r_tank**2)-2*A;
20 V=A_oil*l_tank;
21 P_oil=2*math.pi*r_tank-2*math.pi*r_tank*alpha/(2*math.pi);
22 A_s=P_oil*l_tank+2*A_oil;
23
24 Tm=np.round(Tm)
25 n=0;a=1;i=1;t=[];T=[];T_amb=22
26 rho_226=801.92 #density at 124.66 degrees interpolated between 115 and 125
27 m=V*rho_226 #total mass of oil
28
29 for i in range(0,(len(Tm)-1)):
30     if Tm[i+1]<Tm[i]:
31         T.append(Tm[i])
32         t.append(n*30+30)
33         a=a+1
34         n=0
35     else:
36         n=n+1
37 Cp=[]
38 for i in range(0,len(T)):
39     Cp.append(((2.28042-1.948)*(T[i]-25)/(124-25))+1.948) #kJ/kgK using Cp for ...
       124 degrees and interpolates between 124 and 25 degrees to find Cp for ...
       each temperature step
40 U=[]
41 for j in range (0,len(T)):
42     U.append((m*Cp[j])/(A_s*t[j]*(T[j]-T_amb))*1000) #W/m^2*K
43
44 import statistics
45 print(statistics.mean(U))

```

F Risk assessment: Oil based heat storage rig



Risk Assessment Report

Oil based heat storage rig

| | |
|------------------------------|---|
| Project name | Excess energy to high temperature storage |
| Facility name | Oil based heat storage rig |
| Building and room number | VATL – Thermal Laboratory, C164 |
| Project leader | Ole Jørgen Nydal |
| Facility responsible | Ole Jørgen Nydal |
| HES coordinator | Morten Grønli |
| HES responsible | Terese Løvås |
| Risk assessment performed by | Kristina Berg and Andrea A. Vik |

Approval:

| | |
|---|-----------|
| Apparatur kort (UNIT CARD) valid for: | 12 months |
| Forsøk pågår kort (EXPERIMENT IN PROGRESS) valid for: | 12 months |

| Role | Name | Date | Signature |
|-----------------|------------------|--------|-----------|
| Project leader | Ole Jørgen Nydal | 3/2/22 | |
| HES coordinator | Morten Grønli | | |
| HES responsible | Terese Løvås | | |

TABLE OF CONTENTS

| | |
|--|---|
| INTRODUCTION | 1 |
| DESCRIPTIONS OF EXPERIMENTAL SETUP | 1 |
| EVACUATION FROM THE EXPERIMENTAL AREA | 2 |
| WARNING | 2 |
| Before experiments | 2 |
| Abnormal situation | 3 |
| ASSESSMENT OF TECHNICAL SAFETY | 4 |
| HAZOP | 4 |
| Flammable, reactive and pressurized substances and gas | 4 |
| Pressurized equipment | 4 |
| Effects on the environment (emissions, noise, temperature, vibration, smell) | 4 |
| Conclusion: The experiment shall not generate emission of smoke, gas, odor etc when operated properly. However, there should be a ventilation channel over the node of valves from the three tanks in case of improper operation. The oil should be stored safe in a designated container and considered as special waste when the experiments are done. | 4 |
| Radiation | 5 |
| Chemicals | 5 |
| Electricity safety (deviations from the norms/standards) | 5 |
| ASSESSMENT OF OPERATIONAL SAFETY | 5 |
| Procedure HAZOP | 5 |
| Operation procedure and emergency shutdown procedure | 6 |
| Training of operators | 6 |
| Technical modifications | 6 |
| Personal protective equipment | 6 |
| General Safety | 6 |
| Safety equipment | 7 |
| Special predations | 7 |
| QUANTIFYING OF RISK - RISK MATRIX | 8 |
| ATTACHMENT A: PROCESS AND INSTRUMENTATION DIAGRAM (PID) | 1 |
| ATTACHMENT B: HAZOP | 2 |
| ATTACHMENT C: PROCEDURE FOR RUNNING EXPERIMENTS | 5 |
| ATTACHMENT D: TRAINING OF OPERATORS | 6 |
| FORSØK PÅGÅR /EXPERIMENT IN PROGRESS | 9 |

1 INTRODUCTION

The experiment setup consists of three large steel tanks containing thermal oil (Duratherm 630). The upper tank, the cold reservoir, is initially filled with oil. The second tank is the heat storage, and contains two heating elements (24 V, 500 W). When the oil in the heat storage is sufficiently heated, a bimetallic spring will ensure the opening of a valve, resulting in flow of oil from the cold reservoir to the heat storage. The maximum temperature of the system will be approximately 220 °C. Moreover, all three tanks have a valve to ensure atmospheric pressure.

The purpose of the experiment is to check how much energy is needed to heat the oil (Duratherm 630) by heating it on an electric cooking plate. In addition, a new controller will be tested with solar panels installed on the roof of "Varmeteknisk". This controller will be connected to a 24 V battery to see how much electricity is needed to be stored, in order for the excess electricity to start preheating the three-tank system. The experimental set up will be the same as for previous experiments for this project, except that the rig is powered by PV panels and batteries.

The experimental rig is located at room C164, in Varmeteknisk Lab.

2 DESCRIPTIONS OF EXPERIMENTAL SETUP

The rig consists of the following components (see figure below):

1. Cold oil reservoir, upper tank
2. Heat storage mid tank, with a measurement of oil level.
3. Used oil reservoir, lower tank
4. Cooking arrangement
5. Two heating elements inside the tank. Rated 24V 500W
6. Valve for controlling flow out of heat storage
7. Power connection to controller and PV panels
8. Manually hand pump for transporting oil from lower reservoir to upper
9. Removable lid for refill of oil (and able to see inside tank)



Figure 1: Setup of the rig

The power supply to the heating elements are located at a distance to the rig, to ensure safe monitoring and shutdown of the system if necessary. The system is shut down by unplugging the power supply. Moreover, the system can be drained from oil by opening the valve under the lower tank.

3 EVACUATION FROM THE EXPERIMENTAL AREA

Evacuate at signal from the alarm system or local gas alarms with its own local alert with sound and light outside the room in question

Evacuation from the rigging area takes place through the marked emergency exits to the assembly point, (corner of Old Chemistry Kjelhuset or parking 1a-b.)

Action on rig before evacuation:

Turn off the power supply of the electrical heater by unplugging it.

4 WARNING

4.1 Before experiments

Send an e-mail with information about the planned experiment to:
experiments@ept.ntnu.no

The e-mail must include the following information:

- Name of responsible person:
- Experimental setup/rig
- Start Experiments: (date and time)
- Stop Experiments: (date and time)

Before startup, the laboratory management must have given approval. All running experiments are notified in the activity calendar for the lab to ensure they are coordinated with other activity.

4.2 Abnormal situation

FIRE

If you are NOT able to extinguish the fire, activate the nearest fire alarm and evacuate the area. Be then available for the fire brigade and building caretaker to detect the location of the fire..

If possible, notify:

| |
|---|
| NTNU |
| Morten Grønli, Mob: 918 97 515 |
| Terese Løvås: Mob: 918 97 007 |
| NTNU – SINTEF Beredskapstelefon: 800 80 388 |

GAS ALARM

If a gas alarm occurs, close gas bottles immediately and ventilate the area. If the level of the gas concentration does not decrease within a reasonable time, activate the fire alarm and evacuate the lab. Designated personnel or fire department checks the leak to determine whether it is possible to seal the leak and ventilate the area in a responsible manner.

PERSONAL INJURY

- First aid kit in the fire / first aid stations
- Shout for help
- Start life-saving first aid
- **CALL 113** if there is any doubt whether there is a serious injury

OTHER ABNORMAL SITUATIONS

NTNU:

You will find the reporting form for non-conformance on:

<https://innsida.ntnu.no/wiki/-/wiki/Norsk/Melde+avvik>

5 ASSESSMENT OF TECHNICAL SAFETY

Ensure optimal design of the apparatus with regards to technical safety. Identifying risks related to the design choices, and if necessary initiate re-design to eliminate as much risk as possible through technical security. A description of what the experimental setup can handle and acceptable emissions.

5.1 HAZOP

The experiment set up is divided into the following nodes:

| | |
|--------|---|
| Node 1 | Test the controller with solar panels installed on the roof of "Varmeteknisk" |
|--------|---|

ATTACHMENTS B: HAZOP

Conclusion: Full safety equipment should be used when experimenting/operating with hot oil, including full coverage clothing, gloves, protective footwear and protective glasses.

5.2 Flammable, reactive and pressurized substances and gas

Are any flammable, reactive and pressurized substances and gases in use?

| | |
|----|--|
| NO | |
|----|--|

Attachments: No attachment necessary.

Conclusion: No real dangers.

5.3 Pressurized equipment

Is any pressurized equipment in use?

| | |
|----|--|
| NO | |
|----|--|

ATTACHMENTS D: TEST CERTIFICATE FOR LOCAL PRESSURE TESTING

Conclusion:

5.4 Effects on the environment (emissions, noise, temperature, vibration, smell)

Will the experiments generate emission of smoke, gas, odour or unusual waste?

Is there a need for a discharge permit, extraordinary measures?

| | |
|----|--|
| NO | |
|----|--|

Attachments: No attachment necessary.

- **Conclusion:** The experiment shall not generate emission of smoke, gas, odor etc when operated properly. However, there should be a ventilation channel over the node of valves from the three tanks in case of improper operation. The oil should

be stored safe in a designated container and considered as special waste when the experiments are done.

- **Radiation**

| | |
|----|--|
| NO | |
|----|--|

Attachments: No attachments necessary

Conclusion: No real danger

5.5 Chemicals

Will any chemicals or other harmful substances be used in the experiments? Describe how the chemicals should be handled (stored, disposed, etc.) Evaluate the risk according to safety datasheets, MSDS. Is there a need for protective actions given in the operational procedure?

| | |
|-----|---------------------------|
| YES | Duratherm 630 thermal oil |
|-----|---------------------------|

Attachments: Material Safety Data Sheet

Conclusion: The oil used is a high heat transfer oil but is not dangerous for health. It is declared as to have no known significant effects or critical hazard, so it is safe to smell and touch, like the common oils for use in domestic houses. It is however not applicable for edible use.

5.6 Electricity safety (deviations from the norms/standards)

| | |
|----|--|
| NO | |
|----|--|

Attachments: No attachment necessary.

Conclusion: No real dangers.

6 ASSESSMENT OF OPERATIONAL SAFETY

Ensure that the procedures cover all identified risk factors that must be taken care of. Ensure that the operators and technical performance have sufficient expertise.

6.1 Procedure HAZOP

The method is a procedure to identify causes and sources of danger to operational problems. Procedure:

1. Put a tray in the bottom of the structure to avoid spills of hot oil.
2. Check for leaks by testing the system connections with cold oil.
3. Ensure that the heating elements are working properly.
4. Connecting the heating elements to a power supply that ensures the right power
5. Insulate some of the pipes and heating storage where necessary.
6. Use thermocouples in several places to ensure that the temperature monitored is correct.

ATTACHMENT C: HAZOP PROCEDURE

Conclusion: The procedure is safe, only needs to avoid contact with the hot elements during the heating of the oil.

6.2 Operation procedure and emergency shutdown procedure

The operating procedure is a checklist that must be filled out for each experiment. The emergency procedure should attempt to set the experiment set-up in a harmless state by unforeseen events.

ATTACHMENT E: PROCEDURE FOR RUNNING EXPERIMENTS

Emergency shutdown procedure: Pull out the plug connected to the heat element box (no power means no heat).

6.3 Training of operators

A Document showing training plan for operators

- *What are the requirements for the training of operators?*
- *What it takes to be an independent operator*
- *Job Description for operators*

Attachments: Training program for operators

6.4 Technical modifications

- The cooker is not insulated/closed properly, so the hot oil is open to air. Since water is used as the heating medium in the cooker and has a lower boiling point than the oil, it is extremely important to not spill any water into the oil to avoid water expanding in the hot oil.
- A hole is drilled in the storage tank to ensure atmospheric pressure, which increases the risk of spilling hot oil if water is present.

Conclusion: No water should enter the system, due to the low boiling point of water compared to oil. One must be careful when using water as the heating medium in the cooker.

6.5 Personal protective equipment

- *It is mandatory use of eye protection in the rig zone*
- Gloves should be used when handling the tubes, as some of them can be hot.
- Protective clothing should be used when doing experiments with hot oil.
- Protective shoes should be used when setting up the rig/moving heavy objects and when doing experiments with hot oil.

Conclusion: Plastic glasses and gloves are always necessary special equipment, while protective clothing and shoes should be used during experiments and testing.

6.6 General Safety

Warning signs must be close to the hot elements.

An operator must be controlling the rig.

Conclusion: Signs and monitoring by operator.

6.7 Safety equipment

There should be a welding screen (not flammable) located around the set up to protect from possible oil spill.

6.8 Special predations

One operator must be in the rig zone during tests to make sure the temperature is within safe range and that there are no major leaks.

7 QUANTIFYING OF RISK - RISK MATRIX

The risk matrix will provide visualization and an overview of activity risks so that management and users get the most complete picture of risk factors.

| IDnr | Activity | Consequence | Probability | RV |
|------|------------------------------|-------------|-------------|----|
| 1 | Contact with heating element | 2 | B | B2 |
| 2 | Oil leakage | 2 | B | B2 |
| 3 | Air pollution due to burnout | 3 | C | C3 |
| 4 | Hot oil in contact with skin | 1 | D | D1 |
| 5 | Fire in the storage tank | 2 | E | E2 |
| 6 | Small explosion in tank | 1 | D | D1 |

Actions:




- IDnr 3 requires ventilation above the rig during experiments/operation. Moreover, operators must be observant of the oil level in the storage tank as the outlet is not set over the heating elements in this rig.
- IDnr 4 requires adequate safety equipment; fully covering clothing, shoes, protective glasses and gloves during operation and experiments. Otherwise it would be of a greater probability and characterized as a D3 (unacceptable) risk.
- IDnr 5 is due to the use of variacs. We will not set up and handle the variacs as we do not have the competence to do so, approved personnel at the lab will do this for us so that the heating elements will not be provided with too high voltage. Too high voltage will in the worst case cause the heating elements to start burning.
- IDnr 6 will be caused by water in the tanks, because water has a much lower evaporation point than the thermal oil. It is very unlikely that we will get water into the tanks, however small explosions will increase the risk of hot oil splashing out of the tank. This is also a reason for the importance of wearing safety equipment.

Conclusion: The risk to people, environment and economy is all over considered to be small. The aim of the risk assessment is to avoid all the risks related to the experiments and operation of the system. Burn out is considered as an A1 (acceptable) risk in Tanzania, as the outlet of the storage tank is higher than the heating elements.

RISK MATRIX

| | | | | | | |
|-----------------------|------------------|----|----|----|----|----|
| C O N S E | (E) Catastrophic | E1 | E2 | E3 | E4 | E5 |
| | (D) Extensive | D1 | D2 | D3 | D4 | D5 |
| | (C) Moderate | C1 | C2 | C3 | C4 | C5 |

| | | | | | | |
|--|-------------------|--------------------|--------------|--------------|------------|--------------------|
| Q U E S T I O N | (B) Negligible | B1 | B2 | B3 | B4 | B5 |
| | (A) Insignificant | A1 | A2 | A3 | A4 | A5 |
| | | (1) Rare | (2) Unlikely | (3) Possible | (4) Likely | (5) Almost certain |
| | | PROBABILITY | | | | |

| COLOUR | | DESCRIPTION |
|---------------|---|--|
| Red |  | Unacceptable risk Action has to be taken to reduce risk |
| Yellow |  | Assessment area. Actions has to be considered |
| Green |  | Acceptable risk. Action can be taken based on other criteria |

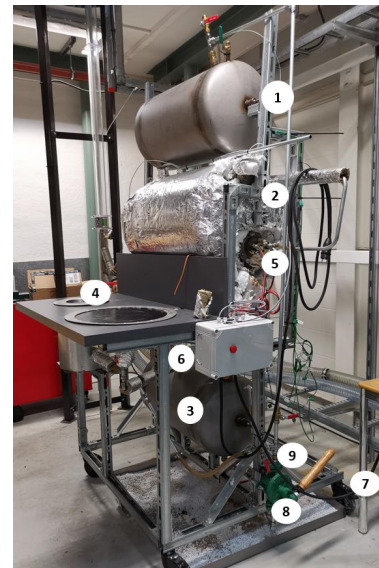
The principle of the acceptance criterion. Explanation of the colors used in the matrix.

● **ATTACHMENT A: PROCESS AND INSTRUMENTATION DIAGRAM (PID)**

The rig consists of the following components (see figure below):

- | |
|--|
| <ol style="list-style-type: none">1. Cold reservoir, upper tank2. Heat storage mid tank, including measurement of oil level3. Used oil reservoir, lower tank4. Cooking arrangement5. Two heating elements inside the mid tank. 24V, 500W6. Valve for controlling flow out of heat storage7. Power connection to controller and PV panels8. Manual hand pump for transporting oil from lower tank to upper tank9. Removable lid for refill of oil |
|--|

The power supply to the heating elements are located at a distance to the rig, to ensure safe monitoring and shutdown of the system if necessary. The system is shut down by unplugging the power supply. Moreover, the system can be drained from oil by opening the valve under the lower tank.



● ATTACHMENT B: HAZOP

| Project: Node: 1 | | | | | | | Page |
|---------------------|--------------------|--|-------------------------------------|--|---|--------|-----------|
| Ref # | Guideword | Causes | Consequences | Safeguards | Recommendations | Action | Date/Sign |
| 1 | No flow | Clogging in tubes | Por oil flow | | Use a thermal oil that does not become sticky | | |
| 2 | Reverse flow | Not relevant | | | | | |
| 3 | More flow | Not relevant | | | | | |
| 4 | Less flow | Temperature valve not correctly working | Overheating of the heating elements | Manual temperature control | | | |
| 5 | Higher level | Over filled | Risk of spilling hot or cold oil | Safety equipment | | | |
| 6 | Lower level | Leakage, under filled | Possible leaking of hot oil | Measure oil volume before experiment, safety equipment | | | |
| 7 | More pressure | | | | | | |
| 8 | Less pressure | | | | | | |
| 9 | Higher temperature | Increasing the oil temperature above autoignition point (368 °C) | Fire | Manual temperature control | | | |
| 10 | Lower temperature | Not relevant | | | | | |

| | | | | | | | |
|----|--------------------|---|---|---|---|--|--|
| 11 | Higher viscosity | Not relevant | | | | | |
| 12 | Lower viscosity | Not relevant | | | | | |
| 13 | Composition Change | Not relevant | | | | | |
| 14 | Contamination | Overcooking of oil in open environment | Smell in the lab | Manual temperature control | Use an oil without significant contamination effects | | |
| 15 | Relief | Leaks | Spill of oil | Manually check for leaks using cold oil | | | |
| 16 | Instrumentation | Not relevant | | | | | |
| 17 | Sampling | Not relevant | | | | | |
| 18 | Corrosion/erosion | Not relevant | | | | | |
| 19 | Service failure | Problems with heating elements | Overheating in the system or no heating | | | | |
| 20 | Abnormal Operation | Not relevant | | | | | |
| 21 | Maintenance | Bimetallic valve or heating elements not working properly | | Safety equipment during operation | | | |
| 22 | Ignition | Exceed autoignition point (368 °C) | Fire in the tank | Manual temperature control | Use safety equipment during experiment, ensure that a fire blanket is located close to the experimental setup | | |
| 23 | Spare equipment | Not relevant | | | | | |

| | | | | | | | |
|----|--------|--------------|--|--|--|--|--|
| 24 | Safety | Not relevant | | | | | |
|----|--------|--------------|--|--|--|--|--|

ATTACHMENT C: PROCEDURE FOR RUNNING EXPERIMENTS

| | | |
|--|-------------|-------------------------|
| Project Excess energy to high temperature heat storage | Date | Signature |
| Facility Oil based heat storage rig | | |
| Project leader Ole Jørgen Nydal | 31/2/22 | <i>Ole Jørgen Nydal</i> |

| | Conditions for the experiment: | Completed |
|--|--|--------------------|
| | Experiments should be run in normal working hours, 08:00-16:00 during winter time and 08.00-15.00 during summer time. Experiments outside normal working hours shall be approved. | |
| | One person must always be present while running experiments, and should be approved as an experimental leader. | |
| | An early warning is given according to the lab rules, and accepted by authorized personnel. | |
| | Be sure that everyone taking part of the experiment is wearing the necessary protective equipment and is aware of the shut down procedure and escape routes. | |
| | Preparations | Carried out |
| | Post the "Experiment in progress" sign. | |
| | <i>Start up procedure</i> | |
| | During the experiment | |
| | Always be aware of the temperature in the storage tank | |
| | Be observant of any leakage | |
| | Be aware of hot surfaces | |
| | End of experiment | |
| | Tidy up and return all tools and equipment | |
| | Tidy and cleanup work areas | |
| | Remove all obstruction/barriers/signs around the experiments | |
| | Remove all obstructions/barriers/signs around the experiment. | |
| | Tidy up and return all tools and equipment. | |
| | Tidy and cleanup work areas. | |
| | Return equipment and systems back to their normal operation settings (fire alarm) | |
| | To reflect on before the next experiment and experience useful for others | |
| | Was the experiment completed as planned and on schedule in professional terms? | |
| | Was the competence which was needed for security and completion of the experiment available to you? | |
| | Do you have any information/ knowledge from the experiment that you should document and share with fellow colleagues? | |

Operator(s):

| Navn | Dato | Signatur |
|----------------|----------|----------------|
| Kristina Berg | 02.02.22 | Kristina Berg |
| Andreas A. Vik | 02.02.22 | Andreas A. Vik |

ATTACHMENT D: TRAINING OF OPERATORS

| | | |
|--|-------------|-------------------------|
| Project Excess energy to high temperature heat storage | Date | Signature |
| Facility Oil based heat storage rig | | |
| Project leader Ole Jørgen Nydal | 31/2/22 | <i>Ole Jørgen Nydal</i> |

| | |
|--|--|
| Knowledge about EPT LAB in general | |
| Lab | |
| <ul style="list-style-type: none"> • Access • routines and rules • working hour | |
| Knowledge about the evacuation procedures. | |
| Activity calendar for the Lab | |
| Early warning, experiments@ept.ntnu.no | |
| | |
| Knowledge about the experiments | |
| Procedures for the experiments | |
| Emergency shutdown. | |
| Nearest fire and first aid station. | |
| | |
| | |
| | |

I hereby declare that I have read and understood the regulatory requirements, have received appropriate training to run this experiment and are aware of my personal responsibility by working in EPT laboratories.

Operator(s):

| | Navn | Dato | Signatur |
|--|---------------|----------|----------------------|
| | Kristina Berg | 02.02.22 | <i>Kristina Berg</i> |
| | Andrea A. Vik | 02.02.22 | <i>Andrea A. Vik</i> |

APPARATURKORT / UNITCARD

Dette kortet SKAL henges godt synlig på apparaturen!
This card MUST be posted on a visible place on the unit!

| | |
|--|--|
| Apparatur (Unit) | |
| Prosjektleder Ole Jørgen Nydal | Telefon mobil/privat (Phone no. mobile/private) |
| Apparaturansvarlig Ole Jørgen Nydal | Telefon mobil/privat (Phone no. mobile/private) |
| Sikkerhetsrisikoer Hot surfaces Oil fumes Heated oil | |
| Sikkerhetsregler (Safety rules) Use safety gloves and goggles Do not touch the rig without approval of the operator | |
| Nødstop prosedyre Unplug the heating element. | |

Her finner du (Here you will find):

| | |
|--------------------------------------|------------------------|
| Prosedyrer (Procedures) | Risk Assessment report |
| Bruksanvisning (Users manual) | Risk Assessment report |

Nærmeste (Nearest)

| | | |
|---|-------|------------------------------|
| Brannslukningsapparat extinguisher) | (fire | First floor , north entrance |
| Førstehjelpsskap (first aid cabinet) | | First floor , north entrance |

NTNU
Institutt for energi og prosessteknikk

Dato

Signert

● FORSØK PÅGÅR /EXPERIMENT IN PROGRESS

Dette kortet SKAL henges opp før forsøk kan starte!
This card MUST be posted on the unit before the experiment startup!

| | |
|--|--|
| Apparatur (Unit) Oil based heat storage rig | |
| Prosjektleder (Project Leader) Ole Jørgen Nydal | Telefon mobil/privat (Phone no. mobile/private) |
| Apparaturansvarlig (Unit Responsible) Ole Jørgen Nydal | Telefon mobil/privat (Phone no. mobile/private) |
| Godkjente operatører (Approved Operators) Paul Svendsen | Telefon mobil/privat (Phone no. mobile/private) |
| Prosjekt (Project) Excess energy to high temperature heat storage | |
| Forsøksstid / Experimental time (start - stop) | |
| Kort beskrivelse av forsøket og relaterte farer (Short description of the experiment and related hazards) <ul style="list-style-type: none">● Hot circulating oil (through insulated pipes and heat storage).● Do not touch the surfaces to avoid scald risk.● Be careful with the electric cable from the heating element and thermocouples. | |

NTNU
Institutt for energi og prosesssteknikk

Dato

Signert

- **ATTACHMENT E: GUIDANCE TO RISK ASSESSMENT**

Chapter 5 Assessment of technical safety.

Ensure that the design of the experiment set up is optimized in terms of technical safety.

Identifying risk factors related to the selected design, and possibly to initiate re-design to ensure that risk is eliminated as much as possible through technical security.

This should describe what the experimental setup actually are able to manage and acceptance for emission.

5.1 HAZOP

The experimental set up is divided into nodes (eg motor unit, pump unit, cooling unit.). By using guidewords to identify causes, consequences and safeguards, recommendations and conclusions are made according to if necessary safety is obtained. When actions are performed the HAZOP is completed.

(e.g. "No flow", cause: the pipe is deformed, consequence: pump runs hot, precaution: measurement of flow with a link to the emergency or if the consequence is not critical used manual monitoring and are written into the operational procedure.)

5.2 Flammable, reactive and pressurized substances and gas.

According to the Regulations for handling of flammable, reactive and pressurized substances and equipment and facilities used for this:

| |
|---|
| Flammable material: Solid, liquid or gaseous substance, preparation, and substance with occurrence or combination of these conditions, by its flash point, contact with other substances, pressure, temperature or other chemical properties represent a danger of fire. |
| Reactive substances: Solid, liquid, or gaseous substances, preparations and substances that occur in combinations of these conditions, which on contact with water, by its pressure, temperature or chemical conditions, represents a potentially dangerous reaction, explosion or release of hazardous gas, steam, dust or fog. |
| Pressurized : Other solid, liquid or gaseous substance or mixes having fire or hazardous material response, when under pressure, and thus may represent a risk of uncontrolled emissions |

Further criteria for the classification of flammable, reactive and pressurized substances are set out in Annex 1 of the Guide to the Regulations "Flammable, reactive and pressurized substances"

<http://www.dsb.no/Global/Publikasjoner/2009/Veiledning/Generell%20veiledning.pdf>

http://www.dsb.no/Global/Publikasjoner/2010/Tema/Temaveiledning_bruk_av_farlig_stoff_Del_1.pdf

Experiment setup area should be reviewed with respect to the assessment of Ex zone

- Zone 0: Always explosive atmosphere, such as inside the tank with gas, flammable liquid.
- Zone 1: Primary zone, sometimes explosive atmosphere such as a complete drain point
- Zone 2: secondary discharge could cause an explosive atmosphere by accident, such as flanges, valves and connection points

5.4 Effects on the environment

With pollution means: bringing solids, liquid or gas to air, water or ground, noise and vibrations, influence of temperature that may cause damage or inconvenience effect to the environment.

Regulations: <http://www.lovddata.no/all/hl-19810313-006.html#6>

NTNU guidance to handling of waste: <http://www.ntnu.no/hms/retningslinjer/HMSR18B.pdf>

5.5 Radiation

Definition of radiation

| |
|---|
| Ionizing radiation: Electromagnetic radiation (in radiation issues with wavelength <100 nm) or rapid atomic particles (e.g. alpha and beta particles) with the ability to stream ionized atoms or molecules. |
| Non ionizing radiation: Electromagnetic radiation (wavelength >100 nm), og ultrasound ₁ with small or no capability to ionize. |
| Radiation sources: All ionizing and powerful non-ionizing radiation sources. |
| Ionizing radiation sources: Sources giving ionizing radiation e.g. all types of radiation sources, x-ray, and electron microscopes. |
| Powerful non ionizing radiation sources: Sources giving powerful non ionizing radiation which can harm health and/or environment, e.g. class 3B and 4. MR ₂ systems, UVC ₃ sources, powerful IR sources ₄ . |
| ₁ Ultrasound is an acoustic radiation ("sound") over the audible frequency range (> 20 kHz). In radiation protection regulations are referred to ultrasound with electromagnetic non-ionizing radiation. |
| ₂ MR (e.g. NMR) - nuclear magnetic resonance method that is used to "depict" inner structures of different materials. |
| ₃ UVC is electromagnetic radiation in the wavelength range 100-280 nm. |
| ₄ IR is electromagnetic radiation in the wavelength range 700 nm - 1 mm. |

For each laser there should be an information binder (HMSRV3404B) which shall include:

- General information
- Name of the instrument manager, deputy, and local radiation protection coordinator
- Key data on the apparatus
- Instrument-specific documentation
- References to (or copies of) data sheets, radiation protection regulations, etc.
- Assessments of risk factors
- Instructions for users
- Instructions for practical use, startup, operation, shutdown, safety precautions, logging, locking, or use of radiation sensor, etc.
- Emergency procedures
- See NTNU for laser: <http://www.ntnu.no/hms/retningslinjer/HMSR34B.pdf>

5.6 The use and handling of chemicals.

In the meaning chemicals, a element that can pose a danger to employee safety and health

See: <http://www.lovddata.no/cgi-wift/ldles?doc=/sf/sf/sf-20010430-0443.html>

Safety datasheet is to be kept in the HSE binder for the experiment set up and registered in the database for chemicals.

Chapter 6 Assessment of operational procedures.

Ensures that established procedures meet all identified risk factors that must be taken care of through operational barriers and that the operators and technical performance have sufficient expertise.

6.1 Procedure Hazop

Procedural HAZOP is a systematic review of the current procedure, using the fixed HAZOP methodology and defined guidewords. The procedure is broken into individual operations (nodes) and analyzed using guidewords to identify possible nonconformity, confusion or sources of inadequate performance and failure.

6.2 Procedure for running experiments and emergency shutdown.

Has to be prepared for all experimental setups.

The operating procedure has to describe stepwise preparation, startup, during and ending conditions of an experiment. The procedure should describe the assumptions and conditions for starting, operating parameters with the deviation allowed before aborting the experiment and the condition of the rig to be abandoned.

Emergency procedure describes how an emergency shutdown have to be done,

- *what happens when emergency shutdown, is activated. (electricity / gas supply) and*
- *which events will activate the emergency shutdown (fire, leakage).*

Chapter 7 Quantifying of RISK

Quantifying of the residue hazards, Risk matrix.

To illustrate the overall risk, compared to the risk assessment, each activity is plotted with values for the probability and consequence into the matrix. Use task IDnr.

Example: If activity IDnr. 1 has been given a probability 3 and D for consequence the risk value become D3, red. This is done for all activities giving them risk values.

In the matrix are different degrees of risk highlighted in red, yellow or green. When an activity ends up on a red risk (= unacceptable risk), risk reducing action has to be taken

RISK MATRIX

| | | | | | | |
|---|-------------------|----|----|----|----|----|
| C O N S E Q U E N | (E) Catastrophic | E1 | E2 | E3 | E4 | E5 |
| | (D) Extensive | D1 | D2 | D3 | D4 | D5 |
| | (C) Moderate | C1 | C2 | C3 | C4 | C5 |
| | (B) Negligible | B1 | B2 | B3 | B4 | B5 |
| | (A) Insignificant | A1 | A2 | A3 | A4 | A5 |

| | | | | | | |
|--------|--|--------------------|--------------|--------------|------------|--------------------|
| S E | | | | | | |
| | | (1) Rare | (2) Unlikely | (3) Possible | (4) Likely | (5) Almost certain |
| | | PROBABILITY | | | | |

| COLOUR | | DESCRIPTION |
|--------|--|--|
| Red | | Unacceptable risk Action has to be taken to reduce risk |
| Yellow | | Assessment area. Actions has to be considered |
| Green | | Acceptable risk. Action can be taken based on other criteria |

The principle of the acceptance criterion. Explanation of the colors used in the matrix

